HARMONIC AND CHAOTIC RESPONSES WITH NONLINEAR VIBRATION ISOLATORS

by

B. RAVINDRA

DEPARTMENT OF MECHANICAL ENGINEERING
INDIAN INSTITUTE OF TECHNOLOGY KANPUR
March 1994

HARMONIC AND CHAOTIC RESPONSES WITH NONLINEAR VIBRATION ISOLATORS

A Thesis Submitted
in Partial Fulfilment of the Requirements
for the Degree of
DOCTOR OF PHILOSOPHY

by

B. RAVINDRA

to the

DEPARTMENT OF MECHANICAL ENGINEERING
INDIAN INSTITUTE OF TECHNOLOGY, KANPUR

MARCH, 1994

If a thing is worth doing, it is worth doing badly

Chesterton

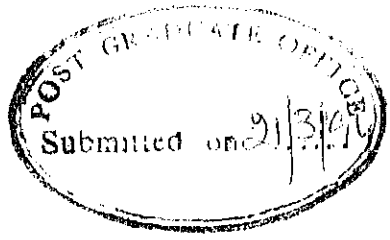

CERTIFICATE

Certified that the work contained in this thesis entitled: **"HARMONIC AND CHAOTIC RESPONSES WITH NONLINEAR VIBRATION ISOLATORS"**, has been carried out by Mr. B. Ravindra under my supervision and that the same has not been submitted elsewhere for a degree.

(Dr. A. K. Mallik)
Thesis Supervisor
Department of Mechanical Engineering
I. I. T. Kanpur - 208 016

ACKNOWLEDGEMENTS

I would appear silly, if I were to thank Professor A. K. Mallik. Working with him has been a great source of joy and inspiration. His guidance has made me understand the importance of diligence, analytical thinking and effective communication. Foremost, I have learned to always keep sight of application to real world problems. I can never forget the care and affection he showered on me during my association with him. One of my ambitions is to overcome my sloppiness and become a great teacher like him.

I am indebted to Professors J. K. Bhattacharjee and K. Banerjee for introducing me to nonlinear dynamics and for offering several valuable suggestions. I want to thank Professors A. Ghosh, H. Hatwal, N. S. Vyas, N. N. Kishore, K. Sriram, V. Sunderarajan, D. Yadav, P. M. Dixit, D. P. Rao, G. S. Murthy, B. S. Murthy, M. R. Madhav, C. V. R. Murthy, K. Ghosh and G. Biswas for their encouragement.

"History of Scientific Ideas" taught by Professors P.R.K. Rao and A.P.Shukla and our thursday and saturday discussion groups are important events in my life. My faculty lounge sessions with Nagarjun, Srikanth, Sanil, Kalyan , Sule, and Ravi Sankar taught me a great deal.

Thanks are also due to ManMohan, Krishna Mohan, Shymal, Rajiv, Chandrasekhar, P.V.M. Rao for their help.

M.M.Singhsaab helped me a great deal in many ways and I thank him for that. Jhaji, Prem Prakashji and others in the Manufacturing Science lab, Shri B. K. Jain of A.C.M.S. and Central workshop staff made a modest experiment possible and I am grateful to them.

Living in Hall 4 with Koshy, Jimmy, Salim, Parmar, Goutam,

Venkata Reddy, Sridhar, Siva Kumar, S.K. Verma, Pradhan, Kanetkar, Vinod Kumar, Venkatesh , Deepak Murthy, Ajit, Karandikar, Sayan Kar, Tarakeswar, Dada, Kapil, Sanjay, Bala, Javed, Nandi, Mandals, Siva, Khadilkar, Praveen and many other friends has been a great fun.

Squirrels on the streets of I.I.T.K. have been a constant source of amusement and day dreaming during my long walks and it is to these that I dedicate my thesis.

B. Ravindra

SYNOPSIS

The various methods of vibration control aim at modifying the source or the system or the transmission path from the source to the system. In vibration isolation, a resilient element is inserted in the path of vibration transmission from the source to the system. The simplest idealisation of vibration isolation system is a single degree-of-freedom model in which a mass is constrained to move only in one direction. The isolator is assumed to be massless with linear stiffness and linear damping. The foundation is considered as ideally rigid. The performance characteristics of isolators under the assumption of linearity have been widely reported in the literature.

Experiments conducted on real-life isolators such as wire-rope vibration isolation systems used in space applications, rubber and pneumatic suspensions used in automobile and other applications indicate the need to include nonlinearity in both the stiffness and damping. In the present thesis, damping forces proportional to pth-power of velocity (p=1, 2, and 3, representing viscous, orifice and cubic damping) and combined Coulomb (p=0) and viscous type are considered. Hard/soft as well as symmetric/asymmetric restoring forces are included. A brief review of previous works of Den Hartog, Ruzicka and other researchers on isolators with linear restoring force and nonlinear damping models is provided in the first chapter of the thesis.

The primary objective of this thesis is to analyse the role of nonlinearity in both stiffness and damping on the performance

of single degree-of-freedom, passive, vibration isolation systems. The governing equation of the isolation system is given by a generalised Duffing's equation with harmonic excitation. Both force and base excitation problems are considered. The method of harmonic balance is used to obtain the transmissibility expressions. These results are presented in chapter 2. The linear stability analysis of the harmonic solution can be carried out using the usual variational technique for only odd values of p. One encounters analytical difficulties for other values of p. A heuristic criterion (based on the notion of equivalent linear damping) is proposed to extend the stability analysis which works for all values of p (except p=0, i.e., Coulomb damping). Even higher order unstable zones can be obtained by this method.

Today, the role of damping in nonlinear vibration poses a new challenge to the theoretician. Even the notions like an attractor, basins of attraction etc., are due to damping in the system. While tremendous progress has been achieved in understanding various features of nonlinear vibrating systems (such as bifurcation structure and chaos), the role of damping and strictly dissipative nonlinear damping in particular (as opposed to self-excited oscillators like the van der Pol system) has not been addressed to in the literature. Therefore, another objective of the present thesis is to understand the role of nonlinear damping on the bifurcations and chaotic phenomena occurring in harmonically excited Duffing's oscillator with pth-power velocity dependent damping. In chapter 3, numerical simulation results are presented to show that the bifurcation structure and routes to chaos are insensitive to the choice of the nonlinear damping model.

In chapter 4, isolation systems with combined Coulomb and viscous damping and cubic, hard nonlinear restoring force are analysed. The method of harmonic balance is used again to obtain the steady-state response and transmissibility indices with the assumption that the motion is continuous without any stop. An anomalous jump in the response, similar to the one obtained in earlier studies on soft systems, is observed when the isolation system is subjected to a base excitation. The phenomenon of break-loose frequency is examined in detail to bypass the jump phenomena in the response.

Numerical simulations on the system discussed in chapter 4 are carried out in chapter 5 to analyse the role of Coulomb damping in bifurcation structure and chaos. It is shown that for a base-excited system, the inclusion of a Coulomb damper with a suitable break-loose frequency can suppress the secondary resonances and chaotic motion. However, for a force-excited system, the introduction of Coulomb damping does not alter the bifurcation structure.

Soft Duffing's oscillators (possessing a saddle point in the unforced situation) such as, single- and double-well potential oscillators represent a variety of engineering and physical problems. These systems are widely studied in literature as some analytical work can be carried out due to the existence of the homoclinic orbits. The role of nonlinear dissipation on the bifurcation structure in these systems is studied in chapter 6. The Melinkov criterion and an analytical criterion for the period-doubling are obtained in the presence of combined viscous and cubic damping.

Some preliminary experimental results are presented in chapter 7 for a soft isolator (made in the form of a hollow rubber tube). The transmissibility characteristics of this system obtained experimentally indicate that the soft characteristics of the hollow rubber tube are beneficial for effective vibration isolation.

The main conclusions of the thesis are:

(i) A nonlinear isolator with a soft characteristic is superior to that with a hard characteristic.

(ii) For a base-excited system, a suitable choice of the Coulomb damping coefficient enables one to maintain the transmissibility at or less than unity over the entire frequency range.

(iii) Both the period-doubling and intermittency routes to chaos occur for all values of the damping exponent p, thus preserving the bifurcation structure of a viscously damped, Duffing's oscillator. It is shown that strictly dissipative nonlinear damping can be effectively used for controlling chaos.

(iv) It has been demonstrated by numerical simulation that in a base-excited system, the instabilities associated with the secondary resonances and chaotic motion, encountered in the low frequency regime, can be eliminated by using a suitably designed friction damper.

(v) For a double-well potential oscillator, with the same value of the damping coefficient, the threshold values of forcing required to cause period-doubling bifurcation are seen to decrease with increasing value of the damping exponent. This feature is just opposite to what has been observed in the case of a hard, Duffing's oscillator.

(vi) Experimental results indicate that a suitable combination of a soft nonlinear spring and the optimum value of the damping can yield a better design than the linear isolator.

CONTENTS

LIST OF FIGURES

CHAPTER I

INTRODUCTION

1.1 Introduction

The quest for safe, reliable and quieter technologies is increasingly becoming important in the present day world. Vibration and noise control engineering is an important component of such an endeavour. Light weight vehicles and machines running at high speeds, performance sensitivity of electronic and optical instruments, design of robust launch vehicles and space structures, protection of buildings from earthquakes and other natural calamities give a fresh impetus for rapid development of new techniques of vibration control. The awareness of ergonomic aspects in designing shop floors and buildings etc., to create a safe and pleasant working environment devoid of noise and vibration is another source of motivation for the progress in vibration control.

In many engineering situations, the source of vibration is either the inertia forces of the moving parts or the oscillatory foundation/base motion. In such cases, it may not be feasible to reduce the level of excitation below the acceptable limit or modify the design so as to bring down the response below the desired level. Therefore, it is apparent that secondary methods of control are necessary to tackle many vibration problems. Vibration isolation is one such important and widely used method.

A vibration isolator in its most elementary form may be considered as a resilient member inserted between the source and

receiver of vibration. Many different materials are used in the form of isolator. Isolators can be rubber springs, air springs and coiled or leaf metal springs. Each one of these has some advantages and disadvantages. The damping capacity of an isolator may originate from various sources. For a bonded-rubber spring, energy dissipation occurs due to the inherent large internal friction within the material. With a coiled metal spring, normally a viscous dashpot is used in parallel to provide the damping. With leaf-springs, interface slip damping is a major contributor towards the overall damping. In the case of air-springs, orifices placed in the flow path cause the desired energy dissipation. Most of these damping mechanisms, like viscous, Coulomb (slip) or orifice, can be adequately treated as special cases of a damping force proportional to pth-power of velocity. This velocity dependent model, however, fails to account for the hysteretic type of damping force.

The function of a vibration isolator is primarily to reduce the magnitude of the motion transmitted from a vibrating foundation to the equipment (referred to as the base excitation problem), or to reduce the magnitude of the force transmitted from the equipment to the foundation (referred to as the force excitation problem). Depending on the method of producing the controlling force, vibration isolation can be classified as passive, active and semiactive. In active vibration isolation, the isolator force is servo-controlled that enhances the system performance. But these active control schemes are expensive and are usually limited to light weight machines. If the isolator force is not controlled using a feed-back strategy, then the

method is referred to as passive vibration isolation. A combination of the above two schemes is referred to as seniactive vibration isolation.

The simplest idealisation of a vibration isolation system is a single degree-of-freedom model in which a mass is constrained to move only in one direction. The isolator is assumed to be massless with linear stiffness and linear damping. The foundation is considered as ideally rigid. More complex vibration isolation systems can be visualised by relaxing these assumptions, such as when (i) the foundation is not ideally rigid, (ii) the isolator inertia cannot be ignored, (iii) several masses with intermediate elastic elements are involved in the model or (iv) the mass can move in any direction producing e.g., heave, roll, yaw and pitch modes. With the advent of modal analysis still more complex models treating the machine as a structure (no longer a rigid mass) connected to the foundation structure by isolators at several points are also not uncommon in the literature. But with increasing complexity, the problem becomes more specific and it is difficult to obtain generalised conclusions.

Further complications of the vibration isolation system may arise out of the type of excitation such as random or impulse excitation. The performance characteristics of isolators under the assumption of linearity have been widely reported in the literature. For such linear systems under harmonic excitations, various transfer functions, e.g., displacement or force transmissibility are used as the indices of effectiveness of an isolator. The various indices are related to one another through simple expressions and the choice of a particular index depends on

the type of the response variable and applications. Though the research on vibration isolation is vast, very little attention is paid to provide guidelines to design or select the isolators on a rational basis. The general practice of designing of the isolators is still on the assumption that all will be well if the natural frequency of the isolated system is appreciably lower than the frequency of excitation.

Consideration of the nonlinearities present in most of the practical isolators becomes important specially during the design and analysis of suspensions of high-speed vehicles, mounts for optical and other sensitive instruments to be used in space vehicles. Experiments conducted on real-life isolators such as wire-rope vibration isolation systems used in space applications, rubber and pneumatic suspensions used in automobile and other applications indicate the need to include nonlinearity in both the stiffness and damping. While, there has been a significant progress in understanding the role of nonlinearity in mechanical systems from the point of view of geometric theory of nonlinear dynamics, these results have not percolated down towards designing/improving the existing isolation systems. In the nonlinear theory of vibration isolation, one encounters with the problem of defining a suitable performance index for the isolator. This is because a harmonic response with the same frequency as that of the excitation is not guaranteed. The response may contain subharmonics , superharmonics and sometimes the response may even be nonperiodic (chaotic). Furthermore, unlike in a linear system, the indices to be used for various types of excitation cannot be related through simple expressions and consequently force and base

excitation problems need to be analysed separately.

The primary objective of this thesis is to analyse the role of nonlinearity in both the stiffness and damping on the performance of vibration isolation systems. In the present work, the isolation system is modelled as a generalised Duffing's oscillator with pth-power damping subjected to a harmonic excitation. Though the results presented are in the context of vibration isolation, emphasis is also laid on understanding the role of strictly dissipative nonlinear damping in the general framework of the geometric theory of dynamical systems.

1.2 Review of Previous Work

The amount of literature available on the general problem of vibration isolation is too vast to be considered in detail. In this section, the literature pertinent to the present work is discussed. A summary of the investigations reporting various features of the Duffing's oscillator is also presented. An overview of the research work in different areas, connected with the present problem, is categorized under the following headings:

(i) Vibration isolation,

(ii) Duffing's equation,

(iii) Systems with a Coulomb damper.

1.2.1 Vibration isolation

The performance characteristics of isolators and other results obtained prior to 1950 have been summarised in Crede's text book [1]. Details of a number of commercial isolators including their hardware constructional features have been

presented in reference [2]. A recent account of the research carried out can be obtained from reference [3]. Researchers have used different indices to express the effectiveness of an isolation system. Some of these are: (1) Force/displacement transmissibility (absolute), (2) Relative transmissibility, (3) Response ratio, (4) Isolation effectiveness, (5) Insertion loss, and (6) Vibration power flow. Log-Log plots of the above mentioned quantities vs. frequency ratio can be found extensively in the literature for various values of the system parameters.

Vibration isolation problems are generally analysed with the assumption that the foundation possesses infinite mechanical impedance. This assumption, although valid in many practical situations, is not applicable when the vibratory system is mounted on, say, ship, aircraft or automobile structures. In such a situation, the finite impedance of the foundation drastically affects the vibration isolation characteristics. Snowdon [4] has studied this problem when the isolator is made of rubber like materials for rigid as well as non-rigid foundations. The frequency dependence of the dynamic modulus and damping factor of rubber like materials has been taken into consideration while calculating the above mentioned indices. The concept of parallel combination of low and high damping rubber for improved performance of the isolation system has been proposed. Snowdon has used 'response ratio' to quantify the effect of vibration isolation for nonrigid foundations. The nonrigid foundations are modelled as simply-supported beams and plates. This analysis has been extended to the case when the feet of the machine supported on the isolator are nonrigid [5]. In this reference, Snowdon has

presented an excellent review of the use of elastomeric materials in vibration isolation. Wave effects may be observed at high frequencies when the rubber mount dimensions become comparable with multiples of the half-wave lengths of the elastic waves travelling through the mounting. Alternatively, wave effects may be thought of as occurring when the elasticity and the distributed mass of the rubber mounting interact at high frequencies. A guide to the character of the wave effects in antivibration mountings has been obtained by assuming that the 'mountings' obey the simple wave equation for the longitudinal vibration of a rod of uniform cross section [4]. Both 'long rod' and 'Love' theories have been used to analyse the wave effects [5]. Also it has been shown that the performance of an isolator is overestimated by ignoring the inertia and the resulting wave effects.

Macinante [6] has considered a two mass model to take care of the flexibility of floors and carried out a detailed parametric study. In reference [7], the criteria of effective isolation of machinery have been derived and the design of isolators complying with these criteria has been described. The concept of vibration power flow has been explained by Goyder and White [8]. Expressions have been derived for vibration power flow to the foundation for single point excitation, taking the foundation mobility into consideration. Design considerations for isolators and foundations, to minimise the transmission of vibration power in the structure, are examined. Pinnington and White [9] have also investigated the parameters controlling the power transmission from machine to the seating structure via vibration isolators. Some vibration isolation problems encountered on ships have been

considered in reference [10].

If added mass can be tolerated, a two stage or compound mounting can provide low values of transmissibility especially at high frequencies. The design of a practical mount based on this idea has been reported in references [4, 5] where a complete analysis of the compound stage mounting with rigid and nonrigid foundations has ben given. High frequency vibration isolation of two-stage isolators has been discussed in reference [11]. Some general design criteria for non-dissipative vibration isolation systems have been given in reference [12]. An analytical procedure for the evaluation of the transmissibility of N degrees-of-freedom viscoelastic mountings has been developed [13], where the transmissibility is expressed through a class of polynomials. The use of four-pole parameters which enables one to take the isolator inertia into account has been demonstrated in references [5, 14]. In reference [15] the wave effects in an isolator, consisting of N equal masses and N intermediate distributed elastic mounts, was analysed by using the four-pole parameters. The resulting transmissibility expressions are lengthy polynomials, especially for increasing values of N. The coefficients of these polynomials have to be evaluated separately for each value of N. In reference [16] the notion of a propagation constant has been used profitably to render the computational effort independent of the number of periodic elements present in the system. The analysis includes isolator inertia, frequency dependence of the isolator stiffness and damping, and the finite foundation impedance. Periodic isolators (antivibration mounts consisting of rubber blocks with intermediate steel spacers) are shown to possess better high

frequency isolation characteristics as compared to a simple one with the same overall dimensions.

Pinnington [17] has derived the expressions for vibration power flow when a motor is supported by four isolators on a flexible seating system. A detailed dynamic analysis of a heavily damped foundation structure designed for the multidirectional isolation of a diesel engine has been presented in reference [18]. The problem of defining suitable performance indices of an isolation system subjected to random excitations has been addressed to in reference [19]. A detailed review of the literature on vibration isolation has been compiled in reference [20] under the following headings: (i) static and dynamic properties of isolator materials, (ii) stress analysis of rubber mounts, (iii) modelling of finite impedance foundations, (iv) analysis of a single point excitation model, (v) analysis of an unidirectional multidegrees-of-freedom model, (vi) analysis of two or multipoint excitation model and, (vii) wave effects in isolators.

A better model of a number of practical isolators should include the nonlinear characteristics inherent in the spring and the damper. A study of the dynamic characteristics of a wire rope isolation system (constructed with helical strands) used in numerous space and military applications has been presented in reference [21]. A semi-empirical model having non-linear stiffness, power-law damping and variable Coulomb friction damping has been developed, and the results have been compared with the experimental data. Ruzicka and Derby [22] have summarised the results of scores of individual investigations on the problem of

vibration isolation of a mass with single degree-of-freedom. Nonlinear damping models considered in this work include linear dampers with clearance, Coulomb friction dampers, hysteretic dampers, and dampers whose damping force is proportional to a general power of velocity across the damper. Several indices of the performance of the isolation system with such nonlinear damping models and linear stiffness characteristics have been presented in a form which is immensely useful to a design engineer.

Kirk [23] has presented a study of the influence of nonlinear spring stiffness-characteristics on the effctiveness of vibration isolators with linear damping, subjected to stationary, random white noise ground acceleration. The results obtained with the cubic hard spring, the cubic soft spring and the tangent spring have been compiled as design charts. Isolators having symmetric and asymmetric nonlinear restoring force characteristics with linear damping have been investigated in reference [24], where the 'jump' phenomenon observed in the response is explained through the bifurcation set and catastrophe theory. The results are compared with those obtained from an experiment conducted with a pneumatic spring of constant area diaphragm. The application of catastrophe theory, rather than the study of isolation characteristics, seems to be the main objective of the work presented in reference [24].

A two degrees-of-freedom model incorporating nonlinear stiffness and damping characteristics is reported by Metwali [25]. Complex motion of the isolated mass at high excitations, taking into account the effects of the nonlinear material behaviour on

transmissibility, has been studied and bifurcations have been observed [26]. Beatty has considered the finite amplitude, periodic motion of a body supported on rubber shear springs [27, 28]. This work has been extended in reference [29]. The effect of the geometric and material nonlinearities of the elastomeric mounts on the transmissibility of a simple system has been studied experimentally by Harris [30, 31]. The types of nonlinearities encountered in mounts of various geometries and modes of loading have been obtained. It has been pointed out that these nonlinear aspects of rubber mounts have been relatively unexplored for antivibration devices. Also the role of nonlinearity in designing better suspensions for automobiles, nonwheeled ground vehicles and vibration control problems in space applications has been discussed. The standard approach to vibration isolation analysis represents the source, the isolator and the receiver by their mobilities. The choice of the appropriate description for each element is not arbitrary, specifically when the isolation system is nonlinear or when the system has noise. At least one of the system components must be represented by its impedance [32]. An interesting discussion of the challenges encountered in the low frequency vibration isolation, required to carry out microgravity science experiments has been presented in reference [33]. In reference [34], design and control aspects of microgravity isolation mounts have been detailed. The steady-state, harmonic response and the transmissibility indices of nonlinear isolators have been discussed in reference [35].

1.2.2 Duffing's equation

In the present work, the governing equation of motion of the isolation system is given by a generalised Duffing's oscillator with nonlinear damping. Hence, a summary of the recent investigations, carried out on various features exhibited by Duffing's oscillator and the role of damping, is presented in this section. Duffing's equation is one of the paradigm cases of nonlinear vibrating systems. Classical results on Duffing's equation can be obtained from the standard text books [36-42]. A modern treatment of Duffing's oscillator from the geometrical theory of dynamical systems has been summarised in references [43-50].

Duffing's oscillators are employed as models of various physical and engineering situations such as Josephson junctions, optical bistability, plasma oscillations, buckled beam, ship dynamics, vibration isolators and electrical circuits, etc.,[35, 43-52]. Since Ueda's [53-55] work on Duffing's equation, it is well-known that nonlinear systems under consideration can exhibit chaotic responses (under harmonic excitation) in certain parameter regimes. Such chaotic responses are studied via phase plots, Poincare maps, power spectrum, Lyapunov exponents etc.[43-45]; all obtained by using numerical methods. Single degree-of-freedom systems with different types of nonlinear restoring force and a linear damping force have been studied by various workers. With a symmetric nonlinear restoring force, the existence of a symmetry-breaking precursor and subsequent period-doubling route to chaos have been explained through the stability analysis using Hill's equation [56].

Crutchfield and Huberman [57, 58] considered the role of fluctuations on the onset of the period-doubling route to chaos. They showed that the structure of the strange attractor is very stable even under the influence of large fluctuating forces and that the role of noise is to introduce a symmetric gap in the deterministic bifurcation sequence. The effects of noisy precursors and the so-called virtual Hopf bifurcation on the period-doubling have been studied by Wiesenfeld [59-61].

Parlitz and Lauterborn [62] examined the connection between the bifurcation set and resonance structure of a forced Duffing's oscillator. In a series of papers [63-66] they employed the notion of 'Torsion Number' to classify resonances and discussed the universal superstructure in driven, dissipative nonlinear oscillators. These results indicate various scenarios in the bifurcation structure of Duffing's equation viz., hysteresis, co-existence of attractors, symmetry-breaking, existence of dual responses, period-doubling route to chaos. The work has also been extended to construct two-dimensional maps capturing similar features [66]. Fang and Dowell [67] also observed dual responses in Duffing's equation. The existence of intermittency transition to chaos in a symmetric potential well is explained in reference [68]. Floquet theory and harmonic balance method have been used to calculate the transition boundaries. In a series of papers, Szemplinska-Stupnicka [69-71] examined the role of classical methods in determining the subharmonic and chaotic zones in the amplitude-frequency plane. Also it has been demonstrated that the classical stability analysis using Mathieu and Hill's equations can capture the period-doubling observed in numerical simulations.

Several authors [72-80] obtained an extra jump in the harmonic response of soft Duffing oscillators indicating a break in the resonance curve. Miles [75, 76] referred to this jump as an 'anomalous jump' and conjectured that this break in the resonance curve for the oscillator is a necessary antecedent to symmetry-breaking.

In all the literature cited so far, the phenomenological model of the dissipative force has been assumed to be linear. In this context it is appropriate to recall what Pippard [81] has said "There is something of a tendency among physicists to try to reduce everything to linearity..... reality may not always conform to what we might wish, rather more so with the damping forces than with the restoring force in small-amplitude vibrations.". In the context of his discussion of the experimental results obtained by Wraight [82], Pippard also suggested that the nonlinear damping curves may give a measure of the pinning and frictional forces involved when the magnetic fields penetrate and move within a superconductor. The role of dissipation in Josephson junctions has received special attention in recent years both from the experimental [83] and theoretical [84] points of view. Landauer [85] presented a nice discussion of ensuing philosophical debate on the origin of dissipation, fluctuations and irreversibility. The modern geometrical theory of the dissipative dynamical systems introduced several new notions like 'strange attractors', 'basins of attraction' etc, [86]. These concepts, being essentially the facets of dissipation in dynamics, seem to inherit all the associated problems. Milnor [87] gave a detailed account of the conceptual difficulties for giving a precise mathematical

definition of an attractor.

A good account of the role of damping in vibrations from the engineering point of view has been given by Crandall [88]. He mentioned that damping is of great relevance as it decides the border of stability and instability. Consideration of nonlinear damping models is necessary in several engineering applications such as the "roll damping" in ship dynamics [51, 52], vibration isolators [21, 35] and the drag forces encountered in flow induced vibration problems [41, 44]. The importance of nonlinear damping in engineering stems from the fact that it can be used as an effective passive control strategy to suppress various instabilities . With these applications in mind a study of the role of nonlinear damping in the dynamics of Duffing's oscillator has been carried out in references [89, 90].

1.2.3 Systems with Coulomb damping

Detailed performance characteristics of a vibration isolation system with directly as well as elastically coupled Coulomb damper have been presented in reference [22]. The notion of equivalent viscous damping was employed to obtain expressions for various transmissibility indices. The importance of the break-loose frequency has been explained and the variations of the high frequency attenuation rate and resonance transmissibility with various values of damping have been discussed. An exact solution for the symmetric, steady-state response of a vibrating system with combined Coulomb and viscous friction has been given by Den Hartog [91]. He considered the motion with and without stops and examined the range of validity of the solution obtained by

assuming continuous motion. An analysis of similar vibrating systems, with combined Coulomb and viscous friction, subjected to base excitation can be found in references [92, 93]. However, in all the references mentioned above, the analysis has been restricted to motion with atmost two stops per cycle. An extension of Den Hartog's work to obtain response with multiple stops per cycle is carried out in reference [94]. Shaw [95] extended the work of Den Hartog by considering a situation where the static coefficient of friction is different from the kinetic coefficient. He also considered the effects of negative viscous damping mechanisms which may arise out of aerodynamic forces acting on turbine blades. The stability analysis was carried out by using bifurcation theory and the possibility of existence of aperiodic motions has been pointed out. It has been shown that the symmetric motion with two stops per period can be unstable and that pairs of unsymmetric motions are generated at the bifurcation points. It has been reported that beating type motions may occur when the equivalent viscous damping coefficient is negative. Some transient motions have also been analysed.

Studies of vibrating systems with various types of friction mechanisms are also important in the context of protection of structures from earthquakes by sliding isolation systems as reported in reference [96]. In this work, the transient and steady state responses of a force-excited system in the presence of various types of damping forces have been reported. The motion under consideration consisted of a number of stops per cycle. It was concluded that with increasing viscous damping, the number of stops per cycle of motion reduces and may even come down to zero.

In a series of papers, Dowell and his co-workers [97-99] have investigated vibrating systems with friction damper. The method of harmonic balance was used in these works. The existence of a strange attractor in a single degree-of-freedom nonlinear oscillator with friction is reported by Awrejcewicz [100]. This work has been extended in reference [101], where a detailed analysis to determine the parameter zones of chaotic motion has been carried out through numerical evaluation of Pioncare maps and Lyapunov exponents. A two degrees-of-freedom, self-excited oscillator with friction has been considered in references [102, 103], where the stability of the equilibrium points received special attention. Different types of stick-slip transition zones, numerical investigation of periodic and chaotic motions and some results on the transient behaviour have also been presented. Chaotic motion in self-excited systems with friction damping has also been dealt with in reference [104].

In reference [105], a hard, Duffing-type (i.e.,with cubic nonlinear restoring force) isolation system with combined Coulomb and viscous damping subjected to a harmonic excitation has been investigated. Both force and base excitation models are presented. The role of subharmonics and chaotic motion in the context of vibration isolation using Coulomb dampers has been addressed to in reference [106].

1.3 Objectives and Scope of the Present Work

The primary objective of the present thesis is to study the performance characteristics of a single degree-of-freedom passive vibration isolation system with nonlinearity in both spring and

damper. The governing equation of the isolation system is given by a generalised Duffing's equation with harmonic excitation. A pth-power velocity dependent damping force and hard/soft as well as symmetric/asymmetric restoring forces are included. Both force and base excitation problems are considered. The method of harmonic balance is used to obtain the transmissibility expressions and the results are presented in a format which can be readily used by the designer of isolation systems.

In 1971, Crandall [22] mentioned in his foreword to a monograph on vibration isolation that vibration theory was essentially complete except for a realistic treatment of damping. He pointed out that though the theoretical advances helped to gain a better understanding of the coupling of various modes due to the damping in multidegrees-of-freedom linear systems, the problems of damping still remain a principal challenge in vibration technology. Today, the role of damping in nonlinear vibration poses a new challenge to the theoretician. As already mentioned in section 1.2.2., even the notions like an attractor, basins of attraction etc., are due to damping in the system. While the literature survey indicates that tremendous progress has been achieved in understanding various features of nonlinear vibrating systems, the role of damping and strictly dissipative nonlinear damping in particular (as opposed to self-excited oscillators like Van der Pol system) has not been addressed to in the literature. Therefore, attention is paid to understand the role of nonlinear damping on the bifurcations and chaotic phenomena occurring in harmonically excited Duffing's equation.

Recently, exploitation of nonlinearity to obtain better

designs is increasingly becoming important [107]. Several attempts are being made to devise control schemes to quench the resulting bifurcations and chaos [108, 109]. In the present work, an effort is also made to understand the role of strictly dissipative nonlinear damping as a passive control strategy to suppress various instabilities occurring in nonlinear isolation systems. The organisation of the thesis is detailed below.

In chapter 2, a wide class of single degree-of-freedom vibration isolation systems subjected to both force and base excitations are considered. The nonlinear restoring and damping forces are assumed to be given by power laws. Symmetric/asymmetric as well as hard/soft spring models are considered. The soft systems are assumed to possess no saddle point in the unforced case. The method of harmonic balance is used to obtain the transmissibility expressions and a parametric study is reported to evaluate the performance characteristics. A heuristic procedure (using the notion of equivalent viscous damping coefficient), for analysing the stability of the harmonic solution of a hard, Duffing's oscillator with pth-power velocity dependent damping ($p \neq 0$, i.e., excluding Coulomb damping) is presented.

In chapter 3, a special case of the systems considered in chapter 2, i.e., Duffing's oscillator with pth-power velocity dependent damper subjected to a harmonic force excitation is studied using numerical simulation. Phase plots and Poincare maps are obtained to study the role of damping on bifurcations and chaos. It is shown that the bifurcation structure and routes to chaos are insensitive to the choice of the nonlinear damping model.

In chapter 4, isolation systems with combined Coulomb and viscous damping and cubic, hard nonlinear restoring force are analysed. The method of harmonic balance is used again to obtain the steady-state response and transmissibility indices with the assumption that the motion is continuous without any stop. An anomalous jump in the response, similar to the one obtained in earlier studies on soft systems, is observed when the isolation system is subjected to a base excitation. The phenomenon of break-loose frequency is examined in detail to bypass the jump phenomena in the response. The obtained results extend the previous works of Den Hartog and Ruzicka who considered a linear restoring element. Numerical simulations are carried out to ascertain the status of anomalous jump and the validity of the results obtained by the method of harmonic balance. It is pointed out that unlike in the case of a soft system, this anomalous jump does not seem to have any bearing on symmetry-breaking and subsequent period-doubling.

In chapter 5, it is shown that for a base-excited system, the inclusion of a Coulomb damper with a suitable break-loose frequency can suppress the secondary resonances and chaotic motion. However, for a force-excited system, the introduction of Coulomb damping does not alter the bifurcation structure.

In chapter 6, the effect of nonlinear dissipation on the response and bifurcations of soft Duffing's oscillator (possessing a saddle point in the unforced situation) is considered. A parametric study is reported to indicate the dependence of threshold values of the parameters, at which bifurcations occur, on the damping index and the damping coefficient. The Melinkov

criterion and an analytical criterion for the period-doubling are obtained in the presence of combined viscous and cubic damping.

In chapter 7, experimental results are presented for a nonlinear vibration isolator made in the form of a hollow rubber tube.

CHAPTER 2

HARMONIC RESPONSES OF NONLINEAR VIBRATION ISOLATORS WITH PTH-POWER DAMPING

2.1 Introduction

The performance characteristics of isolators under the assumption of linearity have been widely reported in the literature [2, 4]. For such linear systems under harmonic excitations, various transfer functions, e.g., displacement or force transmissibility are used as the indices of effectiveness of an isolator. These various indices are related to one another through simple expressions and the choice of a particular index depends on the type of response variable and applications.

In the nonlinear theory of vibration isolation, one encounters with the problem of defining a suitable performance index for the isolator. This is because a harmonic response with the same frequency as that of the excitation is not guaranteed. The response may contain subharmonics and superharmonics, and sometimes the response may even be non-periodic (chaotic) [43]. If other harmonics are present, a working index of isolation effectiveness may be defined as the ratio of the r.m.s. values of the response and the excitation. In the case of a chaotic response, the ratio of the power spectral densities of the response and the excitation may be used. These indices provide an overall measure of transmissibility [19]. However, even these working indices are devoid of any information insofar as the frequency content of the transmitted vibrations is concerned. The

information regarding frequency content is sometimes essential, especially when the foundation is of finite impedance. Furthermore, unlike in a linear system, the indices to be used for various response variables cannot be related through simple expressions and each case needs to be analysed separately. In this chapter, however, the standard index of transmissibility is retained since only the harmonic response is considered. A minor modification, in case the restoring force is asymmetric, has been made to take care of the presence of a frequency independent term in the response. The method of harmonic balance is used to obtain the steady-state, harmonic response and transmissibility under both force and base excitations.

In the present work, the isolator is modelled as one which provides nonlinear restoring and damping forces. The usual pth-power model has been used for damping which encompasses several special cases like Coulomb, linear, and quadratic damping models with p = 0, 1, 2, respectively. The case of Coulomb damping (i.e., p = 0) shows many special features. Therefore, the results with p=0 are not included here and will be reported in a seperate chapter. However, both symmetric and asymmetric nonlinear restoring forces are investigated. These models for isolators are in line with those suggested in references [2, 24, 25]. Force and base excitations are considered separately in each case. With harmonic force excitation on a rigid mass (the source), the foundation (the receiver) has been assumed to be fixed (i.e., of infinite impedance). The jump phenomenon in the response similar to that of Duffing's equation is obtained. The effects of system parameters on the "jump", resonance transmissibility and

high-frquency attenuation rate are presented.

2.2 Modelling of Isolation System and Governing Equations of Motion

As stated earlier, two different types of excitations are investigated. In the first one (Figure 2.1), a rigid mass M is acted upon by a harmonic force f cos ωt, and this mass is isolated from a fixed foundation through an isolator. Hereafter, this situation will be referred to as "force excitation". The second type of excitation, hereafter, referred to as "base excitation" is explained in Figure 2.2. Here the foundation is moving with a harmonic displacement $y = y_0 \cos \omega t$. The governing equations of motion for these two excitations with symmetric and asymmetric restoring force characteristics of the isolator are obtained seperately as detailed below.

2.2.1 CASE I: Isolation system with symmetric restoring force and subjected to force excitation

The governing equation of motion for the system under consideration can be written as [25],

$$M x'' + C x' \mid x' \mid^{p-1} + K x \mid x \mid^{q-1} = f \cos \omega t \qquad (2.1)$$

where a prime denotes differentiation with respect to time t, ω is the frequency of excitation, C and K are the constants of proportionality for damping and restoring forces, respectively. The exponents p and q characterise the nature of nonlinearities present in the damping and stiffness, respectively, of the isolator. This model can be considered as an idealisation of a

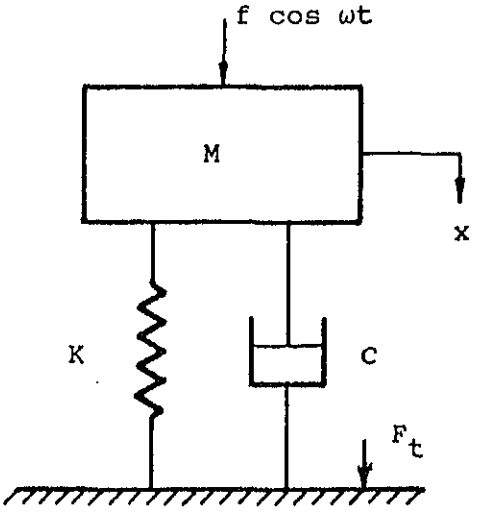

Figure 2.1 Isolation system subjected to force excitation

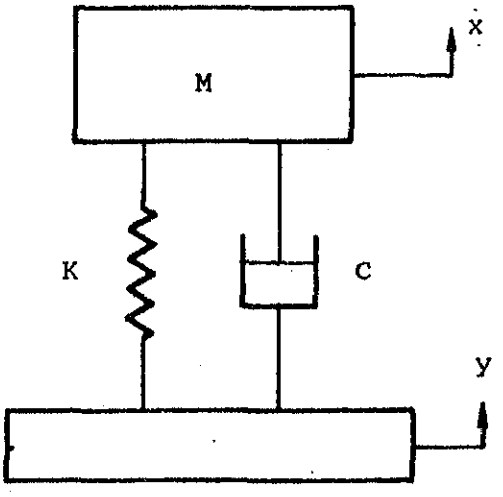

Figure 2.2 Isolation system subjected to base excitation

variable diaphragm pneumatic suspension as suggested in reference [25]. With q=1, equation (2.1) reduces to that considered by Ruzicka [22] and with q=3, we get a generalised Duffing's equation with pth-power damping model. It should be mentioned that a special case of equation (2.1) with p=1, q=2 has been studied by Hayashi [37].

Let us define the following non-dimensional parameters:

$$\tau = \omega_0 \, t, \; \Omega = \omega/\omega_0, \; X = x/x_0,$$

$$\dot{X} = x'/x_0\omega_0, \; \ddot{X} = x''/x_0 \, \omega_0^2, \; \zeta = C \, x_0^{p-1} \, \omega_0^{p-2}/(2 \, M) \qquad \text{with,}$$

$$x_0 = (f/K)^{1/q}, \; \omega_0 = [K \, x_0^{q-1} \, /M]^{1/2},$$

where a dot at the top denotes differentiation with respect to the non-dimensional time τ. Using the above parameters, equation (2.1) is rendered in the following nondimensional form:

$$\ddot{X} + 2 \, \zeta \, \dot{X} \, |\dot{X}|^{p-1} + X \, |X|^{q-1} = \cos \, \Omega\tau \qquad (2.2)$$

2.2.2 CASE II: Isolation system with symmetric restoring force and subjected to base excitation

From Figure 2.2, the relative displacement δ of the isolator is given by, $\delta = x - y$, where x is the response and y is the base excitation. The governing equation of motion for this system can be written as

$$M \, \delta'' + C \, \delta' |\delta'|^{p-1} + K \, \delta|\delta|^{q-1} = -M \, y'' = My_0 \, \omega^2 \cos \, \omega t. \qquad (2.3)$$

Defining the following parameters,

$\tau = \omega_0 t$, $\Omega = \omega/\omega_0$, $\Delta = \delta/y_0$,

$\dot{\Delta} = \delta'/ y_0\omega_0$, $\ddot{\Delta} = \delta''/y_0\ \omega_0^2$ and $\zeta = C\ y_0^{p-1}\ \omega_0^{p-2}/(2\ M)$, with

$\omega_0 = [K\ y_0^{q-1}/M]^{1/2}$,

and substituting in equation (2.3) we get the following nondimensional equation:

$$\ddot{\Delta} + 2\ \zeta\ \dot{\Delta}\ |\dot{\Delta}|^{p-1} + \Delta\ |\Delta|^{q-1} = \Omega^2\ \cos\ \Omega\tau \qquad (2.4)$$

2.2.3 CASE III: Isolation system with asymmetric restoring force and subjected to force excitation

Let us consider an asymmetric restoring force given by $K_1x + K_2x^2 + K_3x^3$. The governing equation of motion can now be written as

$$M\ x'' + C\ x'\ |\ x'\ |^{p-1} + K_1x + K_2x^2 + K_3x^3 = f\ \cos\ \omega t \qquad (2.5)$$

which represents the motion of a mass on a constant-area diaphragm pneumatic isolator as shown in references [2,24]. This equation with p=1 has also been considered in references [37,69].
Defining the following nondimensional parameters:

$\tau = \omega_0\ t$, $\Omega = \omega/\omega_0$, $X = x/x_0$,

$\dot{X} = x'/x_0\omega_0$, $\ddot{X} = x''/x_0\,\omega_0^2$, $\zeta = c\,x_0^{p-1}\,\omega_0^{p-2}/(2M)$,

$\varepsilon_1 = K_2x_0/(M\omega_0^2) = K_2\,x_0/K_1$, $\varepsilon_2 = K_3\,x_0^2/\,K_1$, with

$x_0 = f/K_1$, $\omega_0 = [K_1/M]^{1/2}$,

and substituting these in equation (2.5), one obtains

$$\ddot{X} + 2\,\zeta\,\dot{X}\,|\dot{X}|^{p-1} + X + \varepsilon_1X^2 + \varepsilon_2X^3 = \cos\,\Omega\tau\ . \qquad (2.6)$$

Using a transformation $X^* = X + \varepsilon_1/(3\varepsilon_2)$, equation (2.6) can be changed to

$$\ddot{X}^* + 2\,\zeta\,\dot{X}^*\,|\,\dot{X}^*|^{p-1} + [1 - \varepsilon_1^2/\,(3\,\varepsilon_2)]\,X^* + \varepsilon_2\,X^{*3} =$$

$$\cos\,\Omega\tau + \varepsilon_1/\,(3\,\varepsilon_2) - 2\,\varepsilon_1^3\,/(27\varepsilon_2^2)\ . \qquad (2.7)$$

Since the presence of the linear term does not change the result qualitatively [37], for the sake of simplicity ε_1 is chosen such that the linear term goes to zero. Thus, upon choosing $\varepsilon_1 = \sqrt{3\varepsilon_2}$, equation (2.7) reduces to

$$\ddot{X}^* + 2\,\zeta\,\dot{X}^*\,|\,\dot{X}^*|^{p-1} + \varepsilon_2\,X^{*3} = \cos\,\Omega\tau + B_0 \qquad (2.8)$$

where $B_0 = 1\ /\ (3\,\sqrt{3\varepsilon_2})$.

2.2.4 CASE IV: Isolation system with asymmetric restoring force and subjected to base excitation

The governing equation of motion can be written as

$$M\,\delta'' + C\,\delta'|\delta'|^{p-1} + K_1\,\delta + K_2\,\delta^2 + K_3\,\delta^3 = My_0\,\omega^2\cos\omega t. \qquad (2.9)$$

Defining the following parameters:

$\tau = \omega_0 t$, $\Omega = \omega/\omega_0$, $\Delta = \delta/y_0$,

$\dot{\Delta} = \delta'/\,y_0\omega_0$, $\ddot{\Delta} = \delta''/y_0\,\omega_0^2$ and $\zeta = C\,y_0^{p-1}\,\omega_0^{p-2}/(2\,M)$, with

$\omega_0 = [K_1/M]^{1/2}$,

and substituting these in equation (2.9), the following nondimensional equation is obtained:

$$\ddot{\Delta} + 2\,\zeta\,\dot{\Delta}\,|\dot{\Delta}|^{p-1} + \Delta + \varepsilon_1\Delta^2 + \varepsilon_2\Delta^3 = \Omega^2\cos\Omega\tau, \qquad (2.10)$$

where $\varepsilon_1 = K_2\delta_0/(M\omega_0^2) = K_2\,\delta_0/K_1$, $\varepsilon_2 = K_3\,\delta_0^2/\,K_1$.

By carrying out the transformations along the lines mentioned in section 2.2.3, equation (2.10) can be rewritten as

$$\ddot{\Delta}^* + 2\,\zeta\,\dot{\Delta}^*\,|\,\dot{\Delta}^*|^{p-1} + \varepsilon_2\,\Delta^{*3} = \Omega^2\cos\Omega\tau + B_0\,, \qquad (2.11)$$

where $\Delta^* = \Delta + \varepsilon_1/\,(3\,\varepsilon_2)$, $B_0 = 1\,/\,(3\,\sqrt{3\varepsilon_2})$ and ε_1 is assumed to be satisfy the relation $\varepsilon_1 = \sqrt{3\varepsilon_2}$.

2.3. Solution Procedure

Considering the governing equations of motion for the four different situations, viz., equations (2.2), (2.4), (2.8) and (2.11), we note that the general form of all these equations is

$$\ddot{Z} + 2\zeta \dot{Z} \mid \dot{Z} \mid^{p-1} + g(Z) = F \cos \Omega\tau + B_0 , \qquad (2.12)$$

where Z, g(Z), F and B_0 for the different cases are given in Table 2.1. In this section, first the procedure for solving equations (2.12) in general is outlined. Thereafter, the suitable transmissibility expressions for the four different cases (I-IV) are obtained.

TABLE 2.1

S.No.	Z	g(Z)	F	B_0
CASE I	X	$X\|X\|^{q-1}$	1	0
CASE II	Δ	$\Delta\|\Delta\|^{q-1}$	Ω^2	0
CASE III	X^*	$\varepsilon_2 X^{*3}$	1	$1/(3\sqrt{3\varepsilon_2})$
CASE IV	Δ^*	$\varepsilon_2 \Delta^{*3}$	Ω^2	$1/(3\sqrt{3\varepsilon_2})$

The method of harmonic balance [37] is used to solve equation (2.12). As a first approximation, the solution is assumed to be harmonic, and of the form

$$Z(\tau) = Z_0 + Z_1 \cos (\Omega\tau + \phi) . \qquad (2.13)$$

Let $h(Z,\dot{Z}) = 2\,\zeta\,\dot{Z}\,|\,\dot{Z}\,|^{p-1} + g(Z)$. (2.14)

The periodic function $h[Z(\tau),\ \dot{Z}(\tau)]$ can be approximated by the Fourier expansion up to first order as given below:

$$h[Z(\tau),\dot{Z}(\tau)] \approx R_0 + R_1 \cos(\Omega\tau+\phi) + R_2 \sin(\Omega\tau+\phi) \qquad (2.15)$$

where the Fourier coefficients R_0, R_1 and R_2 are given by,

$$R_0 = 1/(2\pi) \int_{-\pi}^{\pi} h(\vartheta)\ d\vartheta\ ,$$

$$R_1 = 1/(\pi) \int_{-\pi}^{\pi} h(\vartheta) \cos\vartheta\ d\vartheta\ , \qquad (2.16)$$

and $$R_2 = 1/(\pi) \int_{-\pi}^{\pi} h(\vartheta) \sin\vartheta\ d\vartheta$$

where $\vartheta = \Omega\tau + \phi$.

Substituting equations (2.16) in equations (2.15) and (2.12), one obtains

$$\ddot{Z} + R_0 + R_1 \cos(\Omega\tau+\phi) + R_2 \sin(\Omega\tau+\phi) = F \cos\Omega\tau + B_0. \qquad (2.17)$$

Now writing $F \cos\Omega\tau$ as $F\,[\cos(\Omega\tau+\phi)\ \cos\phi + \sin(\Omega\tau+\phi)\ \sin\phi]$ and equating coefficients of the same harmonics and the constant terms from both sides of equations (2.17), one gets

$$R_0 = B_0\ ,$$
$$-Z_1\Omega^2 + R_1 = F \cos\phi \qquad (2.18)$$
and $$R_2 = F \sin\phi,$$

where R_0, R_1 and R_2, given by equations (2.16), are functions of Z_0, Z_1, ϕ and other system parameters. Solving the set of simultaneous nonlinear equations (2.18) in Z_0, Z_1 and ϕ, one finally obtains $Z(\tau)$ from equation(2.13). Detailed expressions for R_0, R_1 and R_2 for the four cases (I-IV) are listed in Table 2.2. The symbols γ_p and γ_q, used in the expressions of R_1 and R_2 in Table 2.2, are given by

$$\gamma_p = (2/\sqrt{\pi})\ \Gamma([p+2]/2)\ /\ \Gamma([p+3]/2) \qquad (19a)$$

and

$$\gamma_q = (2/\sqrt{\pi})\ \Gamma([q+2]/2)\ /\ \Gamma([q+3]/2) \qquad (19b)$$

where Γ is the standard gamma function.

2.3.1 Transmissibility expressions

A minor modification is made in the standard definition of the transmissibility to account for the constant term present in the response of the system with asymmetric restoring force.Two indices, namely the force transmissibity (T_f) in the case of force excitation and the displacement transmissibility (T_d) in the case of base excitation, are defined as given below.

The force transmissibility is defined as the ratio of the maximum magnitude of the force transmitted to the foundation to that of the exciting force (F). From equation (2.17) it can be seen that the ~~the~~ force transmitted to the foundation F_t is given by

$$F_t = R_0 + R_1 \cos(\Omega\tau+\phi) + R_2 \sin(\Omega\tau+\phi) - B_0. \qquad (2.20)$$

Thus, we get

TABLE 2.2

S.No.	Z_0	Z_1	R_0	R_1	R_2
I	0	X_1	0	$X_1^q \gamma_q$	$-2 \zeta \Omega^p X_1^p \gamma_p$
II	0	Δ_1	0	$\Delta_1^q \gamma_q$	$-2 \zeta \Omega^p \Delta_1^p \gamma_p$
III	X_0^*	X_1^*	$\varepsilon_2 X_0^* [1.5 X_1^{*2} + X_0^{*2}]$	$\varepsilon_2 X_1^* [0.75 X_1^{*2} + 3X_0^{*2}]$	$-2 \zeta \Omega^p X_1^{*p} \gamma_p$
IV	Δ_0^*	Δ_1^*	$\varepsilon_2 \Delta_0^* [1.5 \Delta_1^{*2} + \Delta_0^{*2}]$	$\varepsilon_2 \Delta_1^* [0.75 \Delta_1^{*2} + 3\Delta_0^{*2}]$	$-2 \zeta \Omega^p \Delta_1^{*p} \gamma_p$

$$T_f = |[\ R_0 - B_0 + (\ R_1^2 + R_2^2\ )^{1/2}\ ]|. \tag{2.21}$$

The displacement transmissibility (T_d) is defined as the ratio of the maximum displacement of M to that of the base motion. After algebraic manipulation, it can be shown that the generalized expression for T_d is given by

$$T_d = |[\ Z_0 - 3B_0 + (Z_1^2 + 1 + 2\ Z_1\ \cos\phi\ )^{1/2}\ ]|. \tag{2.22}$$

Detailed expressions of T_d and T_f for cases I to IV are given below. These quantities can be evaluated by referring to Table 2.2.

Case I:
$$T_f = \frac{[K_e^2 + c_e^2\ \Omega^2]^{1/2}}{[(K_e - \Omega^2)^2 + c_e^2\ \Omega^2]^{1/2}} \tag{2.23}$$

where
$$C_e = 2\ \zeta\ X_1^{p-1}\ \Omega^{p-1}\ \gamma_p$$

and
$$K_e = X_1^{q-1}\ \gamma_q\ . \tag{2.24}$$

It may be noted that the method of equivalent linearisation [22,110] gives the same results as obtained above, where, C_e and K_e are referred to as the equivalent viscous damping and the equivalent stiffness, respectively.

Case II: T_d is still given by equation (2.23), but in equation (2.24) X_1 should be replaced by Δ_1.

Case III:
$$T_f = |[R_0 - 1/(3\ \sqrt{3\varepsilon_2}) + (R_1^2 + R_2^2)^{1/2}\ ]| \tag{2.25}$$

Case IV: $$T_d = |[\ \Delta_0^* - 1/(\sqrt{3\varepsilon_2}) + (\Delta_1^{*2} + 1 + 2\ \Delta_1^*\ \cos\phi\ )^{1/2}\ ]| \qquad (2.26)$$

2.4 Linear Stability Analysis

In equation (2.12), both restoring and damping forces do not have continuous derivatives with respect to Z and $\dot{Z}$, respectively, for p < 1 or/and q < 1. Hence, the stability analysis by the usual variational technique is not amenable for analytical treatment. A modified procedure described in reference [111] is, therefore, adopted. Considering that Z_0 and Z_1 in equation (2.13) are slowly varying with time and substituting it in equation (2.17), the assosiated autonomous equations of the system are obtained as given below:

$$\dot{\phi} = \frac{(\ R_1 - F\cos\phi\ ) - Z_1\ \Omega^2}{2\ Z_1\ \Omega}\ ,$$

$$\dot{Z}_1 = -(F\sin\phi - R_2\ )\ /\ (\ 2\ \Omega\ )\ , \qquad (2.27)$$

$$\dot{Z}_0 = \psi\ ,$$

and $$\dot{\psi} = -R_0 - B_0$$

While deriving equations (2.27), $\ddot{Z}_1$ but not $\ddot{Z}_0$ has been neglected [42]. The relevant expressions for R_0 , R_1 and R_2 can be substituted from Table 2.2 for different cases I-IV. The stability of the solution, $\dot{\phi} = \dot{Z}_1 = \dot{Z}_0 = \dot{\psi} = 0$ can be studied by considering the linearised equations

$$\dot{\eta} = A\ \eta \qquad (2.28)$$

where $\eta = \{ \phi, Z_1, Z_0, \psi \}^T$ and A is the Jacobian matrix of the system under consideration. The eigenvalues of A provide the requisite information on the stability of the solutions obtained in section 2.3. When both p and q are odd integers, the present method and the usual variational technique yield the same results. An alternative approach to carry out the stability analysis using the notion of "equivalent viscous damping" is proposed in the appendix A for the case of Duffing's oscillator with pth-power damping.

2.5. Results and Discussions

In this section a parametric study depicting the effects of system parameters on the performance indices of various types of isolators is presented. Four typical values of p = 1, 1.5, 2, 3 signifying, respectively, viscous, orifice, quadratic and cubic damping are considered. Results for a symmetric restoring force are reported in section 2.5.1 and those for an asymmetric restoring force are presented in section 2.5.2. A representative curve indicating transmissibility (in dB) vs frequency (Ω) is shown in Figure 2.3.

With refefrence to this figure, the following indices are defined : (i) the maximum value of transmissibility (T_m), (ii) the frequency at which the maximum transmissibility occurs (Ω_m), (iii) the resonance critical frequency (Ω_r), (iv) the non-resonance critical frequency (Ω_n), (v) the jump width (W) and (vi) the high frequency attenuation rate (HAR) of transmissibility. The existence of three possible values of the transmissibility (Figure 2.3) at a given frequency gives rise to the so-called jump

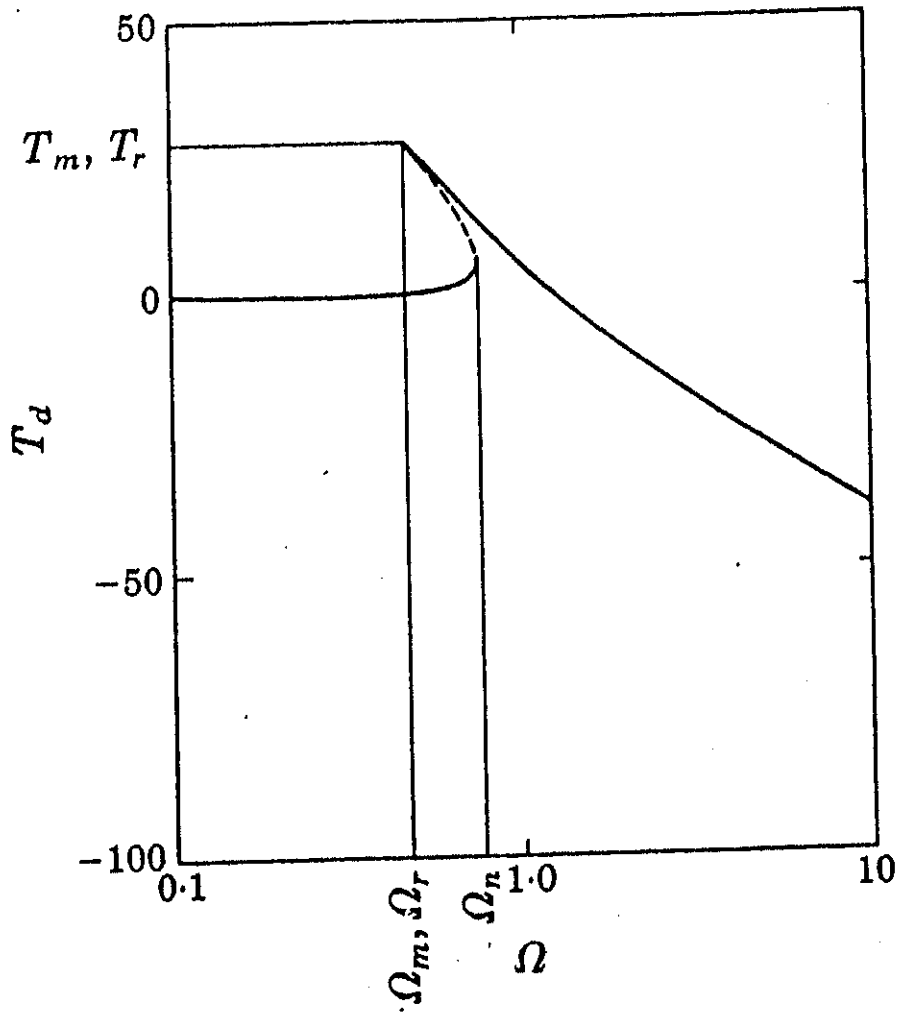

Figure 2.3 Typical transmissibility plot. - - -, unstable; ——, stable.

phenomenon. The upper branch of the jump is known as the resonance branch, the lower one as the non-resonance branch and the middle one as the unstable branch. Two points of vertical tangencies on the transmissibility curve are referred to as the critical frequencies. One on the resonance branch is identified as Ω_r, while that on the non-resonance branch is indicated as Ω_n. The jump width (W) is given by $W = (\Omega_r \sim \Omega_n)$. An unstable solution of the governing equation exists in the frequency range given by the jump width. The high frequency attenuation rate of transmissibility is given by the slope of the transmissibility (in dB) vs Ω curve (as Ω tends to ∞).

It can be seen from Figure 2.3 that the difference between Ω_m and Ω_r is negligible, and one can consider Ω_r and the associated transmissibility (T_r) on the resonance branch as Ω_m and T_m, respectively. Obviously a good isolator should have low values of Ω_r and T_r and a high value of HAR.

2.5.1 Isolation system with symmetric restoring force

The transmissibility expression for a force excitation is given by equation (2.22), and that for a base excitation by equation (2.24). The transmissibility values of a soft system ($q<1$) for these two excitations are shown, respectively, in Figures 2.4 and 2.5. It can be seen from these figures, that a jump similar to the one observed in the response of a soft Duffing's oscillator, occurs. However, a soft Duffing's oscillator, in the absence of excitation, possesses three equilibrium points [36] whereas the present system in the unforced case has only one equilibrium point. Therefore, an anomalous jump

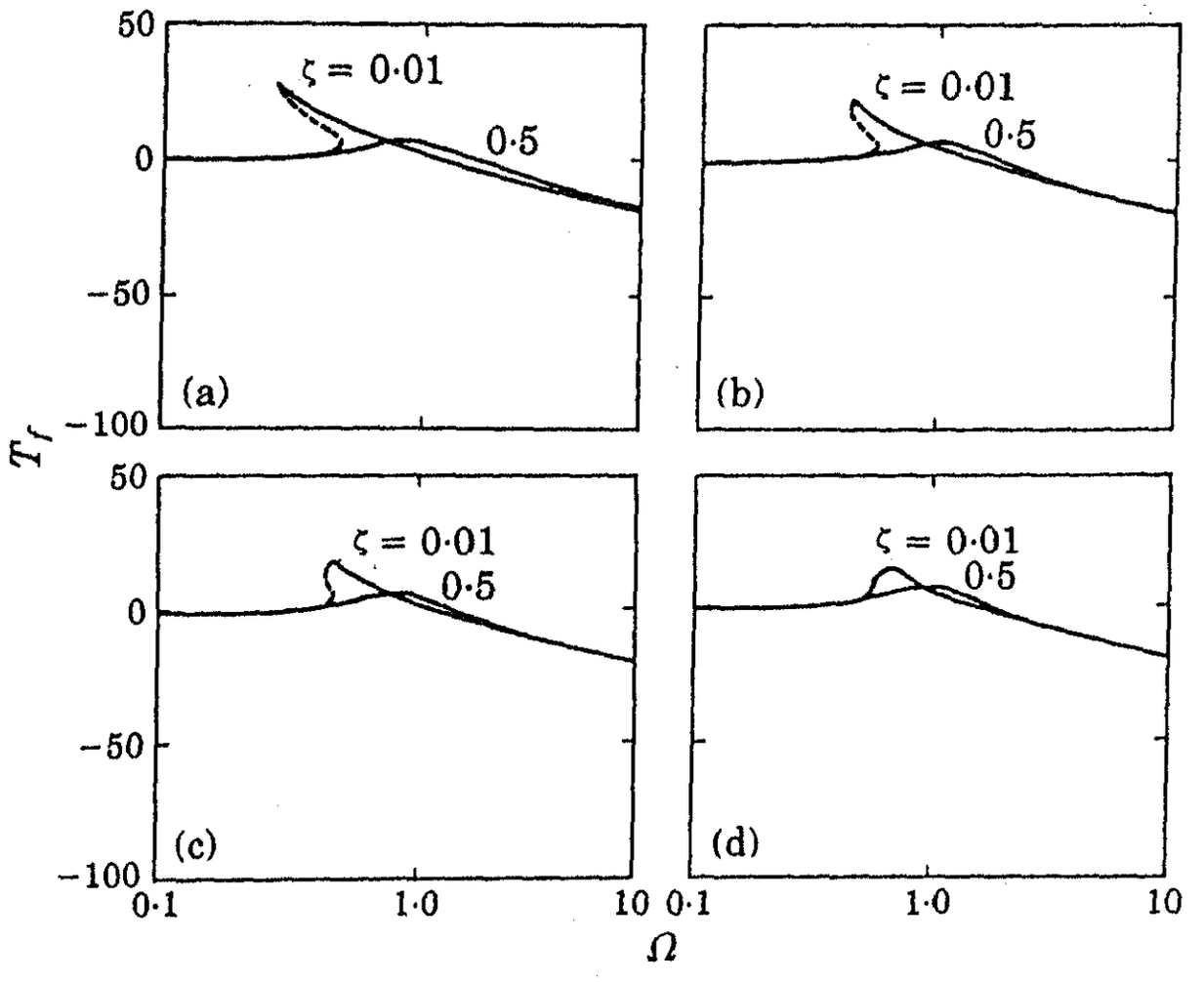

Figure 2.4 Variation of T_f vs Ω. q=0.5 and (a) p=1.0; (b) p=1.5; (c) p=2.0; (d) p=3.0.

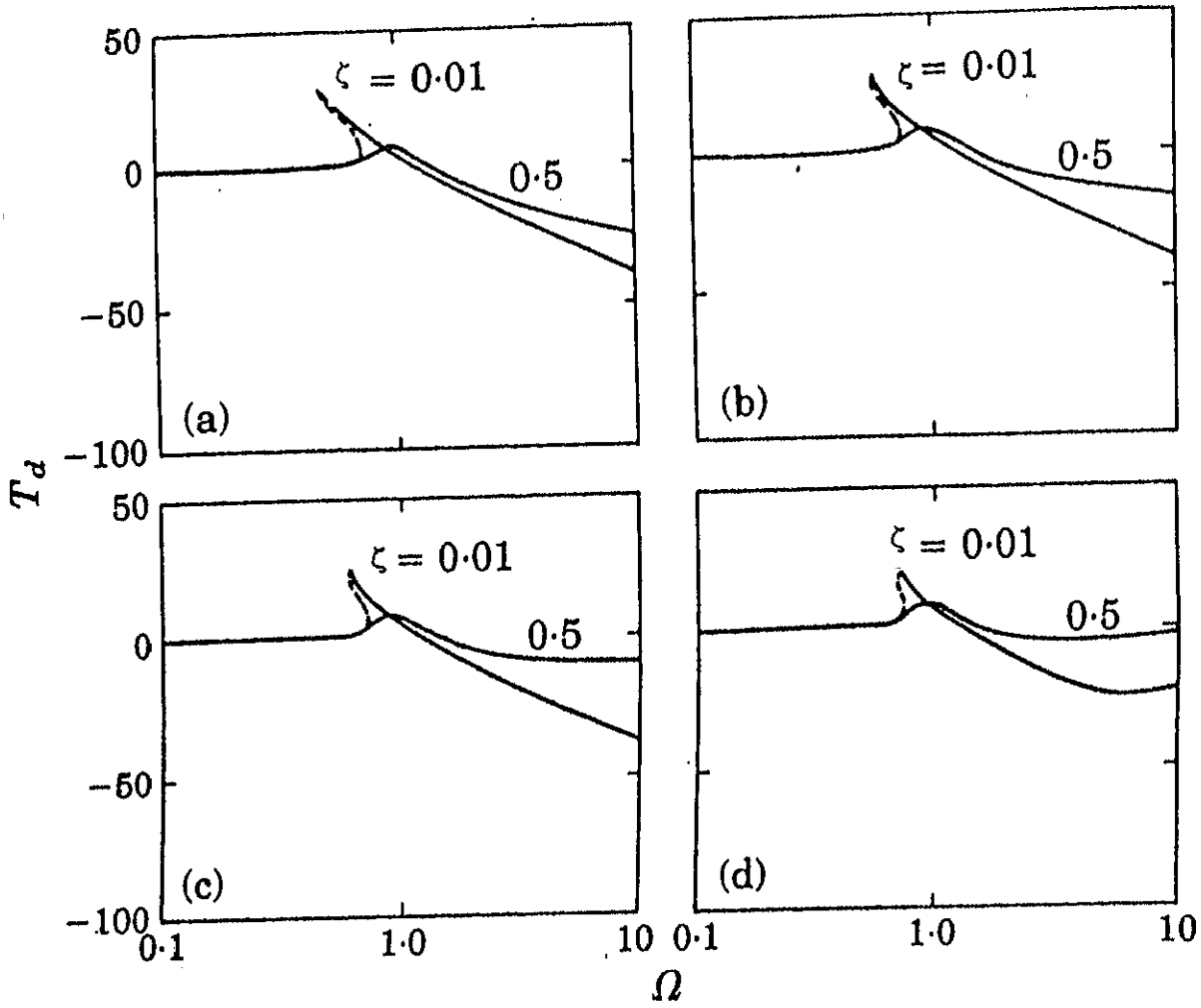

Figure 2.5 Variation of T_d vs Ω. q=0.5 and (a) p=1.0; (b) p=1.5; (c) p=2.0; (d) p=3.0.

observed in the response of a soft Duffing's oscillator with high excitation values [74] is absent in the present system. For a hard system (i.e., q>1), a jump similar to the one observed in the response of a hard Duffing's oscillator occurs as shown in Figures 2.6 and 2.7. In general, an isolator is effective if the resonance frequency (Ω_r in this case) is far below the operating range of interest. One may observe (see Figures 2.6-2.7) that the jump width for a hard system covers the high-frequency range, and consequently such an isolator is not as effective as an isolator with a soft characteristic.

The effect of increasing ζ can be summarised (See Figures 2.4-2.7) as follows: With increasing ζ; (i) the resonance transmissibility T_r decreases, (ii) the high frequency attenuation rate (HAR) decreases, (iii) the jump width (W) reduces and may eventually be entirely eliminated, (iv) the resonance frequency (Ω_r) decreases for q > 1 and increases for q < 1. Thus, the effects of ζ on T_r & HAR are similar to those for a linear isolator.

The jump width (W) reduces as the damping exponent p increases as can be seen from Figures 2.8 and 2.9. It is interesting to note that Ω_n is insensitive to variations in p and ζ. Thus, in many cases one can arrive at an analytical estimate of Ω_n by approximating ζ = 0. As expected, the resonance critical frequency Ω_r is very much sensitive to variations in the damping parameters p and ζ. Furthermore, the jump width in the case of a base excitation is more than that for a force excitation when q > 1 and vice versa when q < 1.

Referring back to Figures 2.5 and 2.7, one sees that HAR

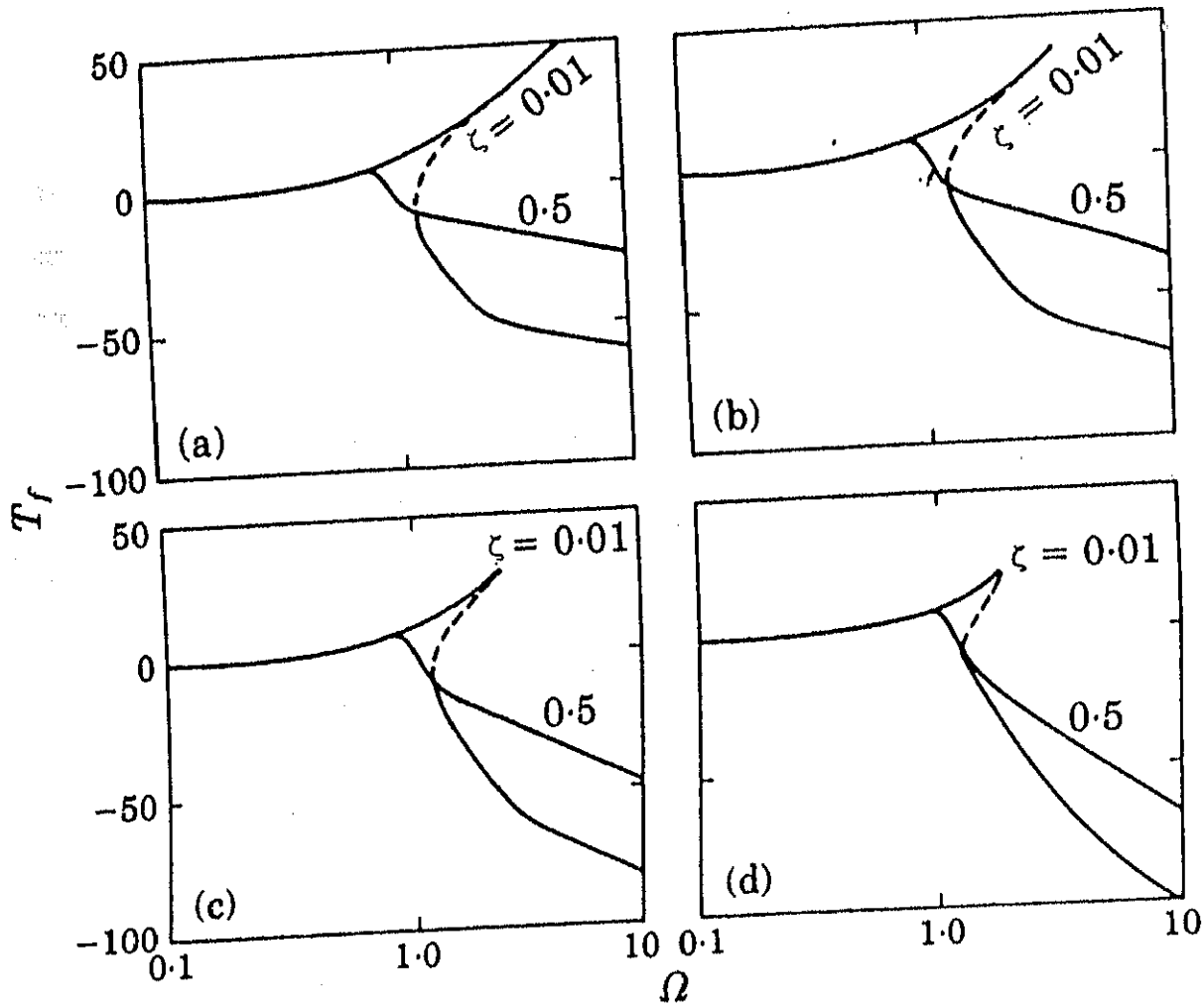

Figure 2.6 Variation of T_f vs Ω. q=3.0 and (a) p=1.0; (b) p=1.5; (c) p=2.0; (d) p=3.0.

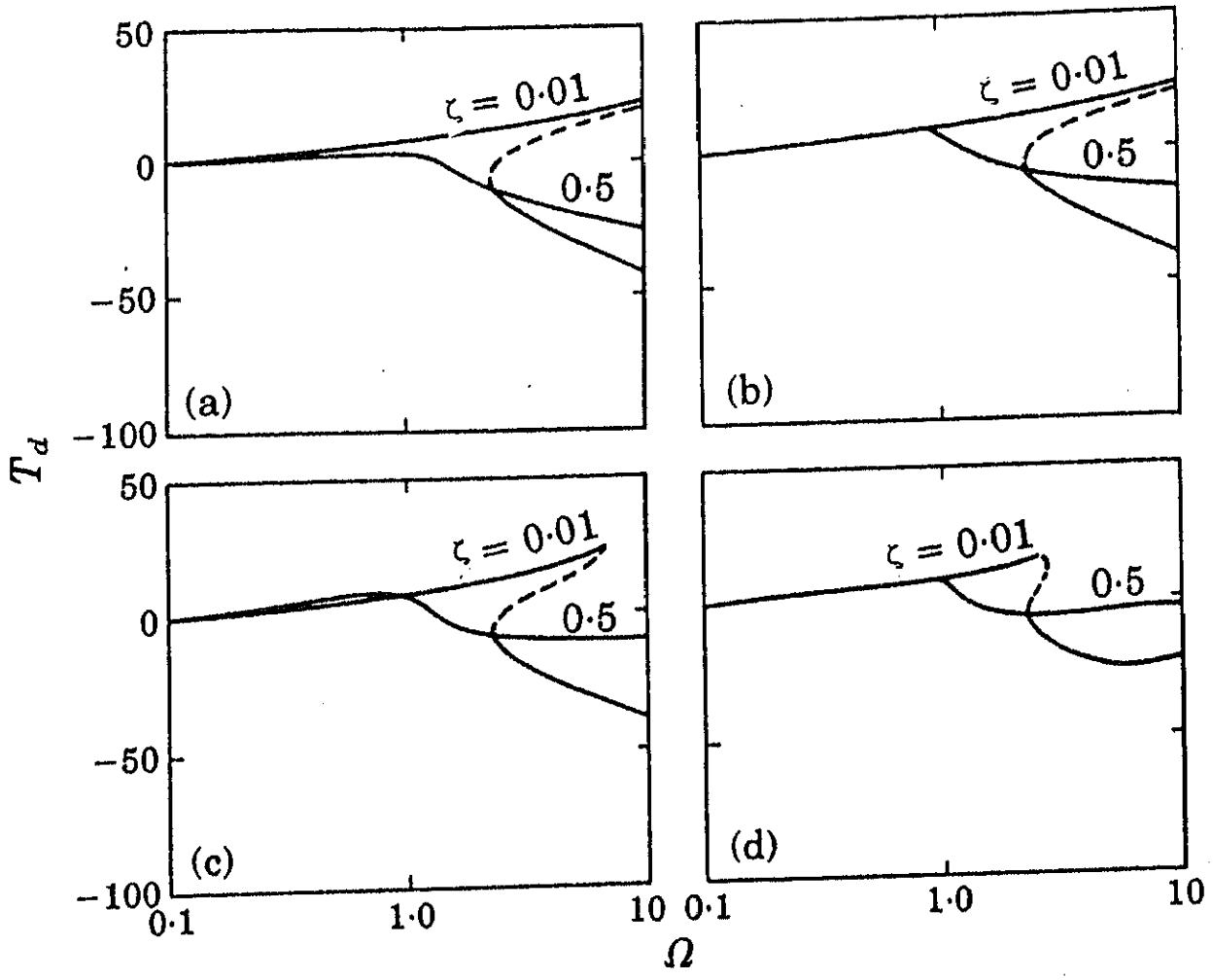

Figure 2.7 Variation of T_d vs Ω. q=3.0 and (a) p=1.0; (b) p=1.5; (c) p=2.0; (d) p=3.0.

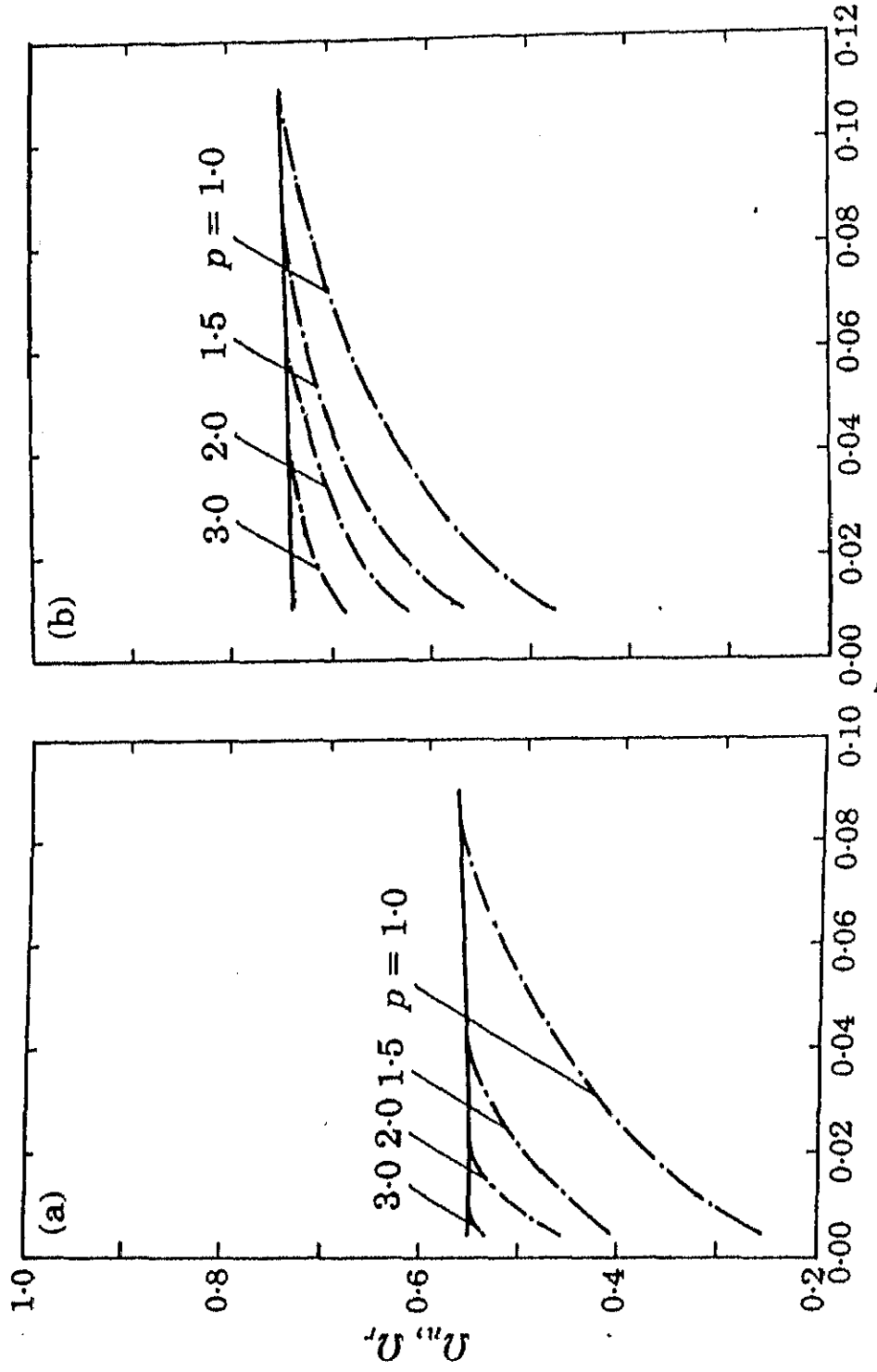

Figure 2.8 Variation of Ω_n and Ω_r with ζ. q=0.5 and (a) force excitation; (b) base excitation.

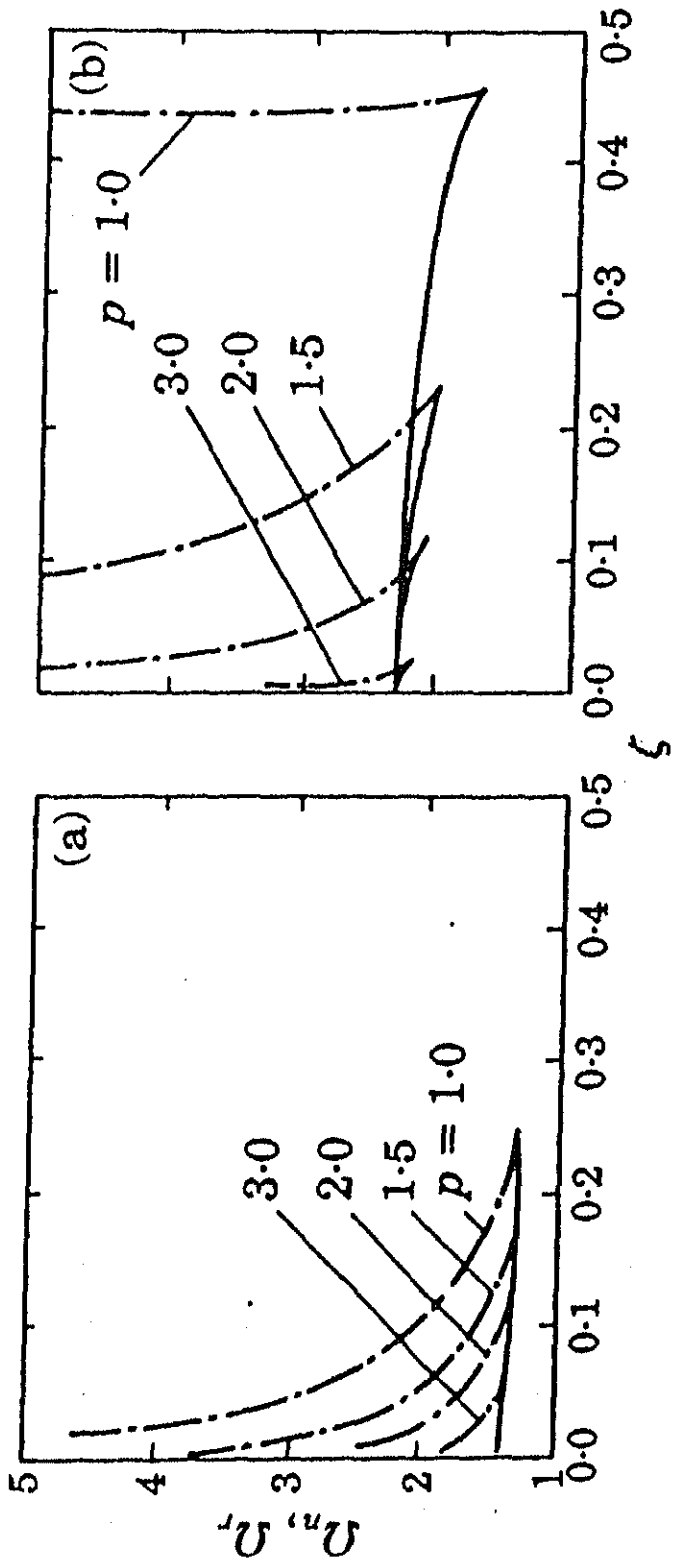

Figure 2.9 Variation of Ω_n and Ω_r with ζ. q=3.0 and (a) force excitation; (b) base excitation.

decreases with an increase in p for the case of a base excitation. It becomes zero for p=2 and even negative for higher values of p. Comparing Figures 2.4 and 2.6 with Figures 2.5 and 2.7, respectively, it is seen that the effects of p on HAR for a force excitation is just the opposite of that for a base excitation. With a force excitation, HAR increases with increasing p. Thus, the trends of HAR are similar to those reported by Ruzicka [22] for the case of an isolator with linear stiffness.

The stability analysis is carried out as explained in section 2.4. The unstable branch in the transmissibility plot is shown by dotted lines in Figures 2.4-2.7. The eigenvalues of the Jacobian matrix A given by equation (2.17) show that this unstable solution corresponds to an unstable saddle point of the associated autonomous equation given by equations (2.16).

2.5.2 Isolation system with asymmetric restoring force

The transmissibilities given by equations (2.25) and (2.26) are plotted in Figures 2.10-2.11. Numerical computations are carried out with $\varepsilon_2 = 1.0$, $\zeta = 0.01$ and 0.5,. A jump similar to that in a 'hard' Duffing's case is observed in all these figures. The unstable branches are marked with dotted lines. The effects of ζ and p on all the quantities associated with the jump are similar to those observed with a symmetric restoring force. But the effects of ζ and p on HAR with a base excitation are at variance from that of the previous section. In the present case, HAR always tends to zero. For the parameter values considered here, one can conclude that an isolation system with asymmetric restoring force

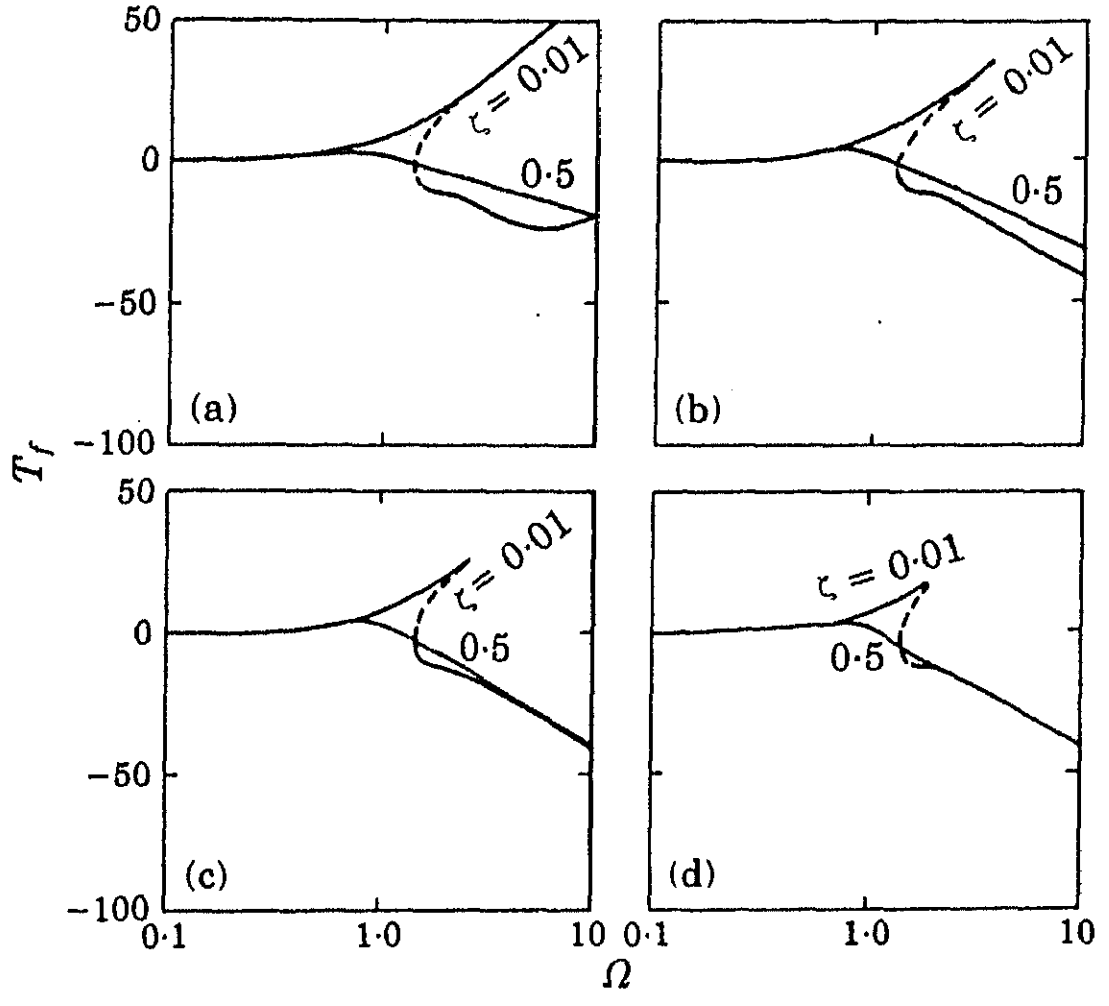

Figure 2.10 Variation of T_f vs $\bar{\Omega}$ for the asymmetric case (a) p=1.0; (b) p=1.5; (c) p=2.0; (d) p=3.0.

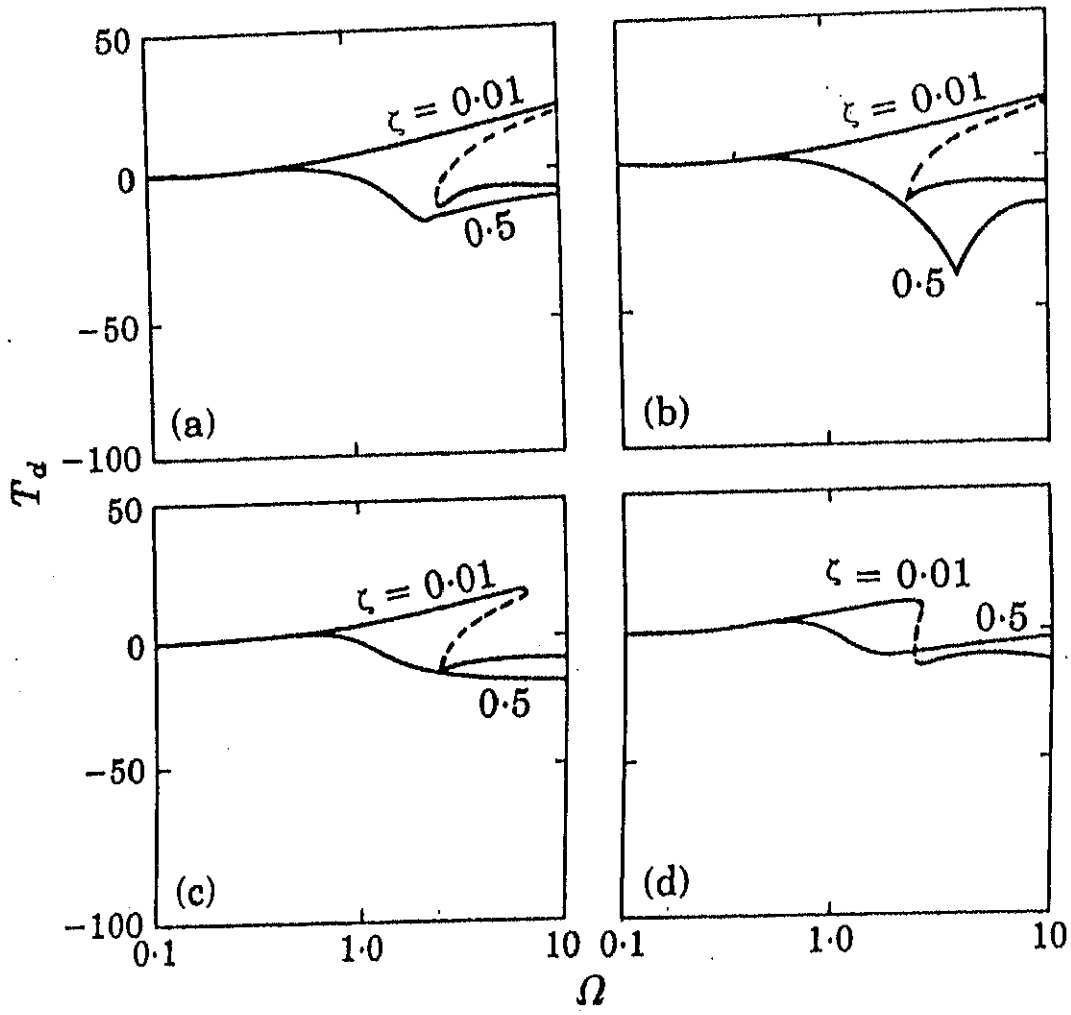

Figure 2.11 Variation of T_d vs Ω for the asymmetric case (a) p=1.0; (b) p=1.5; (c) p=2.0; (d) p=3.0.

may not perform satisfactorily with a base excitation.

2.6. Conclusions

An isolator with a soft characteristic ($q<1.0$) is found to be superior to that with a hard characteristic ($q>1.0$), since in the latter case the jump in the transmissibility curve extends towards high frequencies. The effects of damping on the resonance transmissibility and the high frequency attenuation rate are similar to those reported by Ruzicka for systems with a linear restoring force. The jump width decreases with increasing damping coefficient and may even entirely be eliminated. With increasing damping index p, the jump width reduces making the unstable zone narrower. The resonance critical frequency is very much sensitive to variations in the damping parameters whereas a good approximation for the non-resonance critical frequency can be obtained by assuming the damping to be absent. It is seen that for the parameter values considered in the present work, an isolator with an asymmetric restoring force may not perform satisfactorily for a base excitation.

CHAPTER 3

CHAOTIC RESPONSE OF NONLINEAR ISOLATORS WITH PTH-POWER DAMPING

3.1 Introduction

The steady-state, harmonic response and the transmissibility indices of nonlinear isolators have been discussed in chapter 2. In the present chapter, chaotic oscillations of a harmonically excited mass on a nonlinear isolator are investigated. The magnitude of the strictly dissipative damping force on the mass, provided by the isolator, is assumed to be proportional to pth-power of velocity. Both symmetric and asymmetric nonlinear restoring forces are considered. Numerical simulation is carried out to analyse the subharmonic and chaotic motions in the background of the results obtained in the case of linear damping (i.e., p=1). Two typical routes to chaos, namely through the period-doubling and intermittency, reported already in the literature for linear viscous damping (i.e. p=1), are seen to be present with the damping exponent p=2 and p=3. Thus, the bifurcation structure seems to be unaffected by the damping exponent p. Of course, the values of the damping coefficient (constant of proportionality) needed for complete elimination of the subharmonic and chaotic responses depend on the value of p. A parametric study is presented to indicate the role of the damping exponent, damping coefficient and asymmetry on the onset of chaos. It is revealed that suitable choices of the damping coefficient and damping exponent can entirely eliminate subharmonics and chaotic motions and thus provide a passive rather than an active

3.2. Isolator Model

The governing equation of motion, for a harmonically excited mass on an isolator with pth-power damping and cubic stiffness nonlinearity, can be written as

$$x'' + 2\zeta x'|x'|^{p-1} + x^3 = f_0 + f\cos\omega t;\ \zeta>0,\ p>0 \qquad (3.1)$$

where x is the displacement of the mass and ω is the excitation frequency. It may be noted that equation (3.1) has been obtained by following a non-dimensional procedure different from that used in chapter 2. In this chapter, results are obtained by varying excitation with ω=1.0. The values of the damping exponent p = 1, 2 and 3 correspond, respectively, to linear, quadratic and cubic damping models. The case p=0 representing Coulomb damping with a discontinuous damping force has many special features and will be presented in a later chapter. The parameters ζ and f in equation (3.1) refer to the damping coefficient per unit mass, and the amplitude of the exciting force per unit mass, respectively. The constant term f_0 represents the asymmetry of either the excitation or the restoring force. In a real-life vibration isolation system, this asymmetry can arise due to various factors such as when (i) the gravity effects are included in a vertical system (ii) the restoring force has a quadratic term as in a constant area diaphragm pneumatic spring. In the latter, a suitable scaling [37] gives rise to the constant term f_0 in the excitation. Overall, the degree of asymmetry in the system is represented by f_0 which plays

a major role in the analysis of chaotic motion as will be pointed out later. In this chapter, the symmetric (f_0=0) and asymmetric (f_0*0) cases are discussed separately. It should be noted that a linear term which may be present in the restoring force of a typical isolator has been omitted in equation (3.1) since it is known that the linear term does not qualitatively affect the behaviour of the system in the chaotic regime [53-55].

As indicated by the enormous complexity of the results obtained by numerical simulation over the last ten years [43-71], it is a hopeless task to compute the transmissibility indices for all the parameter zones of interest. Consequently, in this chapter the response of the mass rather than any isolator index has been computed to obtain the qualitative behaviour of the system.

3.3 Numerical Results and Discussions

In this section, detailed numerical simulation of the system governed by equation (3.1) is presented. The effect of nonlinear damping on the bifurcation structure and routes to chaos are discussed. Towards this end, the usual phase plots, Poincare maps and response plots obtained from numerical simulation are used. The Runge-Kutta-Merson method has been employed to carry out the numerical integration of equation (3.1).

3.3.1 Symmetry-breaking and period-doubling route to chaos with symmetric nonlinearity

It should be noted that equation (3.1) has the symmetry such that $x \longrightarrow -x$ as $t \longrightarrow t+\pi/\omega$. In other words, if $x(t)$ is a solution of equation (3.1), then so is $-x(t+\pi/\omega)$. These solutions

may or may not be distinct. The solution is called symmetric if

$$x(t) = -x\ (t+\pi/\omega). \qquad (3.2)$$

It is obvious that any solution consisting of only odd (super) harmonics is symmetric. It can be shown [56, 59] through the stability analysis (using Mathieu's equation) that at certain critical parameter values, the symmetric solution becomes unstable giving rise to even order superharmonics. It may be noted that as soon as even superharmonics appear, the response loses symmetry, i.e., $x(t)$ and $-x(t+\pi)$ solutions become distinct. This loss of symmetry manifests itself in the appearence of dual solutions [62, 67] as confirmed by numerical integration with different initial conditions. With further increase in f, this period-doubling route (i.e., through the introduction of $\omega/2$, $\omega/4$, ... in the response) eventually leads to chaotic response. It has been shown in the literature that the symmetry-breaking precursor is necessary for the period-doubling route to chaos in symmetric systems [61].

Numerical simulation of equation (3.1) is carried out with the following set of parameter values: ω= 1.0, ζ= 0.025, p=2.0 and f_0=0. Bifurcation sequences are observed by varying the amplitude of excitation, f.

The phase plots, obtained after the transients have died down, are shown in Figure 3.1. In Figure 3.1a, the time period of the periodic solution is found to be the same as that of the excitation. The symmetry of the phase trajectories suggest that only odd superharmonics appear in the solution. In Figure 3.1b, the symmetry of the phase trajectory is lost and the dual solution (for the same values of all the parameters) obtained with a different set of initial conditions is shown in Figure 3.1c. Both

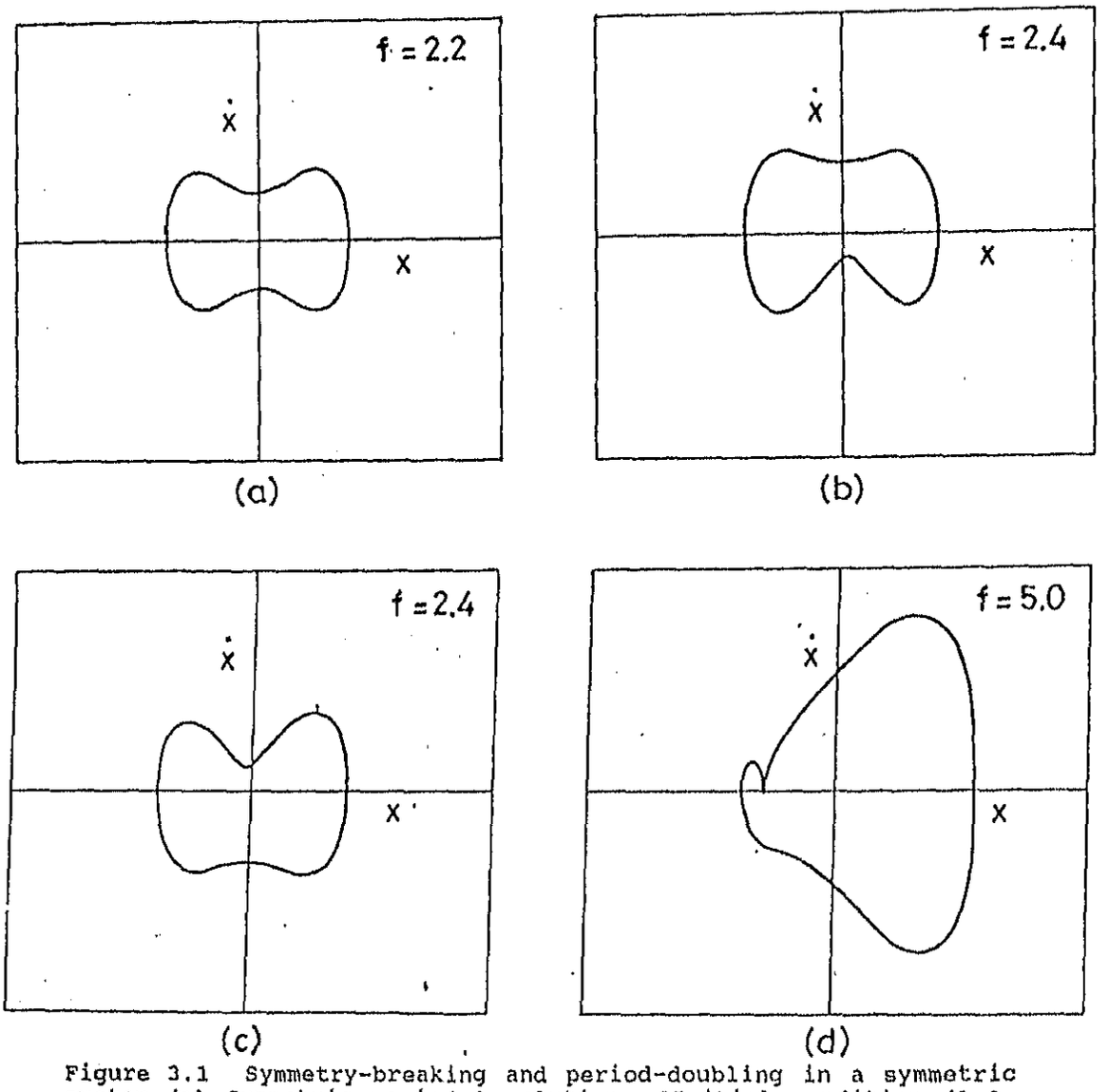

Figure 3.1 Symmetry-breaking and period-doubling in a symmetric system (a) Symmetric period 1 solution [Initial condition (1.0, 1.0)]; (b) Asymmetric period 1 solution [Initial condition (1.0,1.0)]; (c) Dual solution [Initial condition (-1.0, -1.0)]; (d) Period 2 solution [Initial condition (1.0,1.0)]

these solutions have time period equal to that of the excitation. Figure 3.1d shows the phase trajectory when 1/2 subharmonic appears in the solution and consequently the period of the response is twice that of the excitation. Figures 3.2a and 3.2b, respectively, show the Poincare map and the response plot of the chaotic attractor obtained through this period-doubling route.

3.3.1.1 Effect of damping exponent p and damping coefficient ζ

A parametric study is carried out to determine the effects of p and ζ on the onset of chaos via the period-doubling route. Towards this end, the critical forcing amplitudes are obtained for the occurence of symmetry-breaking and the first two period-doubling bifurcations. Figures 3.3a-3.3c refer to the results obtained with p=1, 2 and 3, respectively. It can be seen from Figure 3.3a that a minimum value of ζ is necessary for breaking the symmetry. Further, for a given value of p, the forcing amplitude required to break the symmetry is relatively independent of the value of ζ. However, as ζ increases there is a marked increase in the forcing required for the successive period-doubling bifurcations. It may be noted that with increasing ζ, the cascade of period-doubling bifurcations reduces and chaos is entirely suppressed though the initial period-doubling may still continue. Hence, strictly dissipative nonlinear damping, just like linear damping, can also be used as a passive mechanism to suppress chaos.

Comparing Figures 3.3a-3.3c one can conclude that the basic bifurcation structure is totally independent of the value of p. Only the minimum value of ζ, needed for the symmetry-breaking, or

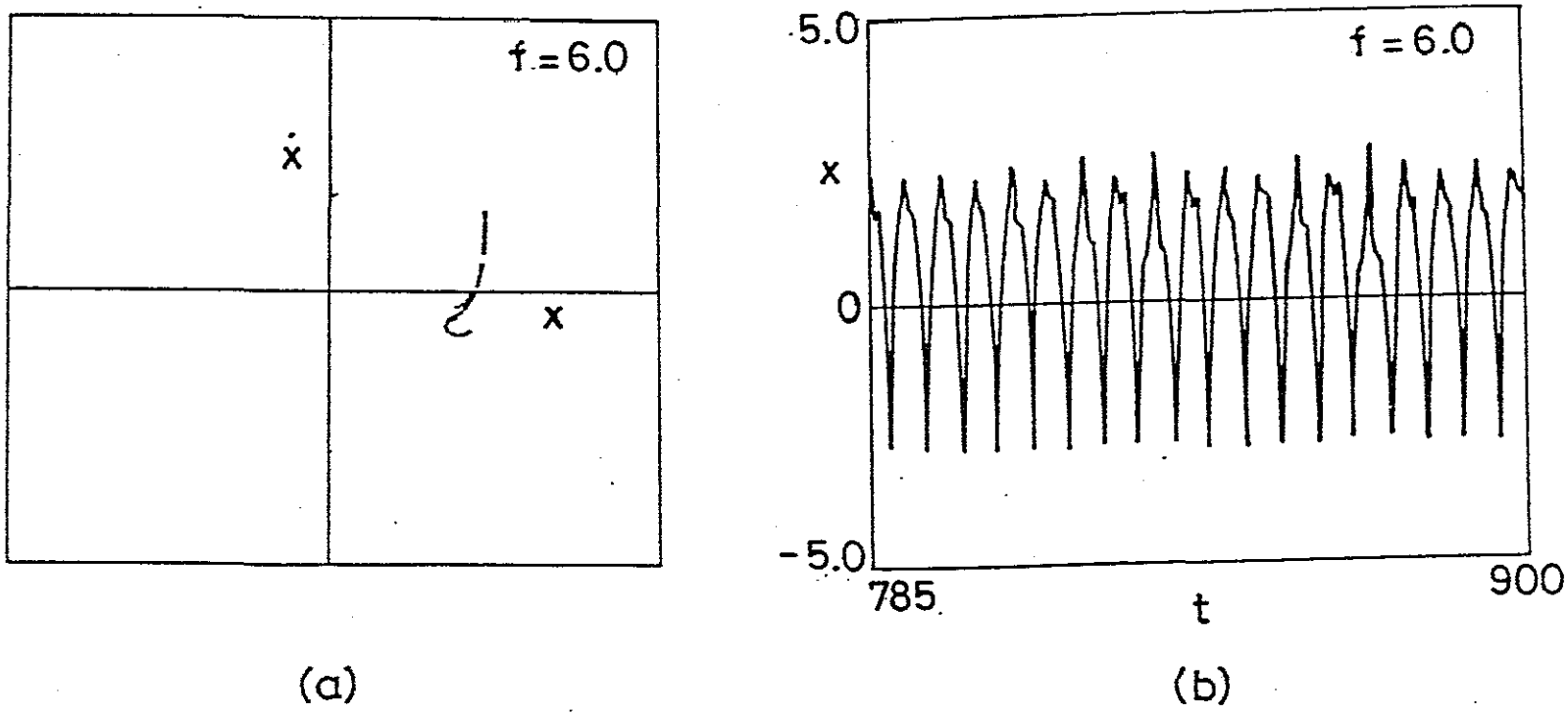

Figure 3.2 Chaotic attractor obtained via period-doubling in a symmetric system [Initial condition (1.0, 1.0)] (a) Poincare map; (b) Response

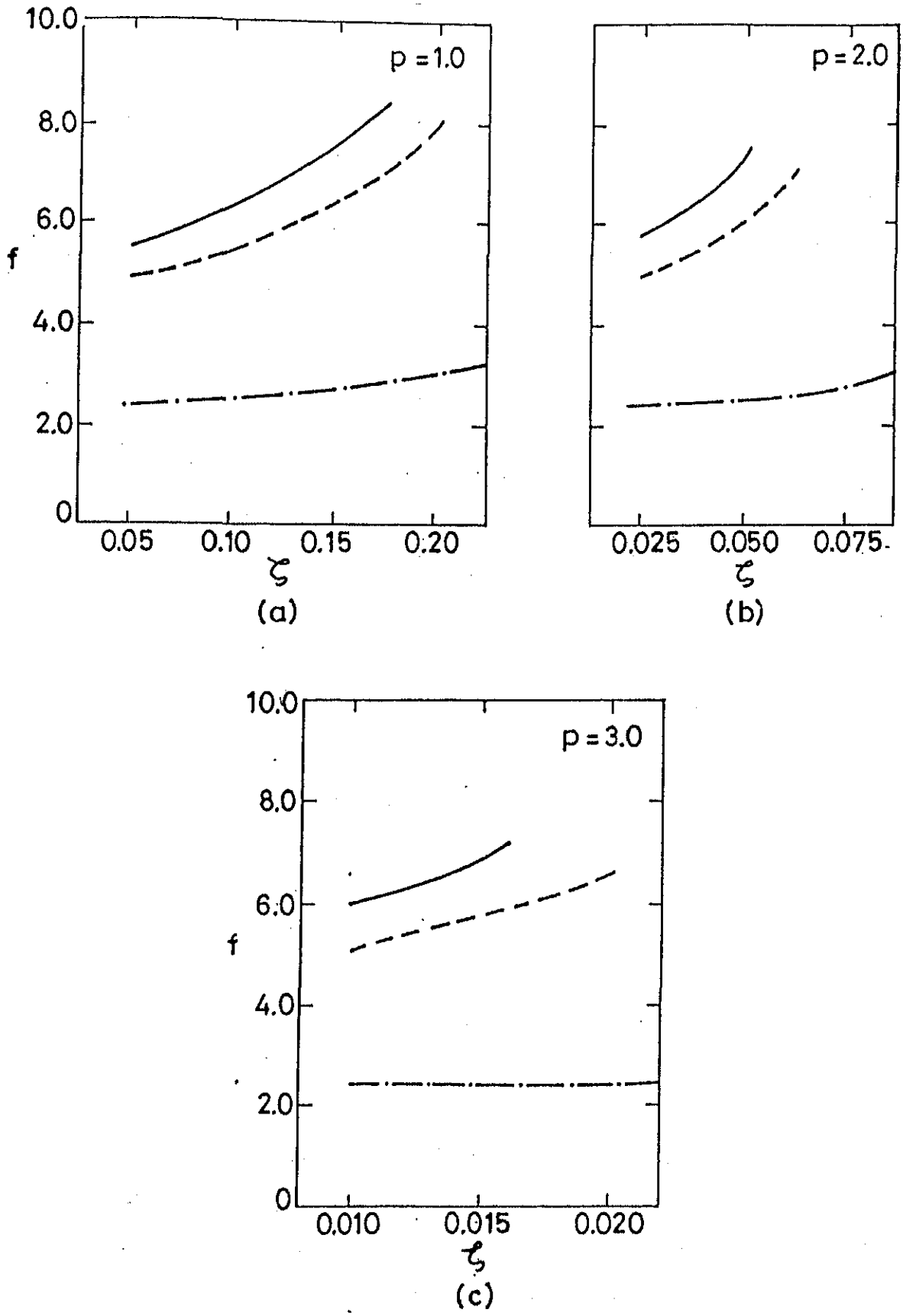

Figure 3.3 Effect of p and ζ on the critical forcing amplitude required for symmetry-breaking and period-doubling (a) p=1.0; (b) p=2.0; (c) p=3.0; Symmetry-breaking -·-; Period 2 ------; Period 4 ———;

for the suppression of period-doubling cascades (and eventual route to chaos) decreases with increasing p. The designer of isolation systems can suitably choose p and ζ to eliminate chaos.

3.3.2 Intermittency route to chaos with symmetric nonlinearity

In the present section, another route to chaos without period-doubling known as intermittency will be illustrated for p=2, through the numerical results obtained by integrating equation (3.1). This chaotic response is seen to be associated with a transition from a period 3 orbit to a period 1 orbit. Detailed mathematical investigations of chaos arising out of period 3 solution has been presented by Li and Yorke for one-dimensional maps [117]. The intermittency transition has been introduced by Pomeau et. al based on the numerical simulation of Lorenz system [118]. Since then, numerous papers have appeared introducing various types of intermittency transitions to chaos [43-46, 119].

The transition from a period 3 orbit to a period 1 orbit via a chaotic zone has been observed in a Duffing's oscillator with linear damping [53, 70] and has been called the sharp transition to chaos in reference [70], where a detailed model is given based on the 1/3 and 7/3 subharmonics. Both Type I and Type III intermittency routes have been observed in Duffing-type oscillators [68]. Detailed literature on the renormalisation procedures in intermittency is available and incidentally this happens to be the only route where exact renormalisation is possible [46]. Even in the logistic map, beyond the critical value r_c (of the Feigenbaum period-doubling route), period three windows

occur which either go to chaos through period-doubling or through Type I intermittency [45]. It is interesting to point out that such a period three orbit and subsequent period-doubling route have also been observed in Duffing's equation [62, 67]. The numerical results of driven dissipative oscillators thus resemble the logistic map more readily than the circle map [64].

Using the same values of the parameter given in section 3.3.1 (i.e., ω= 1.0, ζ= 0.025, p=2.0) and increasing the value of f, a period 3 orbit is revealed whose Poincare map is shown in Figure 3.4a. With further increase in f, a prechaotic zone is obtained. The Poincare map of this zone consisting of three small line segments centered around the period 3 orbit is shown in Figure 3.4b. The Poincare map of the chaotic solution obtained with further increase in f is shown in Figure 3.4c. It can be seen from Figure 3.4d that further increase in the forcing results in a period 1 orbit. The chaotic response is essentially a transition from a period 3 orbit to a period 1 orbit. Thus, even the intermittency route to chaos also appears to be independent of the value of p.

3.3.3 Asymmetric isolation system

As mentioned earlier, the asymmetry of the isolation system reflected by the constant forcing term f_0 in equation (3.1) plays a major role on the onset of chaos. Results of section 3.3.1 indicate that for a symmetric system, the breaking of symmetry is essential for period-doubling. Further, the symmetry-breaking yields a dual solution and both the solutions go to chaos, through period-doubling, resulting in dual chaotic attractors [67]. When

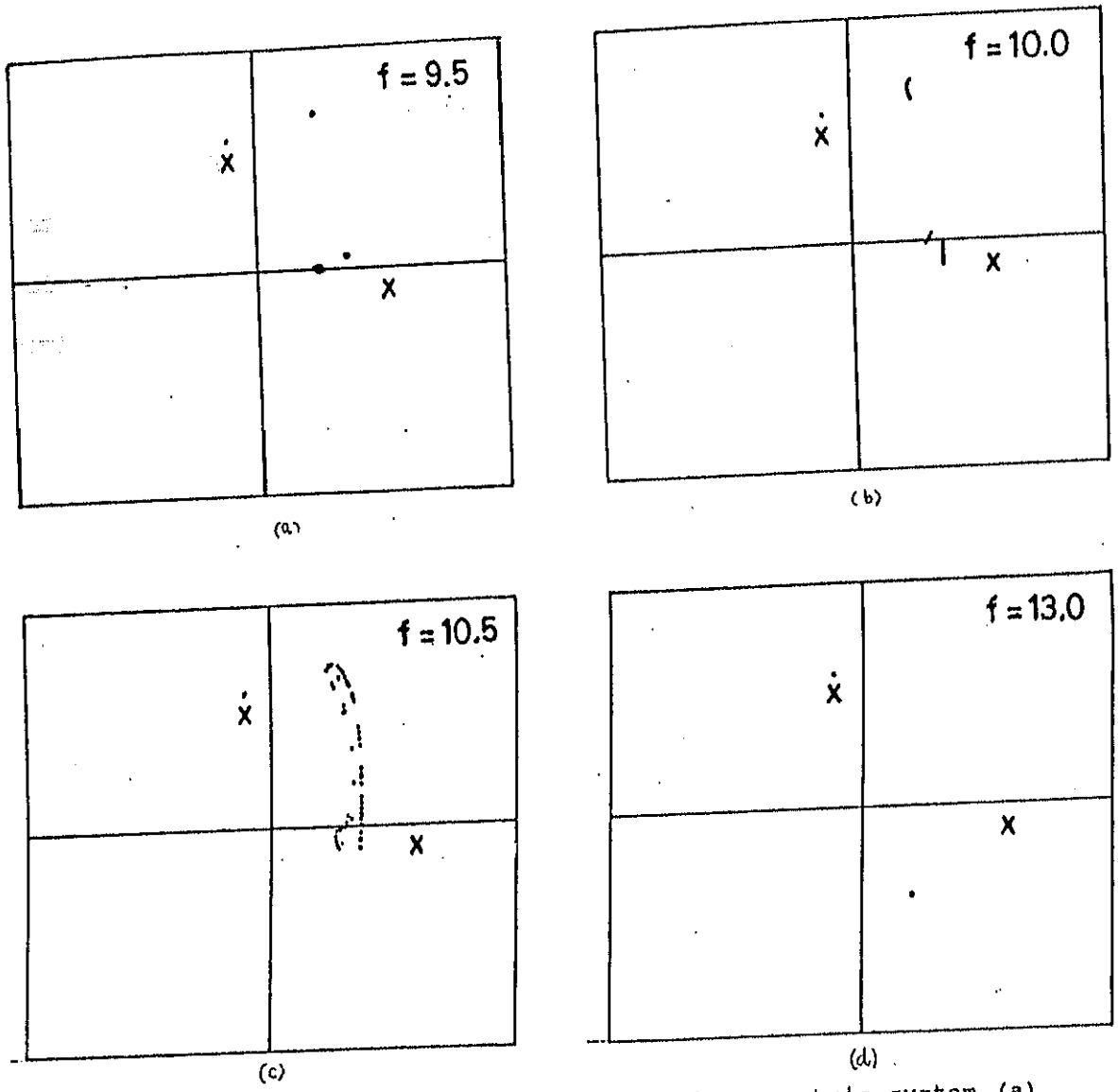

Figure 3.4 Intermittency route to chaos in symmetric system (a) Period 3; (b) Prechaos; (c) Chaos; (d) Period 1 [Initial condition (1.0, 1.0)]

asymmetry is inherent in the system, the symmetry is trivially broken or rather the symmetry-breaking bifurcation is not necessary for period-doubling. Dual solutions appear right from the beginning. Both the solutions undergo period-doubling bifurcations. But one of these routes gets excited for a very small value of the forcing amplitude f even for a slight degree of asymmetry (f_0).

The above scenario is seen to occur for p=1 [54]. In the present section it is shown that similar results are obtained even for p=2. Numerical simulation of equation (3.1) is carried out with the following parameter values: f_0= 0.03, ω= 1.0, ζ= 0.025, p=2.0. The Poincare map of the resulting period 2 orbit is shown in Figure 3.5. With increasing values of f, a chaotic attractor is obtained (via the period-doubling route) whose Poincare map and time response are shown, respectively, in Figures 3.6a and 3.6b. Comparision of the values of f required for the onset of the period 2 orbit in Figures 3.1d and 3.5 confirms that a little asymmetry drastically reduces the necessary forcing amplitude for beginning of one of the period-doubling routes to chaos. Similarly, from Figures 3.2b and 3.6b, it may be noted that the amplitude of the resulting chaotic attractor along this route is small. However, in this asymmetric case, there exists another period-doubling route to chaos for a different set of initial conditions. This route, shown in Figures 3.7a-3.7c, is relatively unaffected by the degree of asymmetry in the system. Along this route, the value of f required to cause the period-doubling and the amplitude of the chaotic attractor are more or less of the same magnitudes as those of the symmetric case. The intermittency

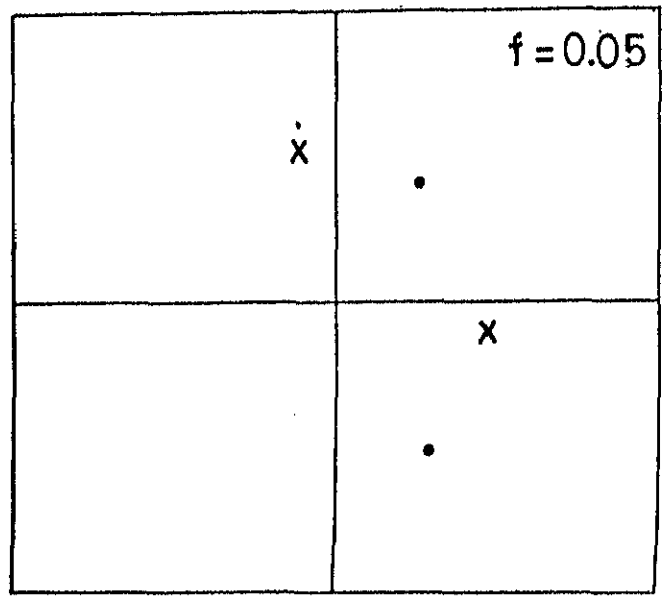

Figure 3.5 Period 2 solution in asymmetric system [Initial condition (0.1, 0.1)]

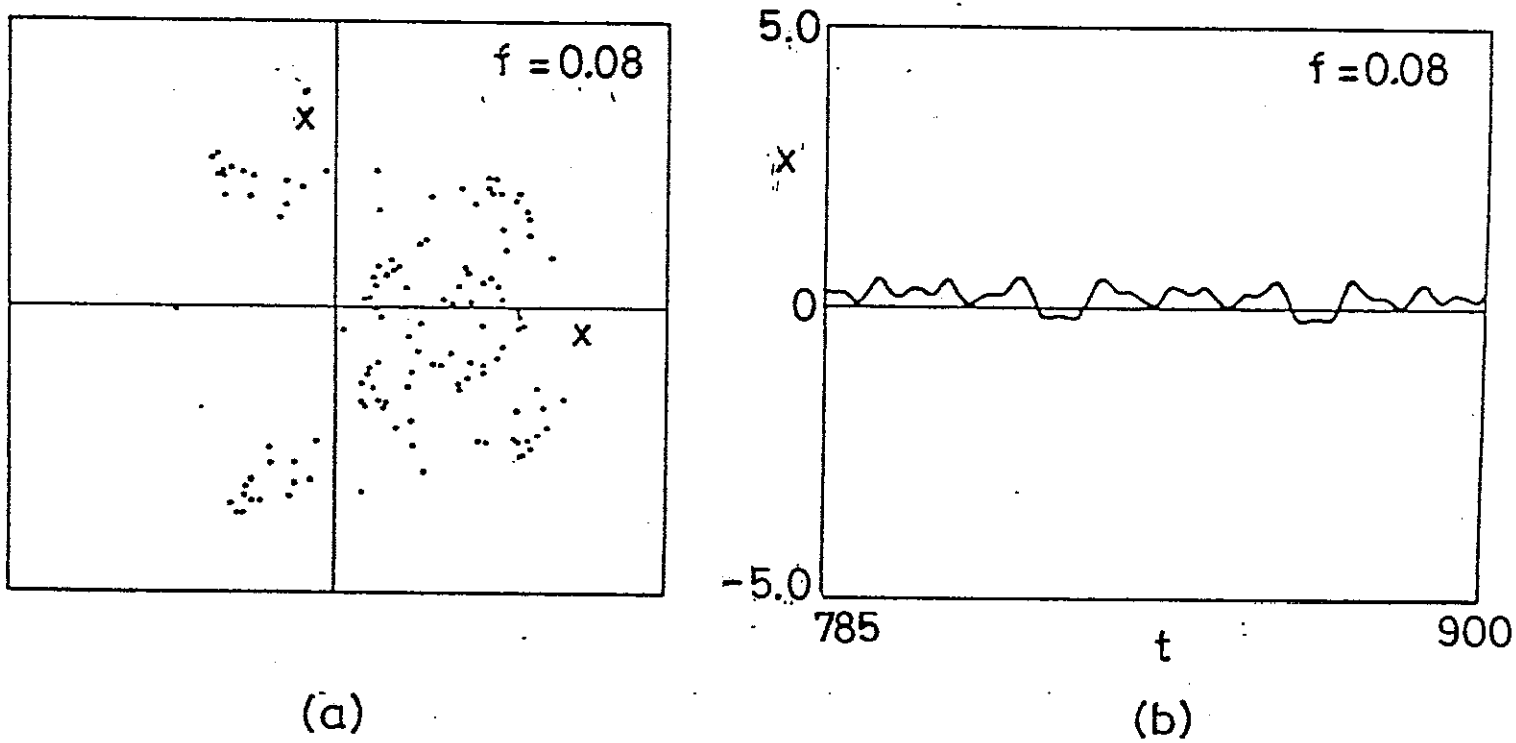

Figure 3.6 Chaotic attractor obtained via period-doubling in asymmetric system [Initial condition (0.1, 0.1)] (a) Poincare map; (b) Response

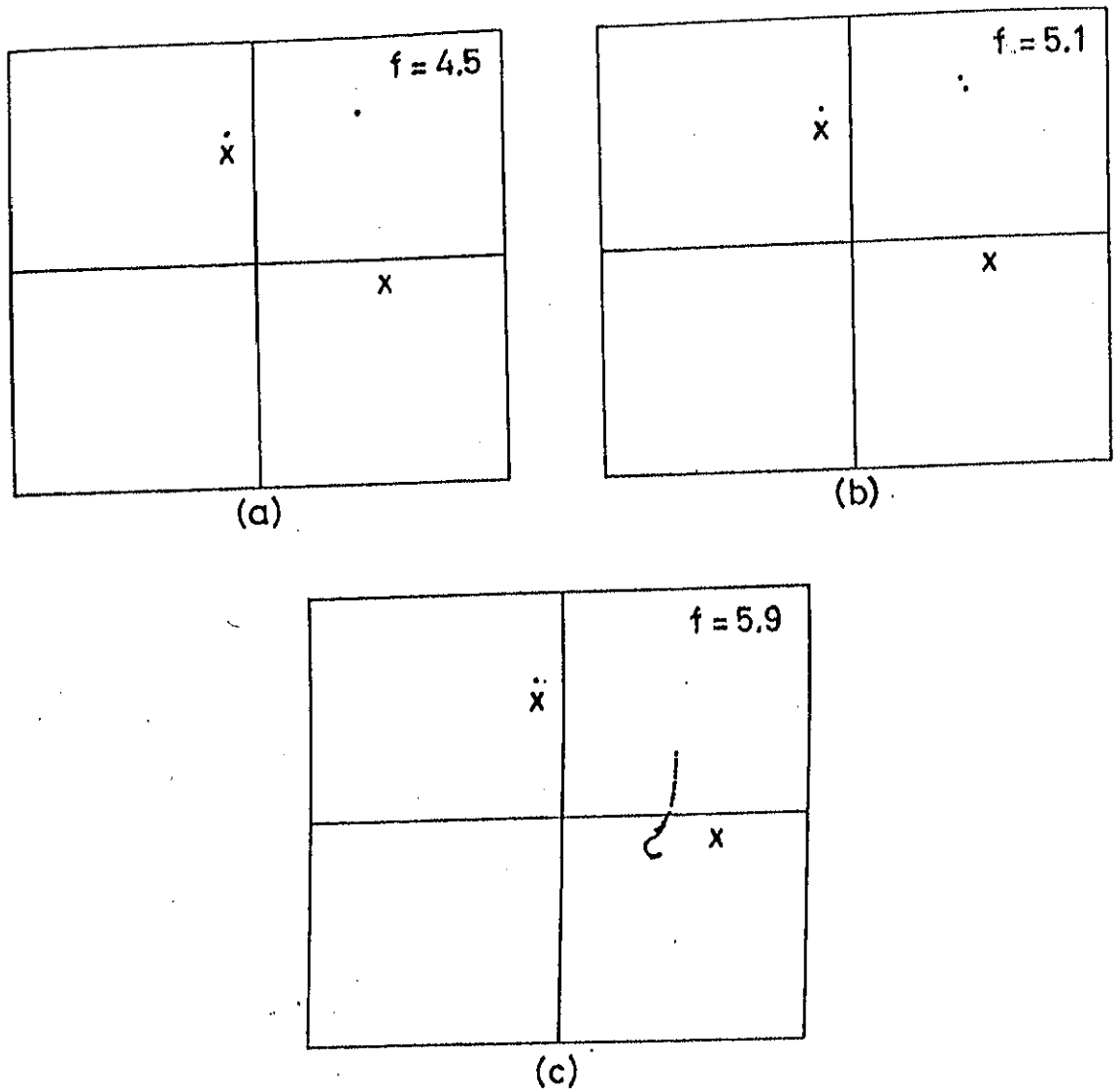

Figure 3.7 Period-doubling in asymmetric system [Initial condition (1.0, 1.0)] (a) Period 1; (b) Period 2;(c) Chaos

route to chaos, explained in section 3.3.2 for the symmetric case, also occurs in the asymmetric case and is shown in Figures 3.8a-3.8d.

3.3.4 Discussion

All the above scenarios presented for quadratic damping are found to exist irrespective of the value of the damping exponent p. Even combinations of various types of damping viz., quadratic and linear or linear and cubic etc., yield similar trends. It is seen that the bifurcation structure associated with the resonances of the system [62-69] is not changed by such nonlinear damping models so long as they are strictly dissipative. However, as reflected by the parametric study, the critical values of forcing at which various bifurcations occur depend on the values of p and ζ. Thus, a proper selection of the damping mechanism with suitable parameters provide the designer with wider choices for passive control of chaos. The fact that the bifurcation structure is not altered by the value of p also points to the possibility of extending the notion of equivalent linear damping to obtain the approximate criteria of chaos based on the stability of harmonic solution.

The results of only the primary resonance region are presented in this work. It is known that the secondary as well as subharmonic resonances exist in these systems and the period-doubling and intermittency routes recursively repeat themselves [62-70]. The results presented in this chapter are for a fixed frequency (ω=1.0) with varying values of f. However, as found earlier with linear damping [70], similar trends are

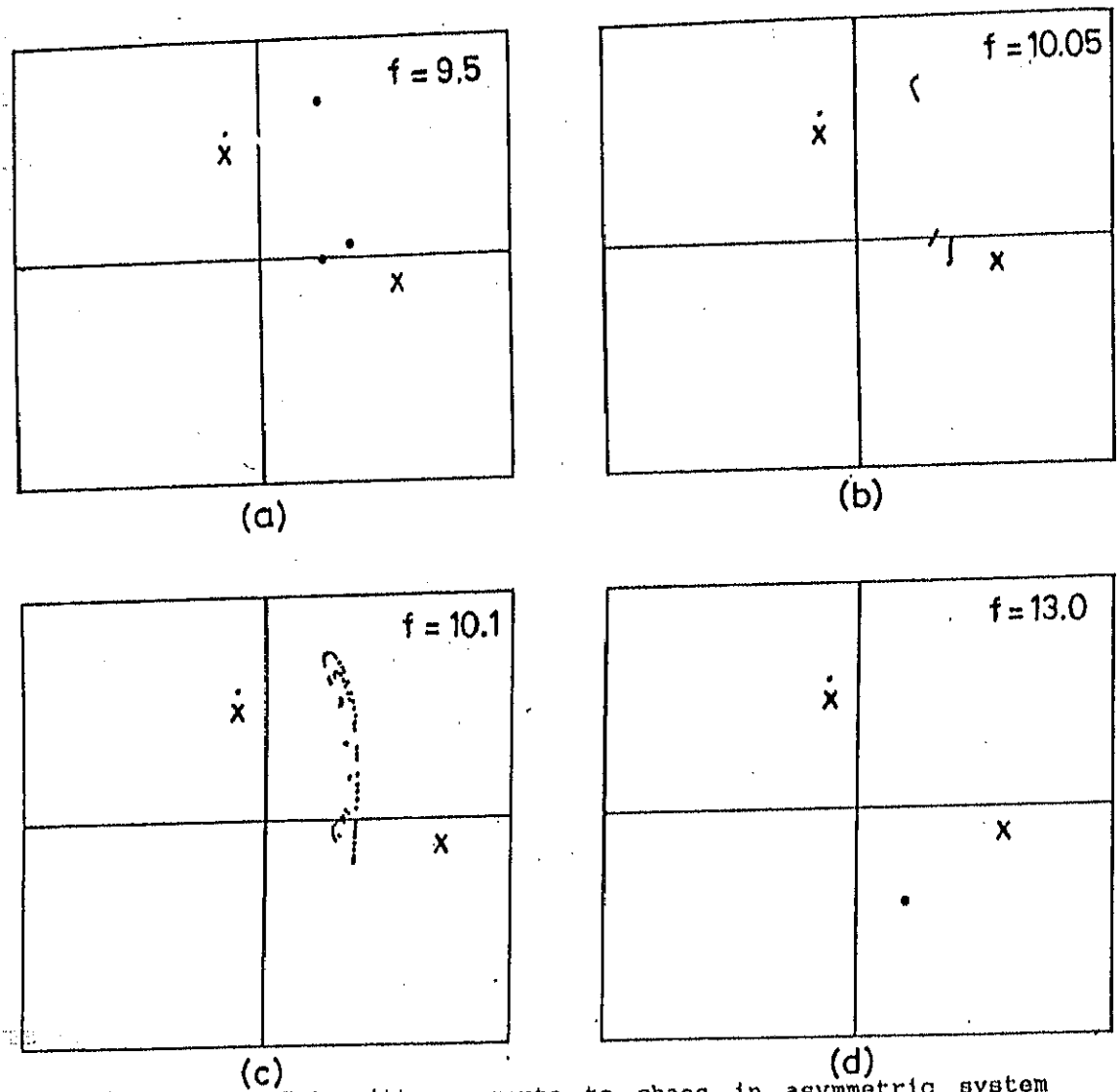

Figure 3.8 Intermittency route to chaos in asymmetric system [Initial condition (1.0, 1.0)] (a) Period 3; (b) Prechaos; (c) Chaos; (d) Period 1

observed for a fixed value of f with varying frequency even with nonlinear damping models.

3.4 Conclusions

Vibration isolators with nonlinearity in stiffness and damping terms are analysed under harmonic excitations. It is shown that both the period-doubling and intermittency routes to chaos occur for all values of p, thus preserving the bifurcation structure of a linearly damped, Duffing's oscillator. A parametric study is reported to indicate the effect of damping on the symmetry-breaking and period-doubling. It is pointed out that asymmetry inherent or arising out of gravity effects in an isolation system plays a major role on the onset of chaos. It is shown that nonlinear damping, just like linear damping, can also be effectively used for controlling chaos.

CHAPTER 4

HARMONIC RESPONSE OF HARD DUFFING-TYPE VIBRATION ISOLATOR WITH COMBINED COULOMB AND VISCOUS DAMPING

4.1 Introduction

In the present chapter, the steady-state, harmonic response of a vibration isolation system with a cubic, hard nonlinear restoring force and combined Coulomb and viscous damping is presented. The results have been obtained by using the method of harmonic balance. It has been assumed that the motion is continuous without any stop. Both force and base excitation models are presented.

While analysing the steady-state response of a viscously damped, soft Duffing-type system by using the method of harmonic balance, an anomalous jump in addition to the standard one has been observed [72-80]. The importance of this anomalous jump in understanding the so-called symmetry-breaking phenomenon in soft systems has been discussed in references [75-77]. It is interesting to note that a similar anomalous jump has been observed in the present work while analysing the steady-state response of a base excited hard, Duffing-type system with Coulomb damping. A linear stability analysis following the method suggested in reference [111] is carried out to ascertain the status of this additional jump response. Also some analytical criteria for merger of the normal jump with the anomalous one are derived. The effect of dissipation on this anomalous jump has been studied in detail. The existence of an anomalous jump in the

response obtained by the method of harmonic balance, is confirmed by direct numerical integration. However, unlike in the case of a soft system, this anomalous jump seems to have no bearing on the symmetry-breaking and subsequent period-doubling route to chaos.

The transmissibility indices have been plotted for relevant parameter values to study the performance characteristics. However, additional features like the effects of negative damping and response with stops have not been addressed to in this thesis. The results of this work extend those obtained previously by Den Hartog and Ruzicka for a linear spring and may thus enhance the scope of the design of vibration isolation systems.

4.2 Theoretical Analysis

4.2.1 Isolation system with base excitation

Referring to Figure 4.1, let a rigid mass M be separated from a harmonically moving base through an isolator consisting of a symmetric, nonlinear spring and combined Coulomb and viscous damper. The equation of motion for the mass can be written as

$$M\,\delta'' + C\,\delta' + C_f\,\mathrm{sgn}(\delta')\, + K\,\delta^3 = -M\,y'' = My_0\,\omega^2\cos\omega t \qquad (4.1)$$

where C and C_f are the viscous and Coulomb damping coefficients, respectively; $\delta = (x-y)$ is the relative displacement of the body to be isolated, and the prime denotes differentiation with respect to time t.

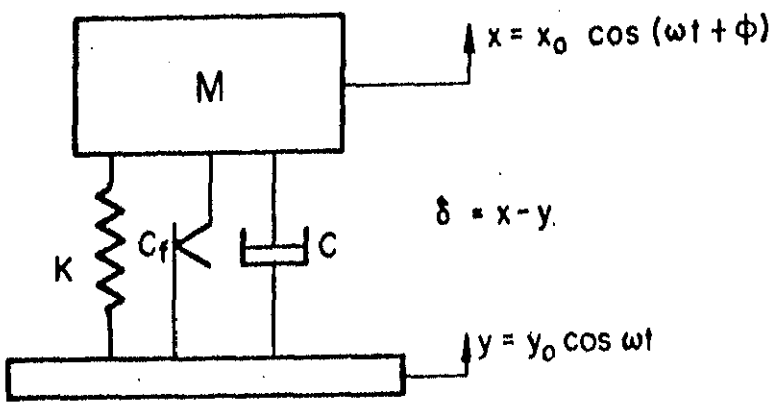

Figure 4.1 Vibration isolation system with combined Coulomb and viscous damper and a cubic nonlinear spring subjected to base excitation

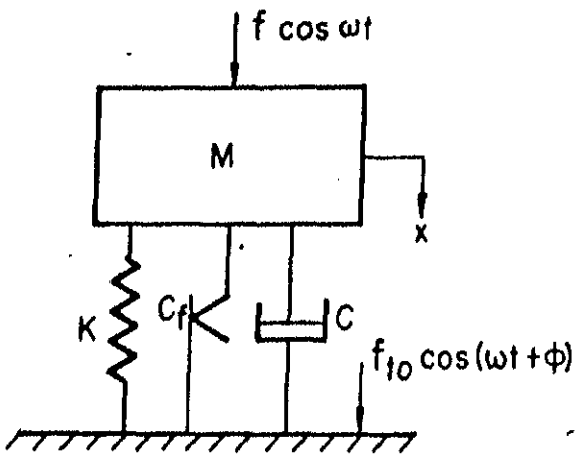

Figure 4.2 Vibration isolation system with combined Coulomb and viscous damper and a cubic nonlinear spring subjected to force excitation

Defining the following non-dimensional parameters:

$$\tau = \omega_0 \, t, \quad \Omega = \omega / \omega_0,$$

$$\Delta = \delta / Y_0 \, , \quad \dot{\Delta} = \delta' / (Y_0 \, \omega_0), \quad \ddot{\Delta} = \delta'' / (Y_0 \, \omega_0^2), \quad \zeta = C/(2M\omega_0),$$

$$\zeta_f = C_f/(2MY_0\omega_0^2) \text{ with } \omega_0 = [\, K \, Y_0^{\,2} \,]^{1/2} / \, M^{1/2} \text{ and}$$

substituting them in equation (4.1), one obtains,

$$\ddot{\Delta} + 2 \, \zeta \, \dot{\Delta} + 2 \, \zeta_f \, \mathrm{sgn}(\dot{\Delta}) + \Delta^3 = \Omega^2 \cos \Omega\tau \qquad (4.2)$$

where the dot denotes differentiation with respect to non-dimensional time τ.

Assuming the steady state solution of equation (4.2) to be given by $\Delta(\tau) = \Delta_1 \cos (\Omega\tau+\phi)$ and using the method of harmonic balance, the following equations are obtained:

$$-\Delta_1\Omega^2 + R_1 = \Omega^2 \cos \phi \qquad (4.3a)$$

and $$S_1 = \Omega^2 \sin \phi \qquad (4.3b)$$

where $$R_1 = \alpha \, \Delta_1^{\,3}, \qquad (4.4a)$$

$$S_1 = -(2\zeta\Delta_1\Omega + 2 \, \zeta_f \, \beta) \qquad (4.4b)$$

with $\alpha = 3/4$ and $\beta = 4/\pi$

Eliminating ϕ from equations (4.3a) and (4.3b), one can write the amplitude equation as

$$\alpha^2 \, \Delta_1^{\,6} - 2 \, \alpha \, \Omega^2\Delta_1^{\,4} + (\Omega^4 + 4 \, \zeta^2\Omega^2)\Delta_1^{\,2} + 8\beta\zeta\zeta_f\Omega\Delta_1 + (4\beta^2 \, \zeta_f^{\,2} - \Omega^4) = 0. \qquad (4.5)$$

In the absence of viscous damping (i.e.,with ζ=0), equation (4.5) reduces to

$$\alpha^2 \Delta_1^6 - 2 \alpha \Omega^2 \Delta_1^4 + \Omega^4 \Delta_1^2 + (4\beta^2 \zeta_f^2 - \Omega^4) = 0. \qquad (4.6)$$

Some simple analytical criteria are derived in the Appendix C for the existence of repeated roots of equation (4.6). The significance of the repeated roots of equation (4.6) will be clear later on.

One can observe that if the constant term in equation (4.5) (same as that in equation (4.6)) is equated to zero, then one root of Δ_1 becomes zero implying no relative movement. Thus, the well-known break-loose frequency (Ω_b) can be obtained by equating this constant term to zero as:

$$4 \beta^2 \zeta_f^2 - \Omega_b^4 = 0 \qquad (4.7)$$

$$\text{i.e, } \Omega_b = (2 \beta \zeta_f)^{1/2} = (8 \zeta_f/\pi)^{1/2} . \qquad (4.8)$$

When the excitation frequency is below the break-loose frquency, the damper gets locked and the relative motion does not take place (i.e., $\delta \equiv 0$). Hence, the present approximate analysis based on continuous relative motion is not valid below the break-loose frequency.

Finally, in the absence of Coulomb damping (i.e., with ζ_f =0), equation (4.5) reduces to

$$\alpha^2 \Delta_1^6 - 2 \alpha \Omega^2 \Delta_1^4 + (\Omega^4 + 4 \zeta^2 \Omega^2) \Delta_1^2 - \Omega^4 = 0. \qquad (4.9)$$

Equation (4.9) is a cubic equation in Δ_1^2 which is nothing but the well-known solution of a viscously damped Duffing's oscillator.It may be noted, that the method of equivalent linearization [110] gives the same results as obtained above with the equivalent stiffness and viscous damping parameters defined by

$$K_e = \alpha \Delta_1^2$$

$$\text{and} \quad C_e = 2\zeta + 2\zeta_f \beta/(\Delta_1 \Omega). \tag{4.10}$$

The absolute displacement transmissibility (T_d) is defined as the ratio of the maximum displacement of the mass to that of the base motion. It can be shown that

$$T_d = x_0/y_0 = [1 + \Delta_1^2 + 2\,\Delta_1 \cos\phi]^{1/2}. \tag{4.11}$$

where Δ_1 is given by equation (4.5). Substituting for $\cos\phi$ from equation (4.3a) in equation (4.11) one can obtain

$$T_d = [\ (\Omega^2 + 2\alpha\Delta_1^4 - \Delta_1^2\,\Omega^2\ )/(\Omega^2)\ ]^{1/2}. \tag{4.12}$$

Alternatively, following the linear vibration theory, one can write [3]

$$T_d = [K_e^2 + C_e^2\,\Omega^2\ ]^{1/2} \ / \ [(K_e - \Omega^2)^2 + C_e^2\,\Omega^2]^{1/2}. \tag{4.13}$$

Substitution for K_e and C_e from equations (4.10) in the above equation results in

$$T_d = [t_1 / t_2]^{1/2} \tag{4.14}$$

where $t_1 = \alpha^2 \Delta_1^6 + 4 \zeta^2\Omega^2\Delta_1^2 + 8\beta\zeta\zeta_f\Omega\Delta_1 + 4\beta^2 \zeta_f^2$

and $t_2 = \alpha^2 \Delta_1^6 - 2 \alpha \Omega^2\Delta_1^4 + (\Omega^4 + 4 \zeta^2\Omega^2)\Delta_1^2 + 8\beta\zeta\zeta_f\Omega\Delta_1 + 4\beta^2 \zeta_f^2$.

With the help of equation (4.5), it is easy to verify that equations (4.14) and (4.12) are identical.

4.2.1.1 Stability analysis

It can be seen from equation (4.1) that the derivative of the damping force with respect to δ' does not exist at $\delta' = 0$. Hence, in place of the usual variational technique, a modified procedure for the stability analysis as suggested in reference [111] is followed. Using this approach, the stability of the steady state response is predicted by the stability of the equilibrium points of the following set of associated autonomous equations:

$$\dot{\phi} = (\alpha\Delta_1^3 - \Omega^2 \cos \phi - \Delta_1 \Omega^2)/(2\Delta_1\Omega)$$

and (4.15)

$$\dot{\Delta}_1 = -(\Omega^2 \sin \phi + 2\zeta\Delta_1\Omega + 2\zeta_f\beta)/(2\Omega).$$

The stability of the equilibrium points of equations (4.15) can be studied by considering the equations

$$\dot{\eta} = J \eta \tag{4.16}$$

where $\eta=(\phi,\Delta_1)^T$ and J is the Jacobian matrix whose eigen values,

when evaluated at the equilibrium points of equations (4.15), provide the requisite information on the stability of the solutions obtained [42]. It is easy to see that the matrix J is given by

$$J = \begin{vmatrix} J_1 & J_2 \\ J_3 & J_4 \end{vmatrix} \tag{4.17}$$

where $J_1 = \Omega \sin \phi/(2\Delta_1)$,

$J_2 = \alpha\ \Delta_1/\Omega + \Omega \cos \phi/(2\ \Delta_1^2)$,

$J_3 = -\Omega \cos \phi\ /2$ (4.18)

and $J_4 = -\zeta$.

4.2.2 Isolation system with force excitation

Referring to Figure 4.2, when the rigid mass M, acted upon by a harmonic force, is seperated by the isolator from an immovable foundation, its equation of motion can be written as

$$M\ x'' + C\ x' + C_f\ Sgn(x') + Kx^3 = f \cos \omega t. \tag{4.19}$$

Defining the following non-dimensional parameters:

$\tau = \omega_0\ t$, $\Omega = \omega/\omega_0$,

$X = x/x_0$, $\dot{X} = x'/(x_0\omega_0)$, $\ddot{X} = x''/(x_0\ \omega_0^2)$, $\zeta = C/(2M\omega_0)$,

$\zeta_f = C_f/(2Mx_0\omega_0^2)$ with $x_0 = (f/K)^{1/3}$, $\omega_0 = [K\ x_0^2\ ]^{1/2}/\ M^{1/2}$

and using them in equation (4.19), one obtains,

$$\ddot{X}\ + 2\ \zeta\ \dot{X} + 2\ \zeta_f\ sgn(\dot{X}) + X^3 = \cos \Omega\tau\ . \tag{4.20}$$

Assuming the steady state harmonic response to be given by $X(\tau) = X_1 \cos\ (\Omega\tau+\phi)$, the response equations for X can be obtained as

$$-X_1\Omega^2 + R_2 = \cos\phi \tag{4.21a}$$

and $$S_2 = \sin\phi \tag{4.21b}$$

where $$R_2 = \alpha X_1^3 \tag{4.22a}$$

$$S_2 = -(2\zeta X_1\Omega + 2\zeta_f\beta) \tag{4.22b}$$

with $\alpha = 3/4$ and $\beta = 4/\pi$.

Now, using equations (4.21) and (4.22), the amplitude equation is finally obtained as

$$\alpha^2 X_1^6 - 2\alpha\Omega^2 X_1^4 + (\Omega^4 + 4\zeta^2\Omega^2)X_1^2 + 8\beta\zeta\zeta_f\Omega X_1 + (4\beta^2\zeta_f^2 - 1) = 0 . \tag{4.23}$$

In the absence of viscous damping (i.e.,with $\zeta=0$), equation (4.23) reduces to

$$\alpha^2 X_1^6 - 2\alpha\Omega^2 X_1^4 + \Omega^4 X_1^2 + (4\beta^2\zeta_f^2 - 1) = 0 . \tag{4.24}$$

Denoting the critical value of ζ_f at which the constant term in equations (4.23) and (4.24) goes to zero as $(\zeta_f)_c$, one can see that

$$4\beta^2(\zeta_f)_c^2 - 1 = 0 \tag{4.25}$$

$$\text{or, } (\zeta_f)_c = 1/(2\beta) = \pi/8 . \tag{4.26}$$

With $\zeta=(\zeta_f)_c$ one root of the amplitude equation goes to zero. As shown by Den Hartog [91] for the isolator with a linear spring and a Coulomb damper, equations (4.23) and (4.24) are not valid if ζ_f

$> (\zeta_f)_c$. Thus, the approximate solution obtained by the method of harmonic balance is valid for $\zeta_f < \pi/8$. The force transmissibility (T_f) is defined as the ratio of the amplitude of the force transmitted to the foundation to that of the exciting force and is given by

$$T_f = f_{t0} / f = [t_1/t_2]^{1/2} \qquad (4.27)$$

where $t_1 = \alpha^2 X_1^6 + 4 \zeta^2\Omega^2 X_1^2 + 8\beta\zeta\zeta_f\Omega X_1 + 4\beta^2 \zeta_f^2$

and $t_2 = \alpha^2 X_1^6 - 2 \alpha \Omega^2 X_1^4 + (\Omega^4 + 4 \zeta^2\Omega^2) X_1^2 + 8\beta\zeta\zeta_f\Omega X_1 + 4\beta^2 \zeta_f^2$.

Comparing equations (4.14) and (4.27) one can conclude that equation (4.27) is nothing but equation (4.14), when X_1 is substituted for Δ_1. The stability analysis of the steady state response is carried out in the same manner as followed for the base excitation model.

4.3 Results and Discussion

Performance characteristics of the isolation systems described in section 4.2 are presented through the transmissibility in dB (i.e., 20 $\log_{10} T_d$ or 20 $\log_{10} T_f$ as the case may be) versus frequency (Ω) plots for various values of ζ and ζ_f.

4.3.1 Base excitation

Case(i) In the absence of viscous damping (i.e. ζ=0):

The absolute displacement transmissibility (T_d) is given by

equation (4.14) where Δ_1 is evaluated from equation (4.6). A typical transmissibility versus frequency (T_d vs Ω) plot is shown in Figure 4.3. One can define all the parameters relevant to the present discussion with respect to this figure. As mentioned earlier, when the excitation frequency is below the break-loose frequency (Ω_b), the Coulomb damper gets locked and the transmissibility is maintained at unity. This portion is denoted as OA in Figure 4.3, with point A corresponding to the break-loose frequency Ω_b. The resonance branch of the usual Duffing jump is labelled DEF, the unstable branch as IG and the non-resonance branch as IH. The frequency corresponding to the point I is denoted as non-resonance critical frequency (Ω_n). It can be seen from Figure 4.3 that the stable resonance branch DEF extends towards infinity resembling the response of an undamped oscillator.

In the case of a viscously damped, soft Duffing oscillator with a high value of excitation, an anomalous response apart from the usual jump phenomenon has been reported [72-80]. It may be noted from Figure 4.3 that a similar peculiar behaviour is observed for the system under consideration when $\Omega > \Omega_b$. Just beyond the break-loose frequency, a small portion with two additional branches (labelled BC and AC in Figure 4.3) appear along with the resonance branch DEF. This portion with two branches BC and AC is denoted as the 'anomalous jump'. Let the frequency at which these two branches meet (at C in Figure 4.3) be denoted by Ω_a. The range of frequency over which this anomalous jump exists depends on the value of ζ_f.

At a given value of ζ_f, equation (4.6) has repeated roots

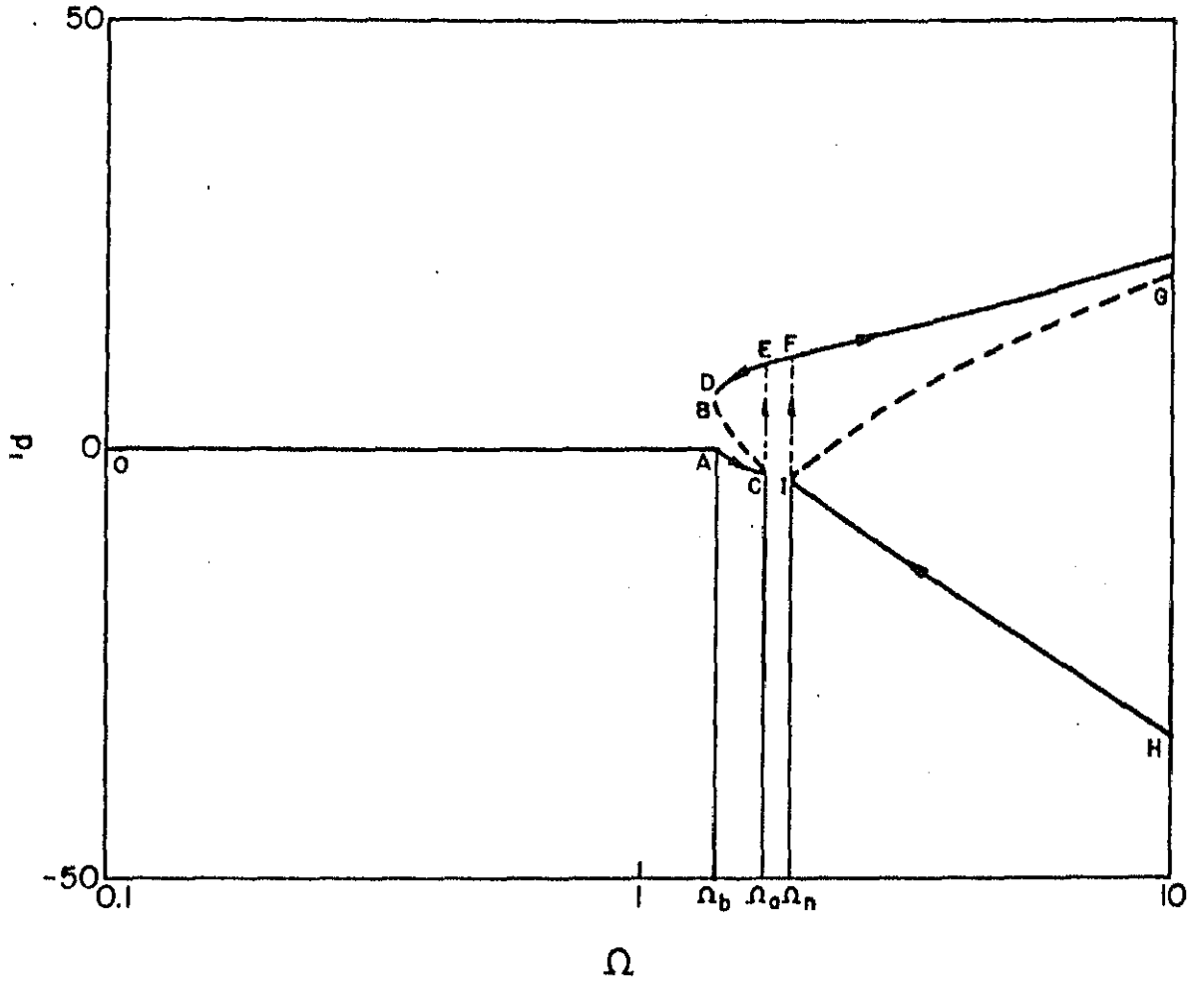

Figure 4.3 Typical plot of T_d (in dB) vs Ω . $\zeta = 0$ and $\zeta_f = 0.75$; ——— stable; ----- unstable;

when $\Omega = \Omega_a$ and $\Omega = \Omega_n$. It is of interest to examine the effect of ζ_f on the values of Ω_a and Ω_n. A procedure for obtaining the condition for repeated roots of equation (4.6) is explained in the Appendix C. Solving equation (C.6) one can obtain Ω_a and Ω_n for various values of ζ_f. These results along with the variation of Ω_b with respect to ζ_f (refer to equation (4.8)) are plotted in Figure 4.4. Upon increasing ζ_f, the range of frequency $(\Omega_a-\Omega_b)$ over which the anomalous jump exists also increases and $(\Omega_n-\Omega_a)$ decreases. At a critical damping value $\zeta_f=(\zeta_f)_m$ (indicated by the point M in Figure 4.4) Ω_n equals Ω_a and the anomalous jump coincides with the main jump. At this critical value $(\zeta_f)_m$ equation (C.6) has repeated roots . The expression for $(\zeta_f)_m$ is also derived in the Appendix C.

The nature of variation of the transmissibility with frequency as ζ_f increases is shown in Figures 4.5(a)-4.5(d). It may be noted from Figures 4.5(a) and 4.5(b) that with low values of ζ_f, the anomalous portion is very small. This is not surprising since the difference $(\Omega_a- \Omega_b)$ is very small with low values of ζ_f as can be verified from Figure 4.4. For $\zeta_f > (\zeta_f)_m$, the main branch of the usual jump opens up and merges with the anomalous jump as clearly seen in Figure 4.5(d).

Now referring again to Figure 4.3, with a low value of $\zeta_f < (\zeta_f)_m$, as the frequency is increased beyond Ω_b, the response takes the lower branch AC of the anomalous portion and at $\Omega=\Omega_a$ (i.e., at the point C) it jumps to the point E on the usual resonance branch DEF . On the otherhand, if the isolator is operating on the non-resonance branch IH, then with decreasing frequency the jump takes place from the non-resonance branch to the resonance branch

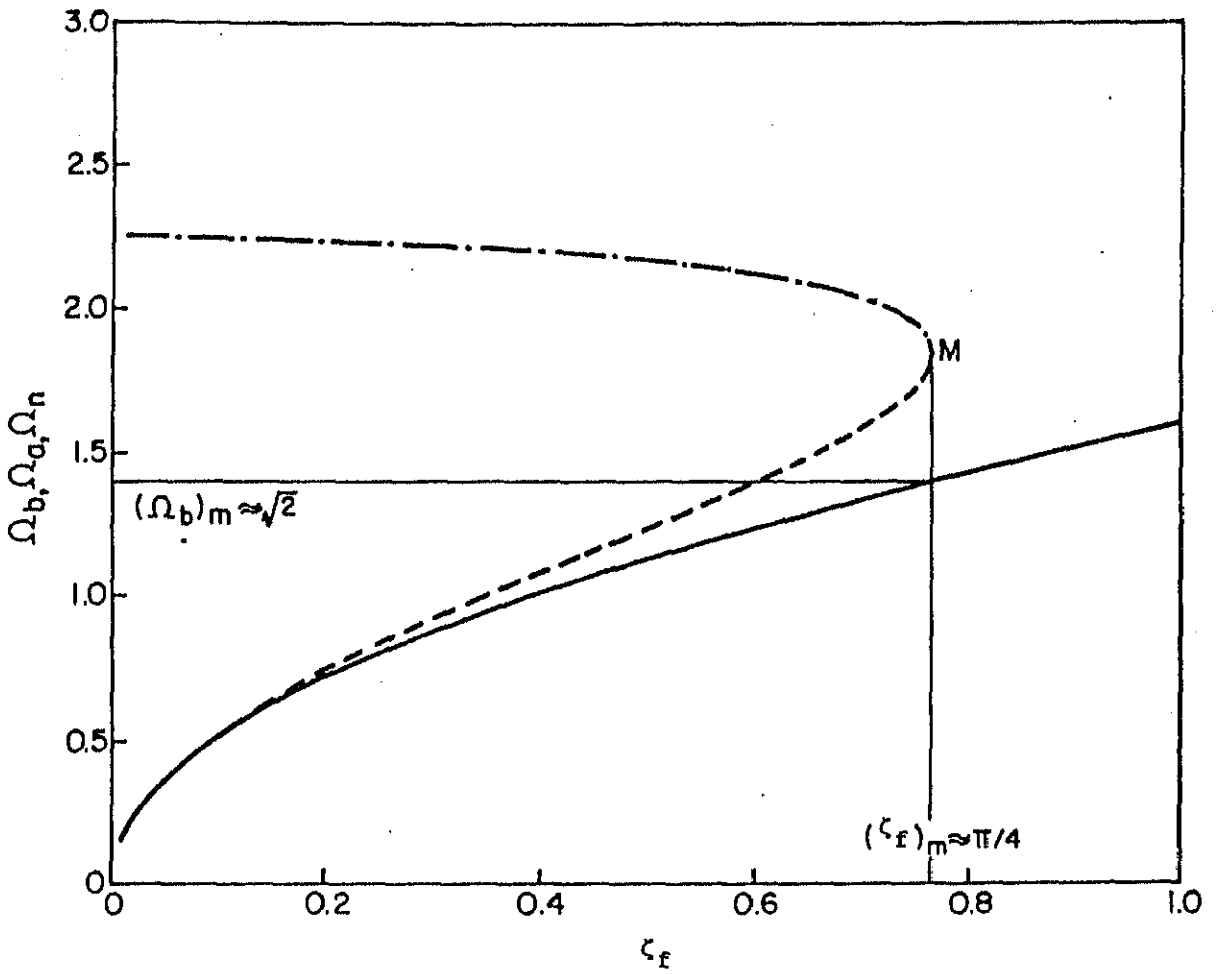

Figure 4.4 Variations of Ω_b, Ω_a and Ω_n with ζ_f in the absence of viscous damping (ζ=0). —— Ω_b; ---- Ω_a; -·-·- Ω_n;

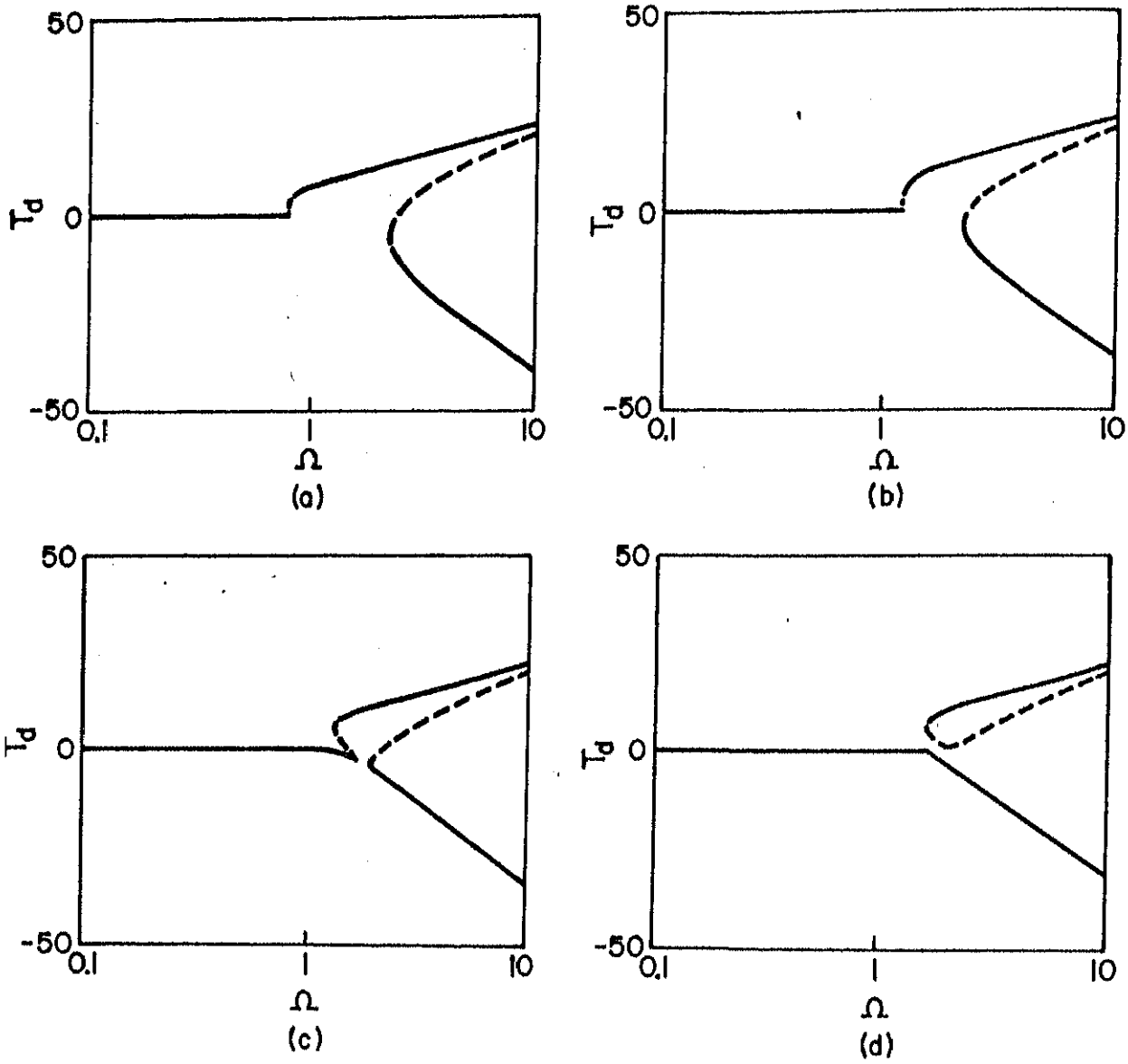

Figure 4.5 Variation of T_d with Ω. $\zeta = 0$ and (a) $\zeta_f = 0.25$; (b) $\zeta_f = 0.5$; (c) $\zeta_f = 0.75$; (d) $\zeta_f = 1.0$;

at $\Omega = \Omega_n$ i.e., from the point I to F, and the response follows the curve FED. The response again jumps back to the locked region at the point D.

It is known that in the case of a linear spring and a Coulomb damper [3], with a suitable choice of the break-loose frequency, (i.e., with a friction coefficient > $\pi/4$), one can maintain the transmissibility less than or equal to unity. Also the unbounded transmissibility at resonance can be avoided if the break-loose frequency is made atleast equal to 1 (i.e, with a friction coefficient > $\pi/8$). In the present case, by choosing $\zeta_f > (\zeta_f)_m$ as shown in Figure 4.5d, one can maintain the transmissibility to be equal to or less than unity over all frequencies as no jump occurs towards the resonant branch. It can be seen from the Appendix C (refer equations C.7 and C.8) that $(\zeta_f)_m \approx \pi/4$ and the corresponding break-loose frequency $(\Omega_b)_m \approx \sqrt{2}$.

The stability analysis of the anomalous jump portion (see Figure 4.3) is carried out in a manner detailed in section 4.2.2. It is found out that near the break-loose frequency with $\Omega_b < \Omega < \Omega_a$, the upper and lower branches i.e. AC and DE are either stable nodes or stable spirals and the middle branch (i.e.,BC) corresponds to unstable saddle points. Due to the transition from a stable node to a stable spiral near $\Omega=\Omega_b$, some interesting transient behaviours are expected.

Case(ii) Effect of viscous damping:

The effect of ζ_f on the anomalous jump in the presence of viscous damping can be seen in Figures 4.6-4.8. The break-loose frequency Ω_b is of course independent of ζ (see equation (4.8)).

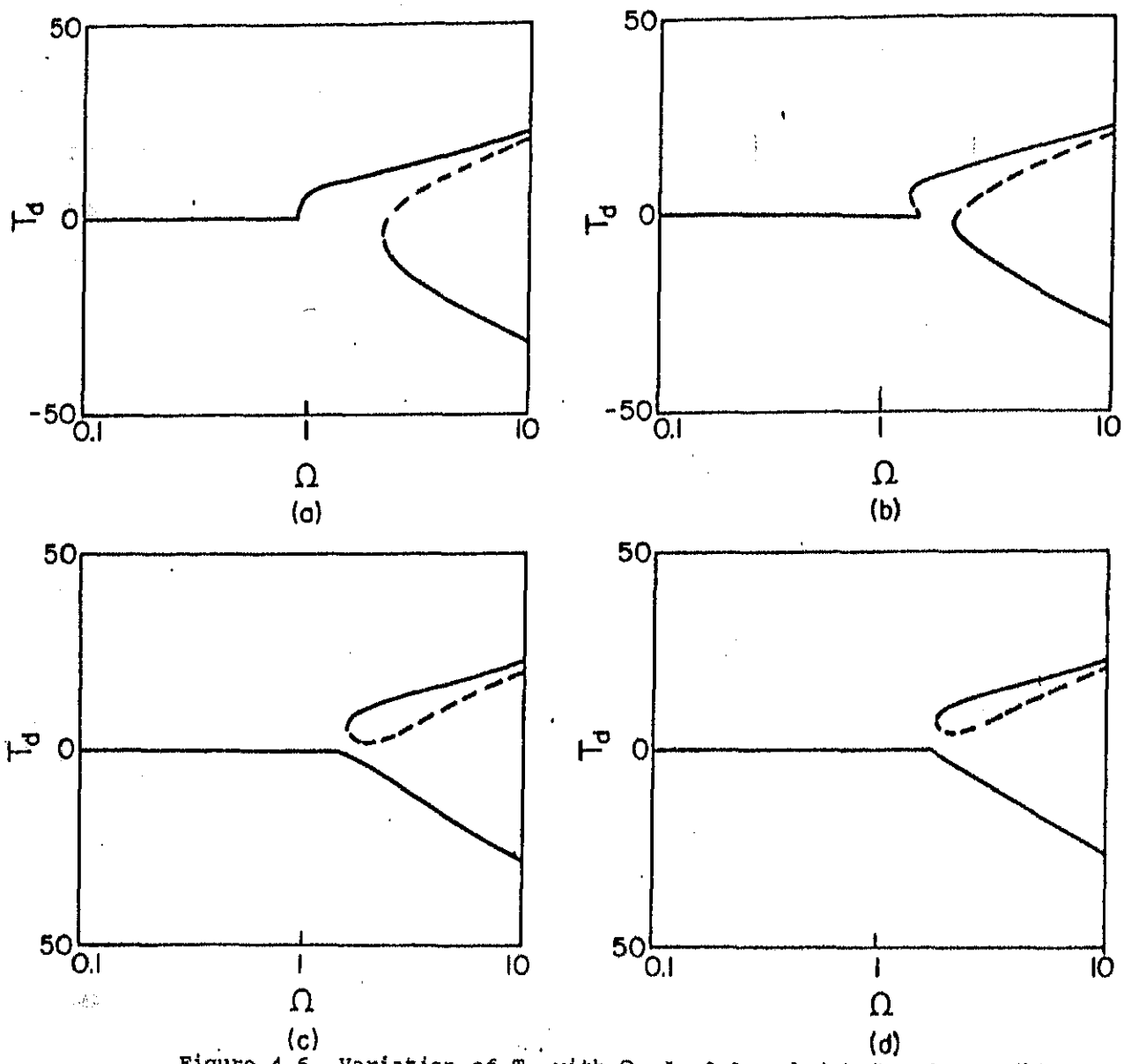

Figure 4.6 Variation of T_d with Ω, ζ =0.1 and (a) ζ_f =0.25; (b) ζ_f = 0.5; (c) ζ_f = 0.75; (d) ζ_f = 1.0;

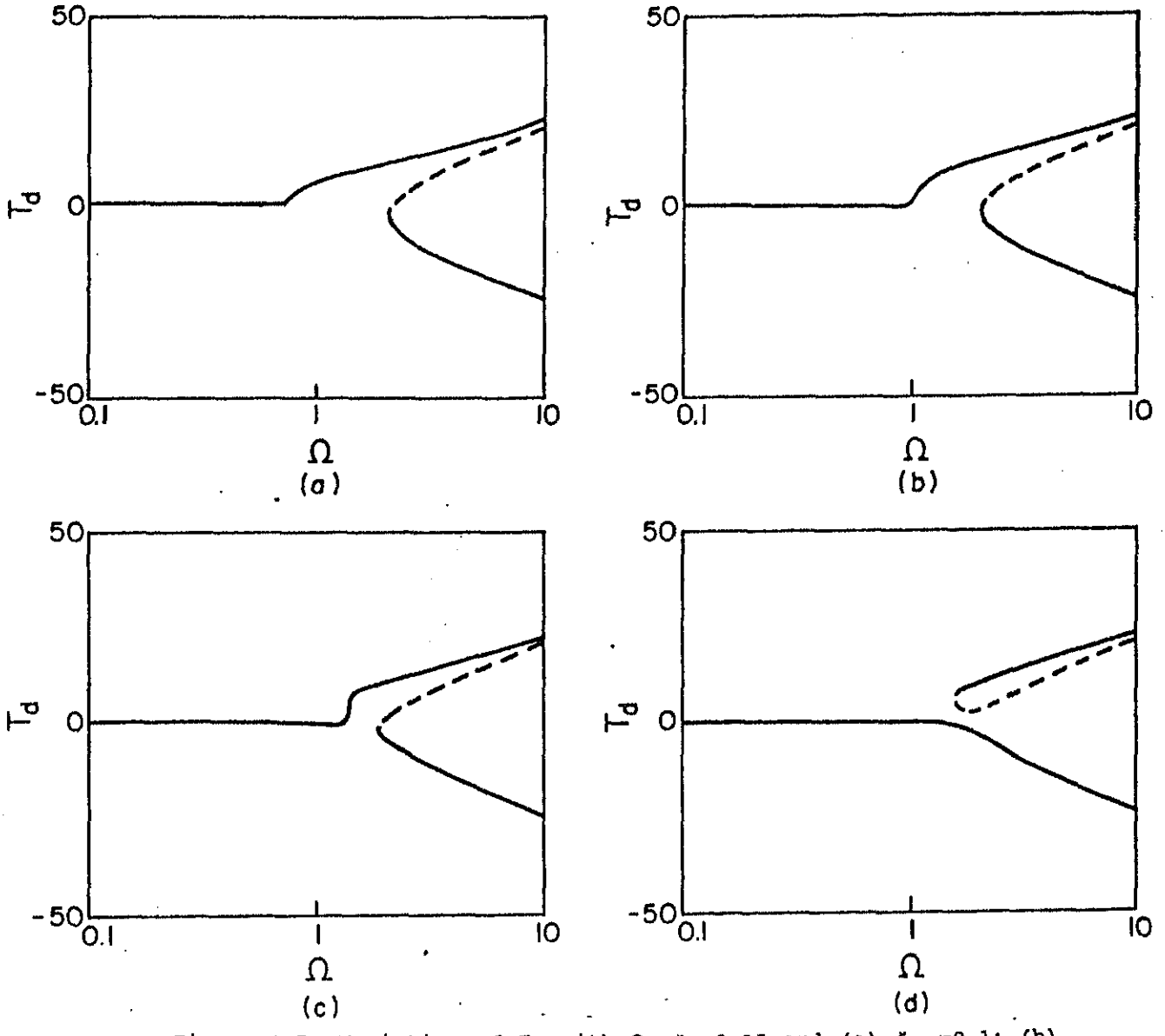

Figure 4.7 Variation of T_d with Ω. ζ= 0.25 and (a) ζ_f =0.1; (b) ζ_f = 0.2; (c) ζ_f = 0.3; (d) ζ_f = 0.4;

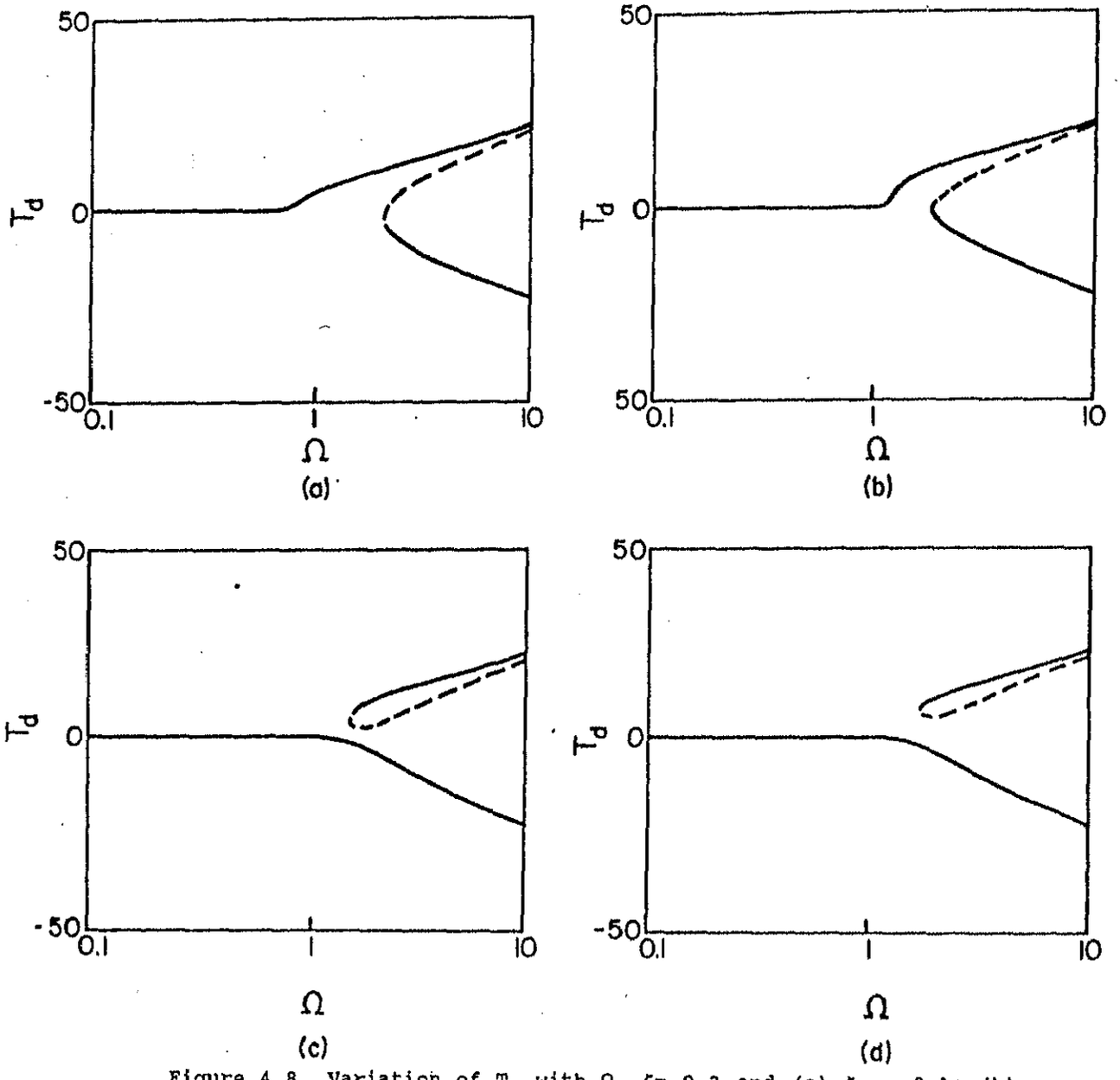

Figure 4.8 Variation of T_d with Ω. ζ= 0.3 and (a) ζ_f = 0.1; (b) ζ_f = 0.2; (c) ζ_f = 0.3; (d) ζ_f = 0.4;

But with $\zeta = 0$, the anomalous jump does not occur immediately after breaking loose. There exists a very small difference between the frequency corresponding to the point A and that for the points B and D of Figure 4.3. However, the difference is too small to be noticed e.g. in Figure 4.6(b). An increase in the viscous damping results in a reduction of the anomalous jump portion and may even eliminate it altogether as can be confirmed from Figures 4.6-4.8. Figure 4.9 shows the variations of Ω_b, Ω_a and Ω_n with ζ_f for a non-zero value of ζ. It may be noted that unlike in the case with $\zeta = 0$ (Figure 4.4), here the repeated roots of equation (4.5) signifying Ω_a and Ω_n can only be obtained through numerical computation.

Comparing Figures 4.4 and 4.9, one can observe that the critical value $(\zeta_f)_m$, where the main and anomalous jumps coincide, is decreased with the addition of viscous damping. The plot of $(\zeta_f)_m$ versus ζ is shown in Figure 4.10. An approximate linear variation is seen to take place. In this figure, ζ is restricted to less than 0.2 since for higher values of ζ it is found that the anomalous jump may be entirely absent (see Figures 4.7 and 4.8). However, the opening up of the usual jump still occurs as shown in Figures 4.7(d) and 4.8(c). Furthermore, it occurs at a lower value of ζ_f as ζ is increased. This implies that the break-loose frequency which depends only on ζ_f is also lowered and hence the range of frequency over which the transmissibility can be maintained less than unity is increased. However, just like in a linear isolator [3,22], the transmissibility at high frequencies increases with increase in ζ as can be observed by comparing corresponding diagrams in Figures 4.6-4.8. Thus suitable

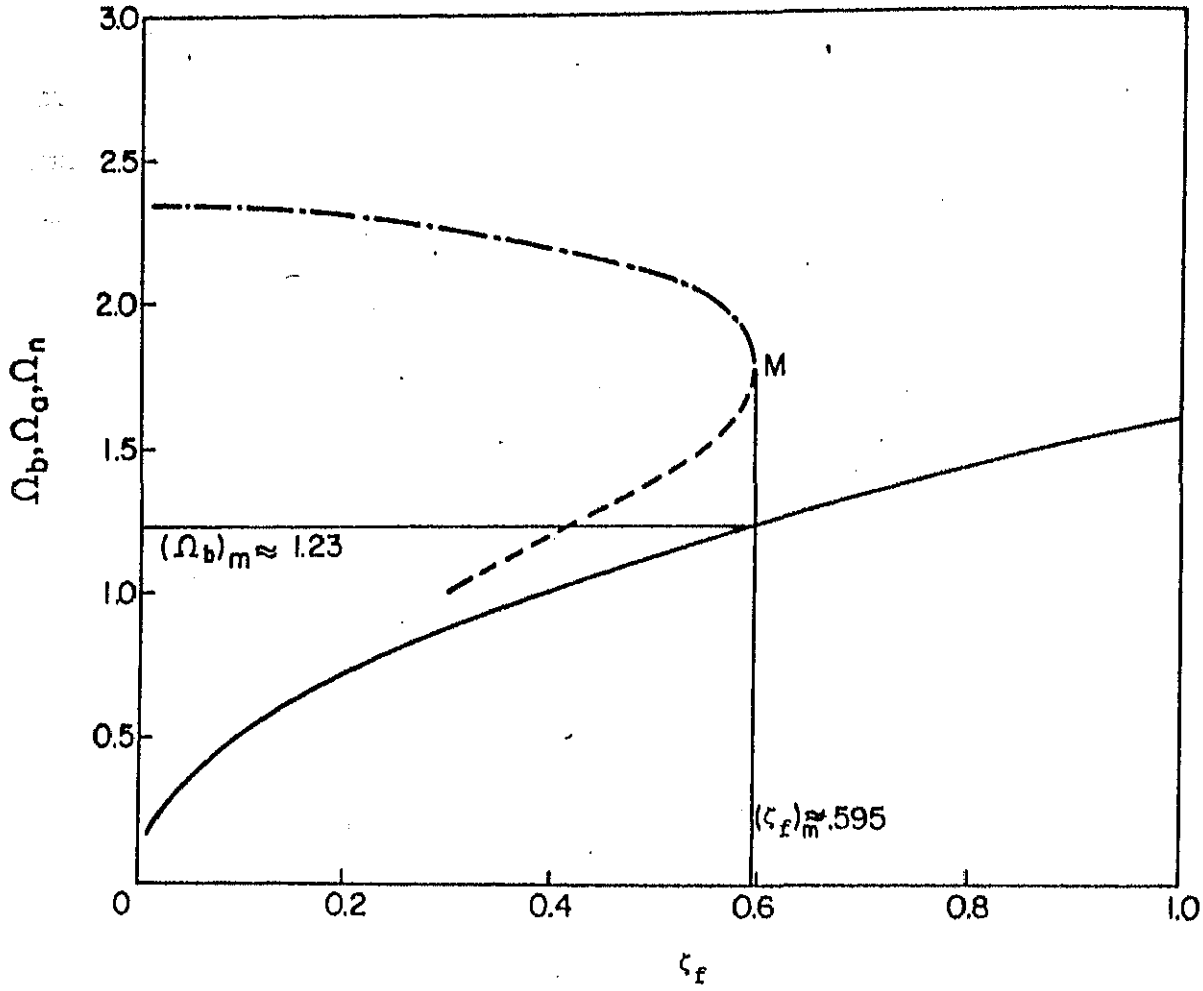

Figure 4.9 Variations of Ω_b, Ω_a and Ω_n with ζ_f in the presence of viscous damping (ζ=0.1). —— Ω_b; ---- Ω_a; ····· Ω_n;

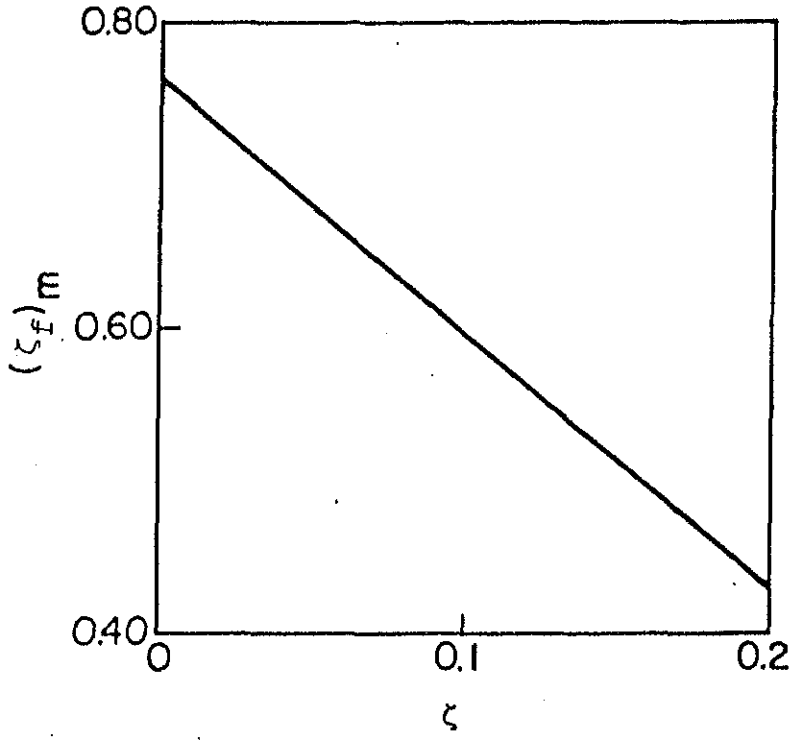

Figure 4.10 Variation of $(\zeta_f)_m$ with ζ

choices of ζ and ζ_f are to be made for the desired performance of the isolation system according to the application on hand. Results obtained, not presented here, with an asymmetric restoring force and Coulomb damping also show the anomalous jump.

4.3.1.1 Numerical integration results

In the present section, equation (4.2) is integrated numerically (using Runge-Kutta-Merson method) and the absolute displacement transmissibility T_d is obtained as

$$T_d = |x|_{max} / y_0 \tag{4.28}$$

where $|x|_{max}$ is the absolute of the maximum steady-state displacement.

In the absence of viscous damping (ζ=0) with ζ_f =0.75, the values of T_d so obtained are expressed in dB (=20 $\log_{10}$ T_d) and are indicated in Figure 4.11 by a circle mark along with the results obtained by the method of harmonic balance (same as Figure 4.3).

It can be seen from Figure 4.11 that the numerical results also show the stable branch (AC) associated with the anomalous jump. To get a clear picture of the response near the anomalous jump the phase plots of equation (4.2) are shown in Figures 4.12 and 4.13 with appropriate initial conditions. Figures 4.12a and 4.12c show the anomalous response at Ω=1.7 and 1.8 respectively whereas Figures 4.12b and 4.12d show the resonance responses for the same frequencies obtained with a different set of initial conditions. Figure 4.13a shows the jump to resonance branch at Ω=2.1 obtained with the same set of initial conditions for which the anomalous response was obtained in Figures 4.12a and 4.12c.

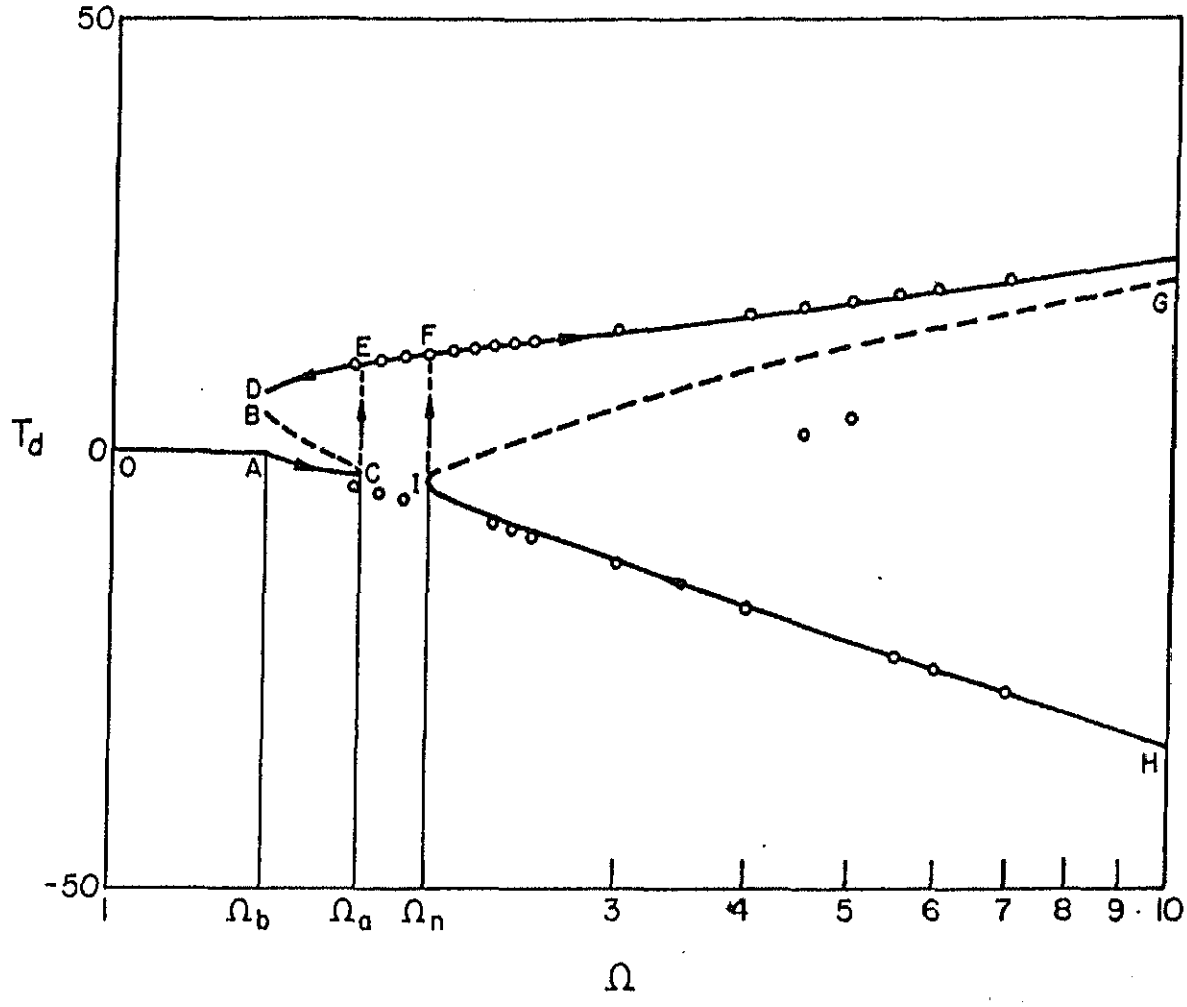

Figure 4.11 Variation of transmissibility, T_d (in dB), versus frequency, Ω. $\zeta' = 0$ and $\zeta_f = 0.75$; (——)stable;(- - -)unstable; (o o o)numerical simulation results.

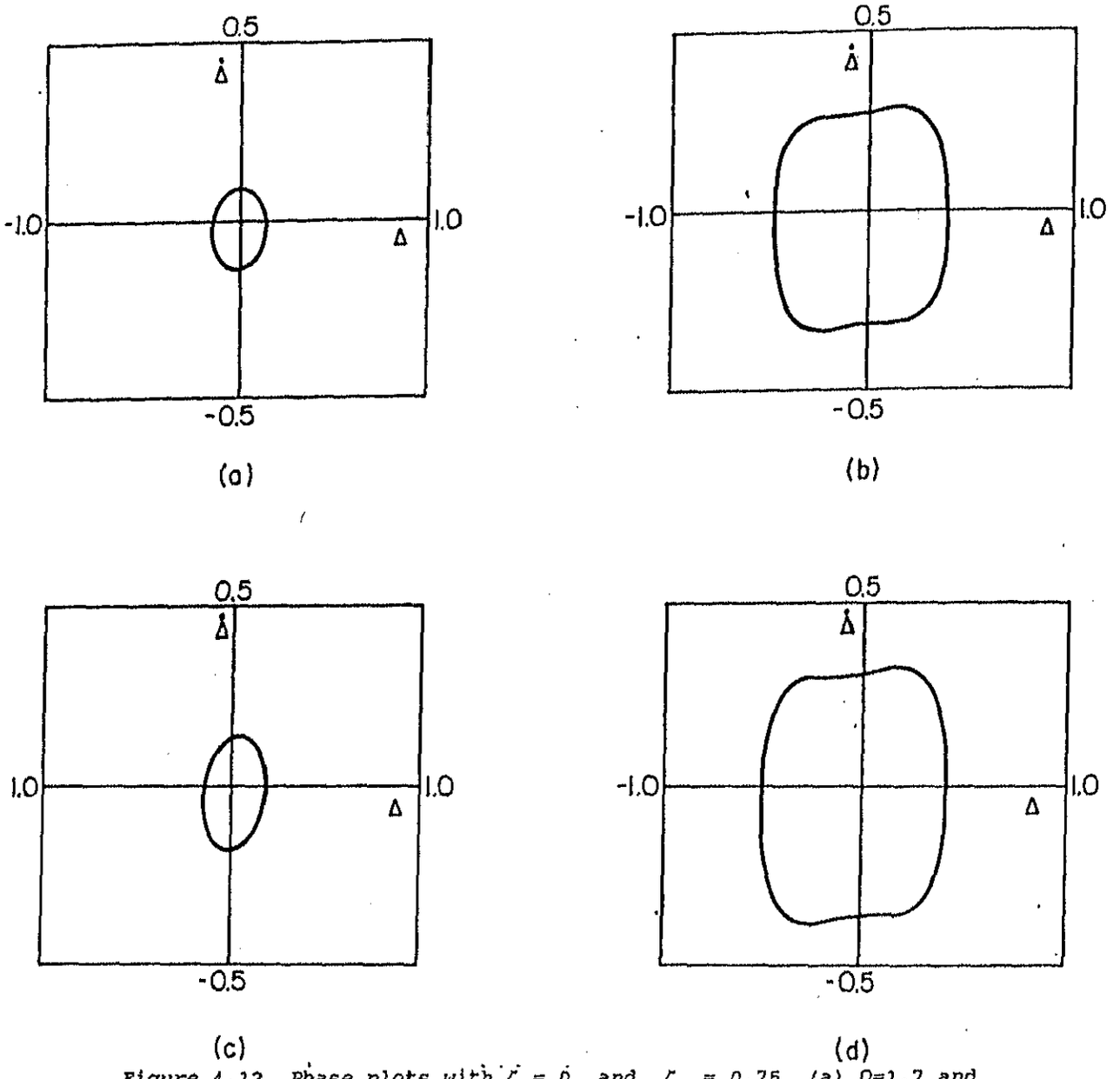

Figure 4.12 Phase plots with $\zeta = 0$ and $\zeta_f = 0.75$ (a) Ω=1.7 and Δ_0=$\dot{\Delta}_0$=0.001 (b) Ω=1.7 and Δ_0=$\dot{\Delta}_0$=3.0 (c) Ω=1.8 and Δ_0=$\dot{\Delta}_0$=0.001 (d) Ω=1.8 and Δ_0=$\dot{\Delta}_0$=3.0.

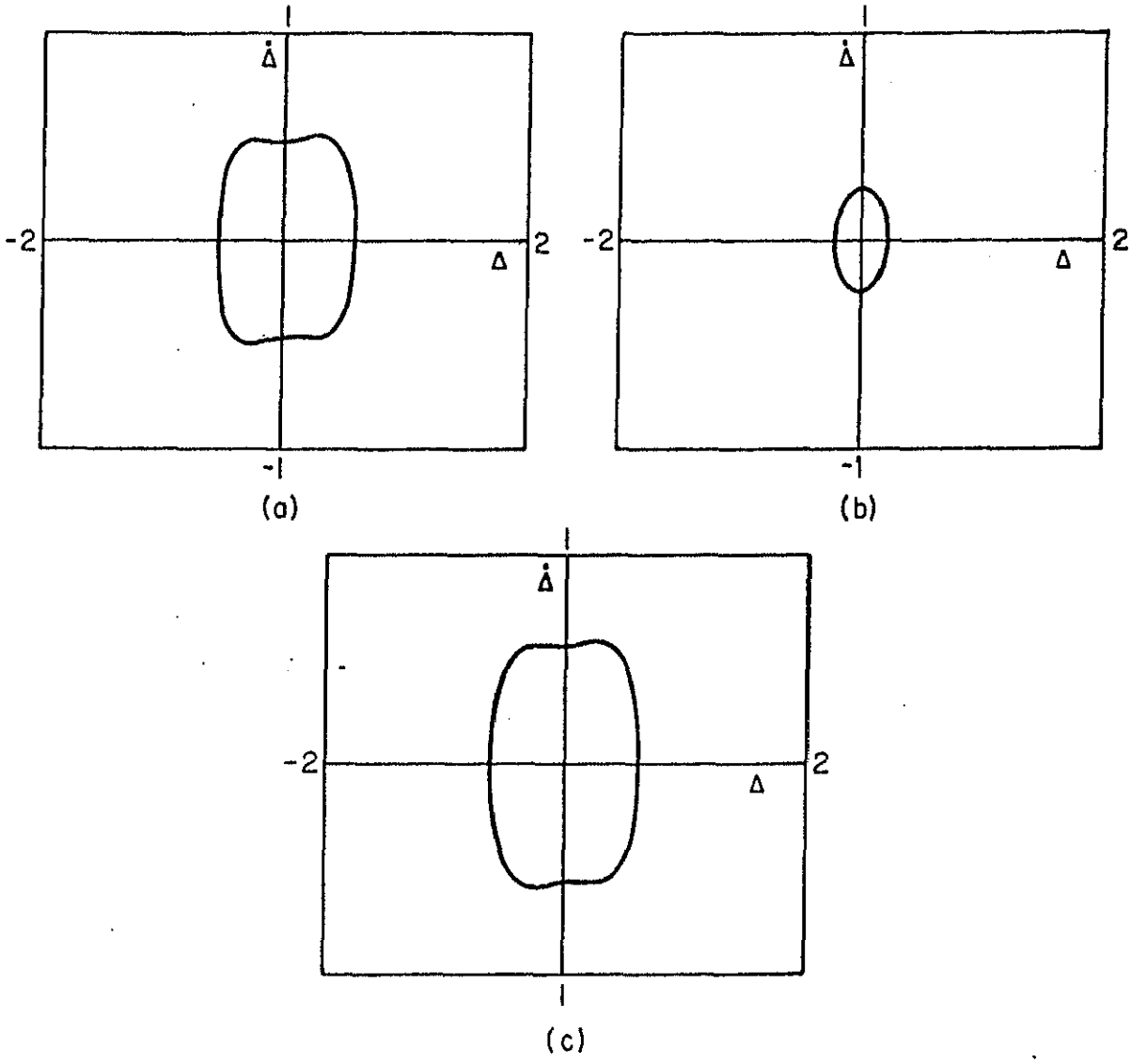

Figure 4.13 Phase plots with $\zeta = 0$ and $\zeta_f = 0.75$ (a) $\Omega = 2.1$ and $\Delta_0=\dot{\Delta}_0=0.001$ (b) $\Omega = 2.3$ and $\Delta_0=\dot{\Delta}_0=0.001$ (c) $\Omega=2.3$ and $\Delta_0=\dot{\Delta}_0=3.0$.

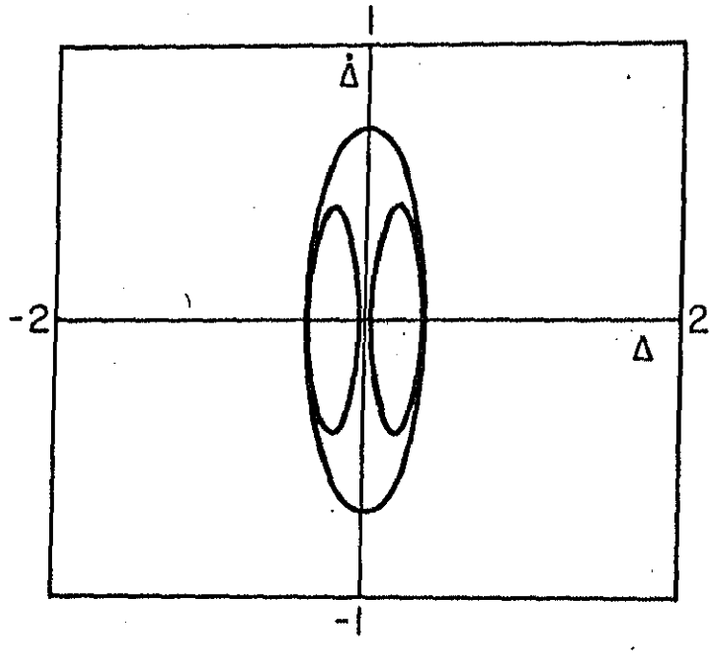

Figure 4.14 Phase plot of the one-third subharmonic response with ζ=0.0, ζ_f=0.75, Ω=4.5 and Δ_0=$\dot{\Delta}_0$=0.01.

Again for Ω=2.3, both the non-resonance and resonance responses can be seen in Figures 4.13b and 4.13c. Thus the numerical simulations confirm the existence of an anomalous jump in the response predicted by the harmonic balance. It was observed that the basin of attraction for the anomalous response is very small as compared to those of the resonance and non-resonance responses.

It can be noted from Figure 4.11, that though the response of equation (4.2) may not be harmonic, the values of T_d, obtained from equation (4.28) by numerical simulation match with those computed from the assumed harmonic motion. Thus one can rely on the method of harmonic balance to provide a good approximation to the transmissibility. However, around Ω=4.5 the non-resonance response predicted by the harmonic balance differs significantly from that obtained by the numerical simulation of equation (4.2). A phase plot of equation (4.2) with Ω=4.5 is shown in Figure 4.14. It can be seen from this figure, that this phase plot corresponds to a one-third subharmonic in the response which has not been accounted for in the harmonic approximation. It is evident that the presence of the subharmonic resonance decreases the high frequency attenuation rate (given by the slope of the non-resonance branch) and consequently the isolator effectiveness. The effect of the subharmonic resonances on transmissibility is analogous to the wave effects, caused by the isolator inertia, in a linear isolator [4]. From the above discussion one can conclude that consideration of subharmonic resonances, which occur well within the normal operating range of frequencies, is important in vibration isolation.

It is shown in Figure 4.5d that when ζ=0 and $\zeta_f > \pi/4$, the

anomalous jump merges with the main jump. This situation is depicted in Figure 4.15 along with the numerical results. Again, the results obtained by numerical integration match with those obtained from the harmonic balance method. The phase plots of equation (4.2), shown in Figure 4.16, also clearly indicate the merger of the two jumps.

In a soft Duffing's oscillator the anomalous response is seen to be related with the so-called symmetry-breaking phenomenon when the higher order harmonics are included in the solution [75-80]. However, in the present case, analysis of the anomalous portion including higher harmonics is difficult due to the presence of the Coulomb damping and therefore, a numerical investigation was carried out. It was seen that in the case of a base-excited, hard, Duffing's system numerical simulation did not reveal any further bifurcations around the anomalous jump region. Thus, one may conclude that in the system under consideration, the occurence of an anomalous jump in the response is not a signature for symmetry-breaking and period-doubling.

4.3.2 Force excitation

The force transmissibility (T_f), given by equation (4.27) with X_1 calculated from equation (4.23), is shown in Figures 4.17-4.19 for various values of ζ_f and ζ. It may be noted that apart from the usual jump observed in a hard Duffing equation, no anomalous behaviour exists. This can be verified readily following the procedure outlined in the Appendix C. In the absence of viscous damping (ζ=0), the resonance branch extends to infinity as

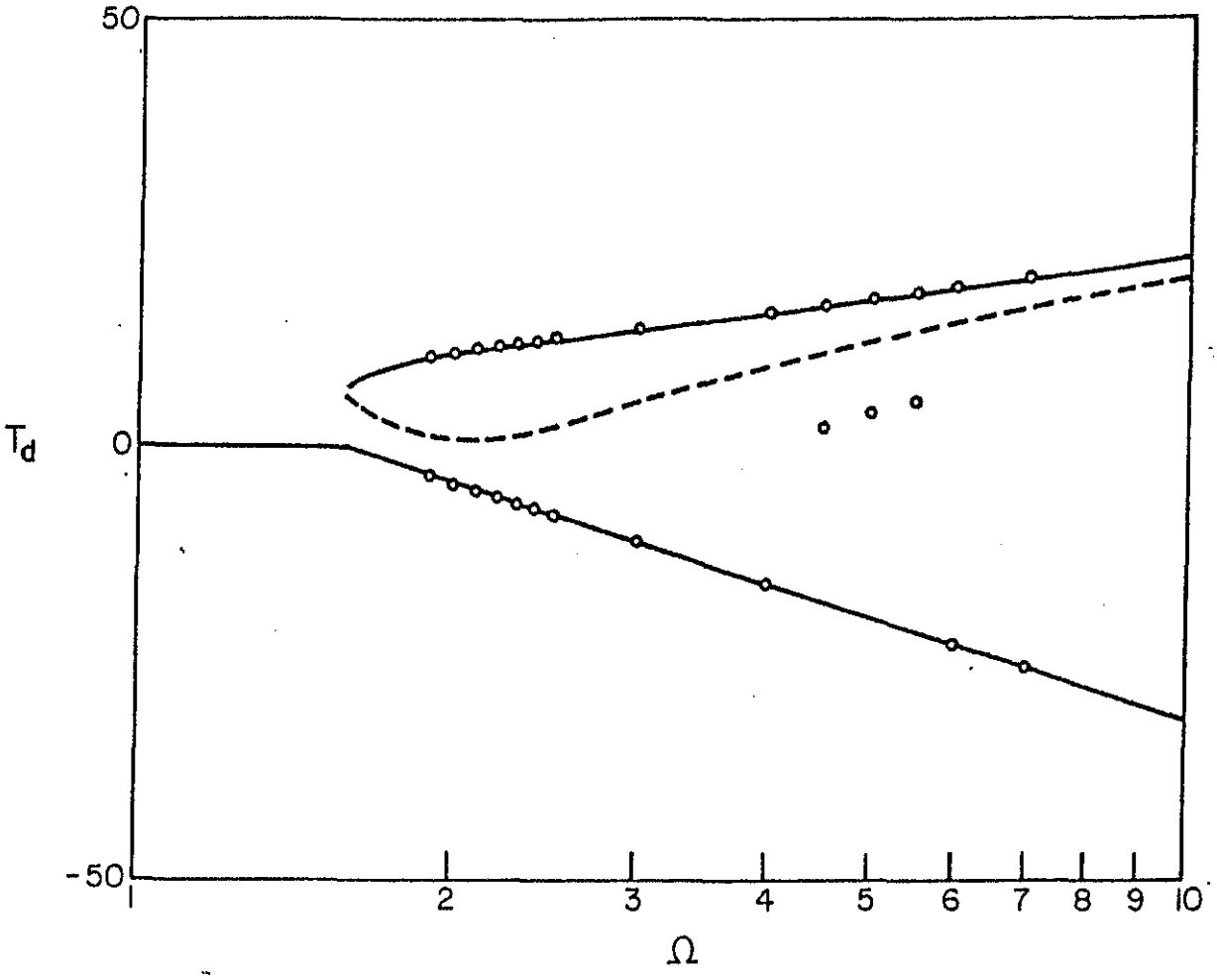

Figure 4.15 Variation of transmissibility, T_d (in dB), versus frequency, Ω. ζ=0 and ζ_f=1.0 ; (——)stable; (- - -)unstable; (o o o) numerical simulation results.

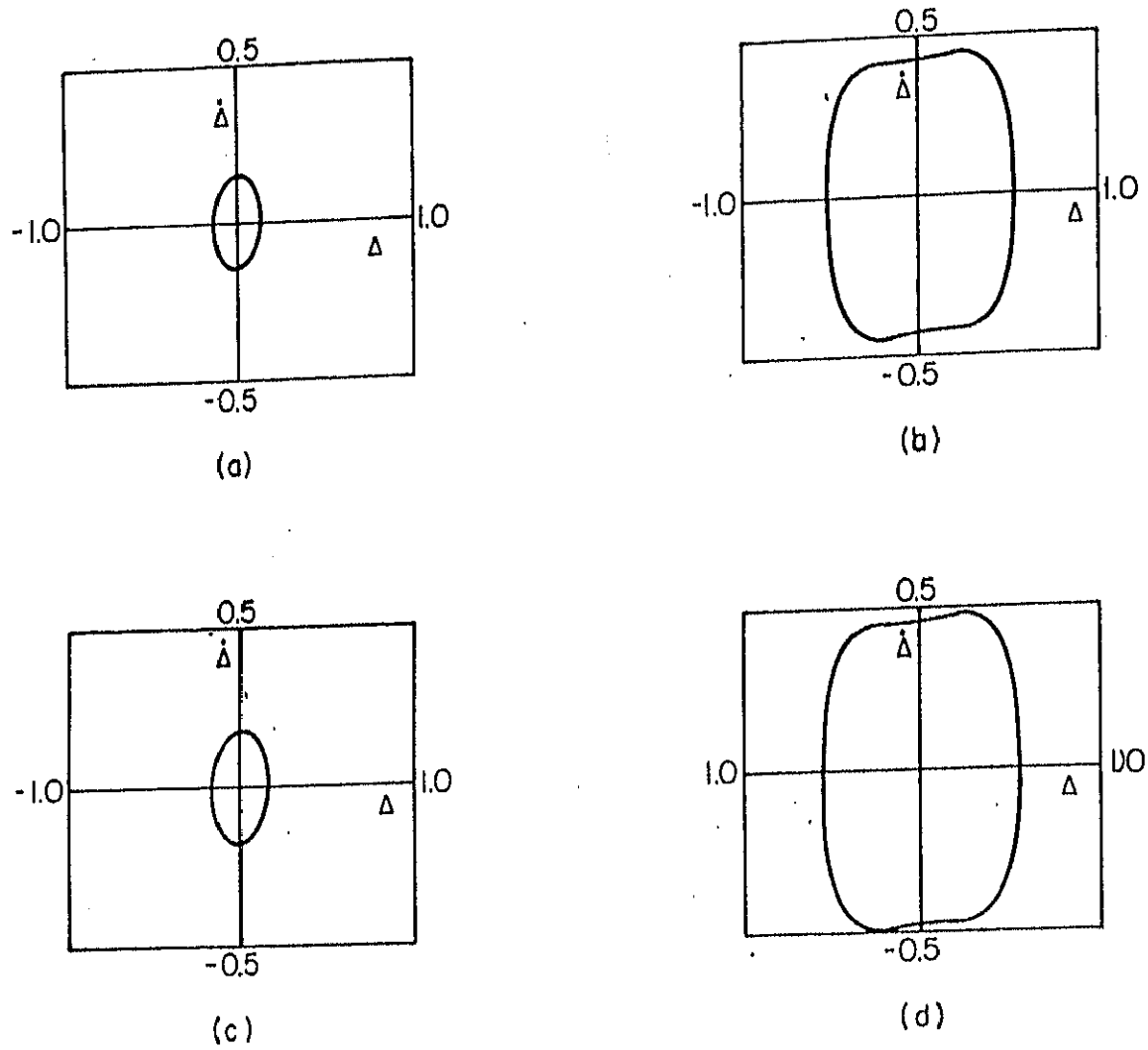

Figure 4.16 Phase plots with ζ=0 and ζ_f=1.0 (a) Ω=2.0 and Δ_0=$\dot{\Delta}_0$=0.001 (b) Ω=2.0 and Δ_0=$\dot{\Delta}_0$=3.0 (c) Ω=2.1 and Δ_0=$\dot{\Delta}_0$=0.001 (d) Ω=2.1 and Δ_0=$\dot{\Delta}_0$=3.0.

shown in Figures 4.17a-4.17d. However, with a suitable choice of ζ one can make the resonance transmissibility bounded as seen in Figures 4.18 and 4.19. It is observed from Figures 4.17a-4.17d that the transmissibility at high frequencies is almost constant when the viscous damping is absent. In the presence of viscous damping, the high frequency transmissibility is no longer constant as can be observed from Figures 4.18 and 4.19. With simultaneous increase in both ζ and ζ_f , the high frequency transmissibility increases as shown in Figures 4.17-4.19.

As mentioned earlier, the approximate method used in the present analysis breaks down when $\zeta_f > (\zeta_f)_c (\approx \pi/8)$. Den Hartog [91] presented the exact analysis for a linear restoring force and gave the expressions for finite resonance response when $\zeta > (\zeta_f)_c$. Moreover, he also considered the motion with atmost two stops and determined the range of motion without stops. However, the present problem with nonlinear spring characteristics is not amenable to analytical treatment.

4.4 Conclusions

This chapter extends the work of Den Hartog and Ruzicka on isolators with combined Coulomb and viscous damping by including a nonlinear restoring force. The effect of the nonlinear damping terms on the usual jump response of the hard Duffing's equation is studied by using the method of harmonic balance. A peculiar behaviour in the response of the base excited system is pointed out. Analytical results related with the anomalous jump have been derived. The existence of an anomalous jump in the transmissibility curve of a base-excited, hard, Duffing's

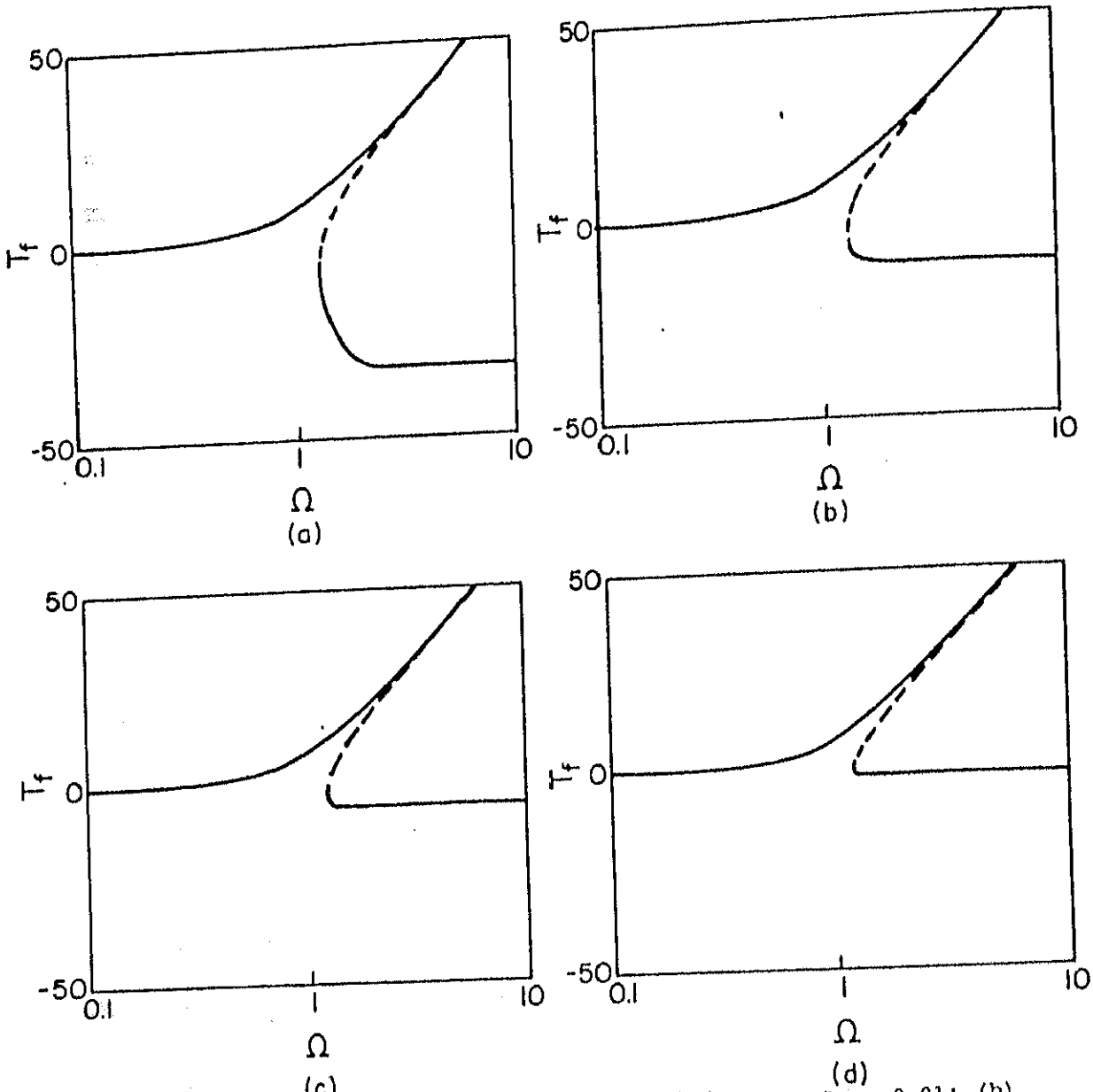

Figure 4.17 Variation of T_f with Ω. ζ= 0 and (a) ζ_f = 0.01; (b) ζ_f = 0.1; (c) ζ_f = 0.2; (d) ζ_f = 0.3;

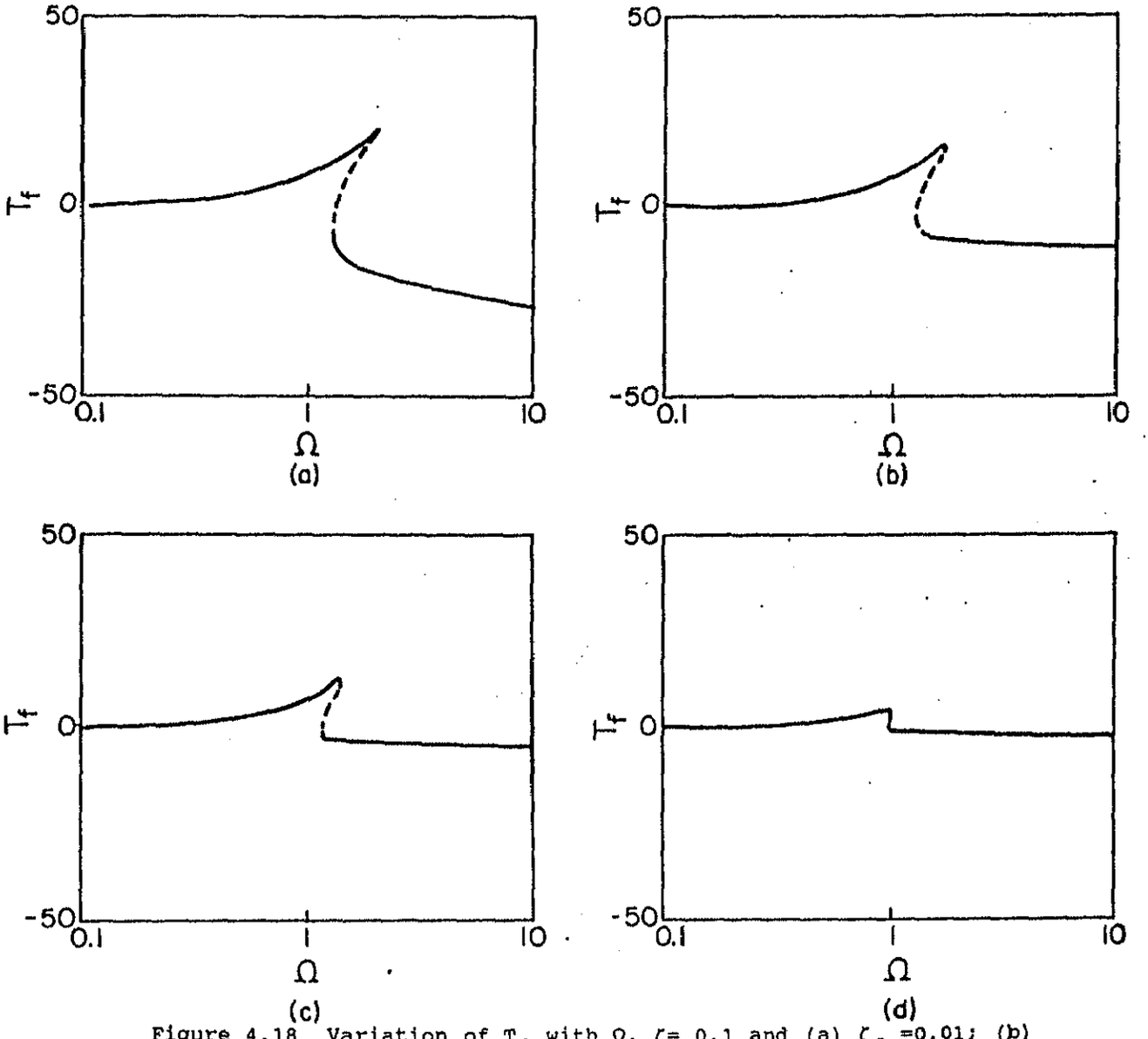

Figure 4.18 Variation of T_f with Ω. ζ= 0.1 and (a) ζ_f =0.01; (b) ζ_f = 0.1; (c) ζ_f = 0.2; (d) ζ_f = 0.3;

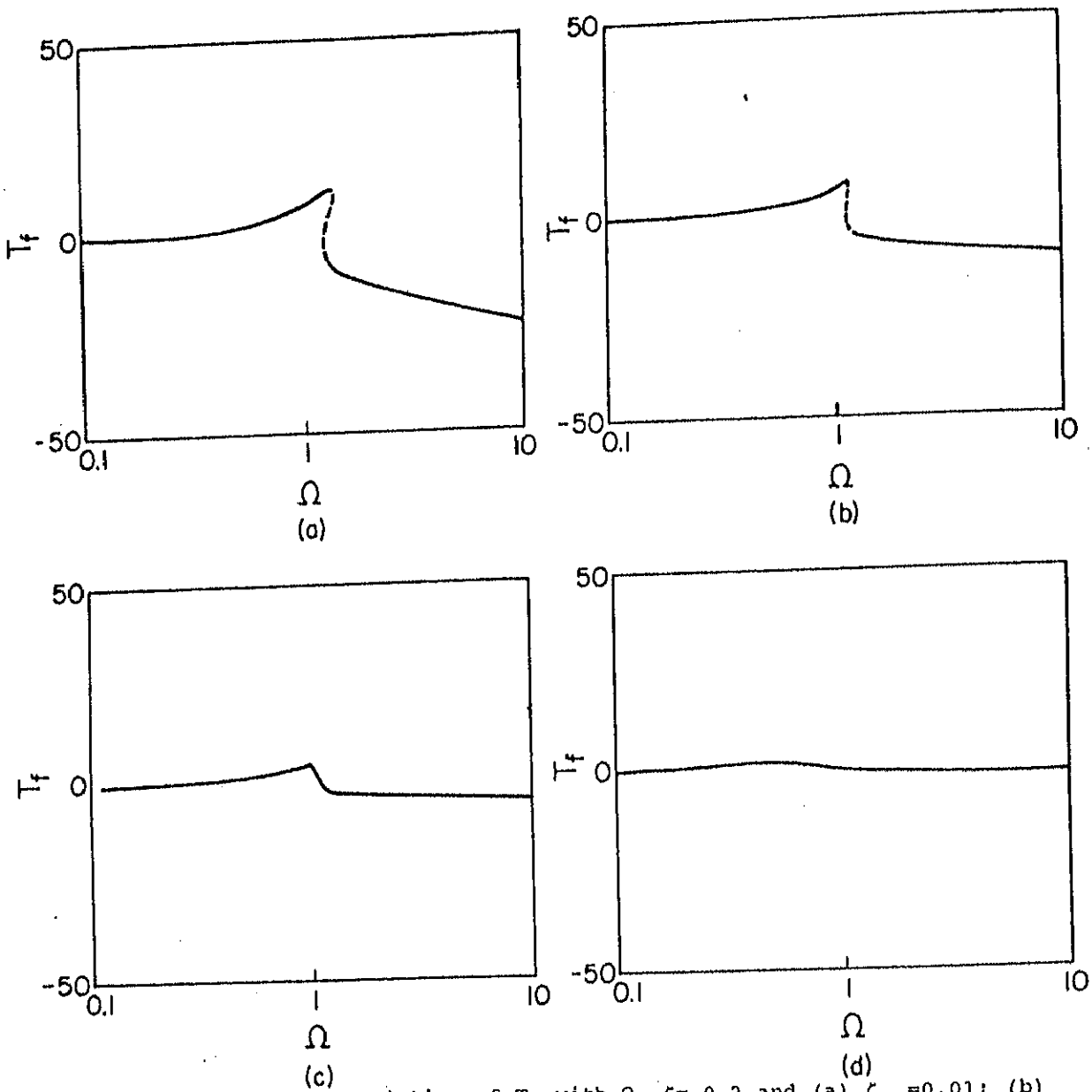

Figure 4.19 Variation of T_f with Ω. ζ= 0.2 and (a) ζ_f =0.01; (b) ζ_f = 0.1; (c) ζ_f = 0.2; (d) ζ_f = 0.3;

isolator, is also confirmed by direct numerical integration. Unlike in the case of a soft system, this anomalous jump is not associated with the symmetry-breaking and period-doubling. The transmissibility indices show that the subharmonic resonances can impair the performance of such a nonlinear isolator. The stability analysis is carried out and it is found that a transition from a stable node to a stable spiral takes place near the break-loose frequency. Performance characteristics are presented through a detailed parametric study. It is pointed out that with a suitable choice of Coulomb damping one can maintain the transmissibility at or less than unity even for this nonlinear system. Addition of viscous damping contracts the anomalous jump and thereby enhances the range of frequency over which the transmissibility can be maintained at less than unity. The analysis is done by assuming continuous motion and hence it is valid strictly for low damping cases. It is known that the secondary resonances and chaos occur on the low frequency regime around the jump in the resonance response curve of a hard Duffing's equation with linear damping. Hence, it is interesting to find out whether or not a suitable choice of break-loose frequency (i.e., the Coulomb damping coefficient) can eliminate these phenomena. The effects of a friction damper on secondary resonances and chaotic motion will be taken up in the next chapter.

CHAPTER 5

CHAOTIC RESPONSE OF A HARD DUFFING-TYPE VIBRATION ISOLATOR WITH COMBINED COULOMB AND VISCOUS DAMPING

5.1 Introduction

Numerical simulations of the response of a harmonically excited mass on an isolator with a cubic, hard, nonlinear restoring force and combined Coulomb and viscous damping are presented. These computations have been carried out on an HP-8000 UNIX system with a subroutine of NAG library using Runge-Kutta-Merson method. Appropriate tolerance values have been selected to get consistent results. Both force- and base-excited systems, in the absence of Coulomb damping, exhibit the period-doubling (with a symmetry-breaking precursor) and (Type I) intermittency routes to chaos as the system parameters are varied. An addition of a little friction damping quenches the chaotic responses in the base-excited system. In the force-excited system, however, it is shown that the addition of friction damping does not alter the bifurcation structure.

5.2 Isolation System With Base Excitation

Let a rigid mass be separated from a harmonically moving base through an isolator consisting of a cubic, non-linear spring and combined Coulomb and viscous dampers. The equation of motion for the mass can be written as (see chapter 4)

$$\ddot{\Delta} + 2\,\zeta\,\dot{\Delta} + 2\,\zeta_f\,\mathrm{sgn}(\dot{\Delta}) + \Delta^3 = \Omega^2 \cos \Omega\tau \qquad (5.1)$$

where the dot denotes differentiation with respect to non-dimensional time τ.

5.2.1 Control Of Chaos

The control of the chaotic responses is recently receiving attention of the researchers from several disciplines [107-109]. A control strategy for suppressing the chaotic responses in maps is presented in reference [108] and has been applied to the Poincare map, obtained from an experimental investigation of a parametrically driven magnetoelastic ribbon [109]. It is reported in reference [109] , that no model for the dynamics is required for determining a control strategy. Though several feedback strategies have been proposed for vibration control, their hardware may be quite expensive and designing a robust controller may not be an easy task. Hence, a suitable passive control strategy is still an attractive option for a practicing engineer. As opposed to the feedback control, the present work examines a passive control of chaos based on the conventional vibration control methods [3] by incorporating a proper friction damping mechanism.

In fact, the roìe of the chaotic responses in the design of a nonlinear vibration isolation system needs to be critically examined. First of all, the amplitudes of the chaotic responses are usually quite small compared to those of the resonant responses [70]. Secondly, the global bifurcation structure [62, 68] indicates that the secondary resonances and chaotic responses

lie to the left of the primary resonance towards the low frequency region. Thirdly, the chaotic responses usually occur with a high level of excitation and that too within a narrow regime of the parameter values. However, in case the chaotic responses need to be controlled, it is proposed to achieve this by a suitable choice of the break-loose frequency (Ω_b) i.e., of the friction damping coefficient, ζ_f. To substantiate this suggestion, numerical simulation of equation (5.1) is carried out with ζ_f=0 (i.e., only with viscous damping) and ζ=0.01 by varying Ω. As the frequency is decreased, the periodic orbit (shown in Figure 5.1a for Ω =0.5) loses its symmetry due to the symmetry-breaking bifurcation and the resulting dual, unsymmetric solutions (at Ω=0.4) are shown in Figures 5.1b and 5.1c with the corresponding initial conditions. Decreasing Ω further, a period-doubling bifurcation takes place (at Ω=0.2) and the resulting period-two orbit can be seen in Figure 5.1d . At a still lower value of the frequency (Ω=0.17), a chaotic attractor (not shown here) resulting from the usual period-doubling route is obtained. Further reduction of Ω shows the emergence of a period-three orbit followed by the (Type I) intermittency route to chaos as reported in references [53, 70 and 89].

Numerical simulation of equation (5.1) for the same value of ζ (=0.01) is now carried out after including a small friction damping (ζ_f=0.005). These results are shown in Figures 5.2a to 5.2d. Figure 5.2a shows a symmetric, periodic orbit at Ω=0.5. It can be seen from Figure 5.2b that the symmetry-breaking bifurcation occurs again at Ω=0.4 (same as that in Figure 5.1b). Thus, it appears that the symmetry-breaking bifurcation is quite

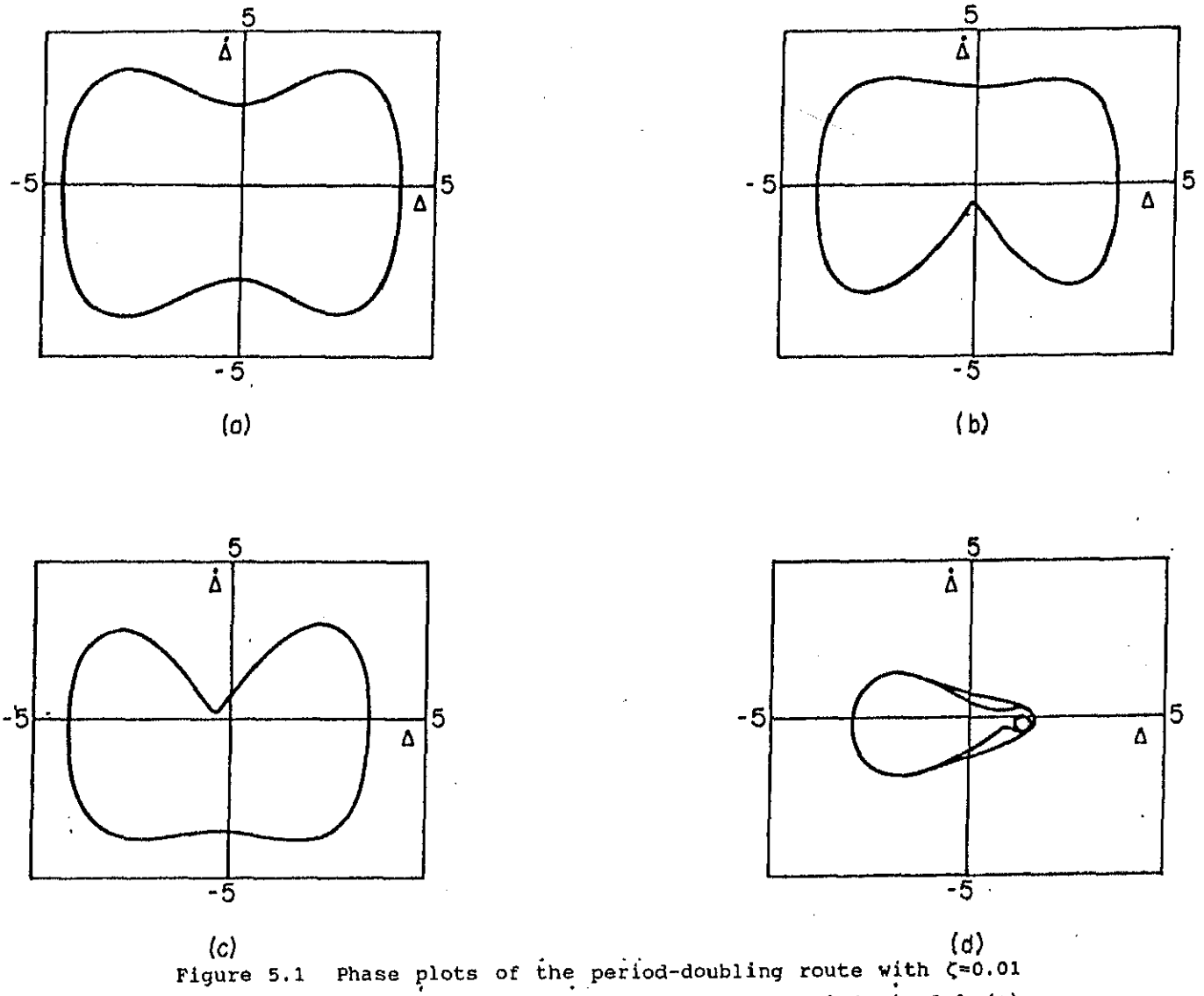

Figure 5.1 Phase plots of the period-doubling route with ζ=0.01 and ζ_f=0.0. (a) Ω=0.5 and $\Delta_0=\dot{\Delta}_0$=0.1 (b) Ω=0.4 and $\Delta_0=\dot{\Delta}_0$=0.1 (c) Ω=0.4 and $\Delta_0=\dot{\Delta}_0$= -0.1 (d) Ω=0.2 and $\Delta_0=\dot{\Delta}_0$=0.1.

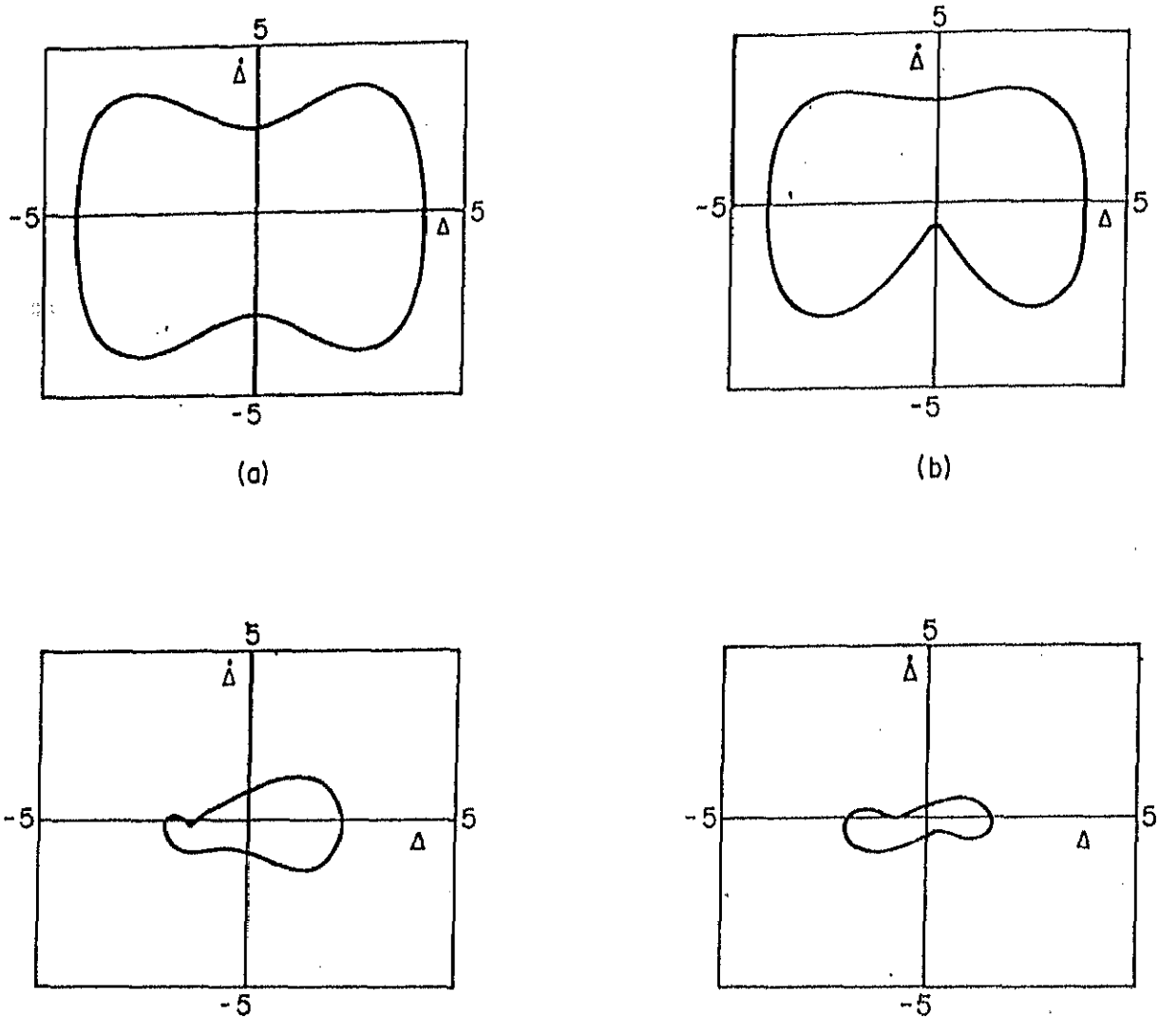

Figure 5.2 Phase plots with ζ=0.01 and ζ_f=0.005. (a) Ω=0.5 and $\Delta_0=\dot{\Delta}_0$=0.1 (b) Ω=0.4 and $\Delta_0=\dot{\Delta}_0$=0.1 (c) Ω=0.2 and $\Delta_0=\dot{\Delta}_0$=0.1 (d) Ω=0.15 and $\Delta_0=\dot{\Delta}_0$=0.1

insensitive to the value of ζ_f. However, any further reduction of Ω even up to 0.15 does not reveal the period-doubling cascade as confirmed by Figures 5.2c and 5.2d. Thus, the addition of friction damping effectively suppresses the chaotic responses observed in the presence of viscous and other non-linear damping forces [89].

It may be noted that with $\zeta_f=0$, the period-doubling occurred at around $\Omega=0.2$ (Figure 5.1d) and the chaos at $\Omega=0.17$. In order to eliminate the period-doubling route to chaos, one would tend to choose $\Omega_b=0.2$ (i.e., $\zeta_f=(\pi/8)\Omega_b^2 \approx 0.0157$ [105]). However,it is evident from Figures 5.2a to 5.2d that, a much lower value of ζ_f ($=0.005$ with corresponding $\Omega_b\approx 0.113$) is sufficient to quench chaos. Hence, it can be said that the period-doubling bifurcation (unlike the symmetry-breaking) is quite sensitive to the value of ζ_f.

The phase plot of equation (5.1) for $\Omega=0.15$, shown in Figure 5.2d, indicates the onset of the characteristic stick-slip of a friction damper. Such responses can be accurately obtained by using numerical integration only after incorporating special conditions [94]. However, these studies are not carried out in the present work. It has been reported that the low frequency chaos and escape phenomenon are common features in soft, Duffing's oscillators [44, 47, 52]. The present method of controlling chaos with a friction damper is worth exploring in such systems.

5.3 Isolation System With Force Excitation

Referring to chapter 4 (see Figure 4.2), if the rigid mass M is excited by a harmonic force (f cos ωt) and is isolated from an immobile foundation, then the equation of motion can be written as

$$M\,x'' + C\,x' + C_f\,\mathrm{Sgn}(x') + Kx^3 = f\cos\omega t\ . \qquad (5.2)$$

Defining the following non-dimensional parameters :

$\tau = \omega t$,

$X = x/x_0$, $\dot{X} = x'/(x_0\omega)$, $\ddot{X} = x''/(x_0\omega^2)$, $\zeta = C/(2M\omega)$,

$\zeta_f = C_f/(2Mx_0\omega^2)$, $F = f/(M\omega^2 x_0)$ with $x_0 = (M\omega^2/K)^{1/2}$,

and using them in equation (5.2), one obtains

$$\ddot{X} + 2\,\zeta\,\dot{X} + 2\,\zeta_f\,\mathrm{sgn}(\dot{X}) + X^3 = F\cos\tau\ . \qquad (5.3)$$

In this section, the effect of friction damping on the bifurcation structure [62, 68] is examined by analysing the results obtained by numerical integration of equation (5.3).

Equation (5.3) is numerically integrated for various values of F with $\zeta = 0.05$ and $\zeta_f = 0.005$. The stroboscopic maps (sampled at $\tau=2\pi$), obtained from these results, are shown in Figures 5.3 and 5.4. Figures 5.3a to 5.3c indicate the period-doubling route to chaos as F is increased from 4.9 to 5.7. Figure 5.3a shows the period-doubling , Figure 5.3b shows the period-quadrupling and Figure 5.3c represents the chaotic response. Upon further increasing the value of F, a period-three solution is obtained at F=9.8 (Figure 5.4a). The (Type I) intermittency route to chaos is resulted at F=10.0 (Figure 5.4c) with a prechaotic regime (Figure 5.4b) at F=9.9. When the value of F is increased to 13.4, again a period-one solution is obtained (Figure 5.4d). This transition

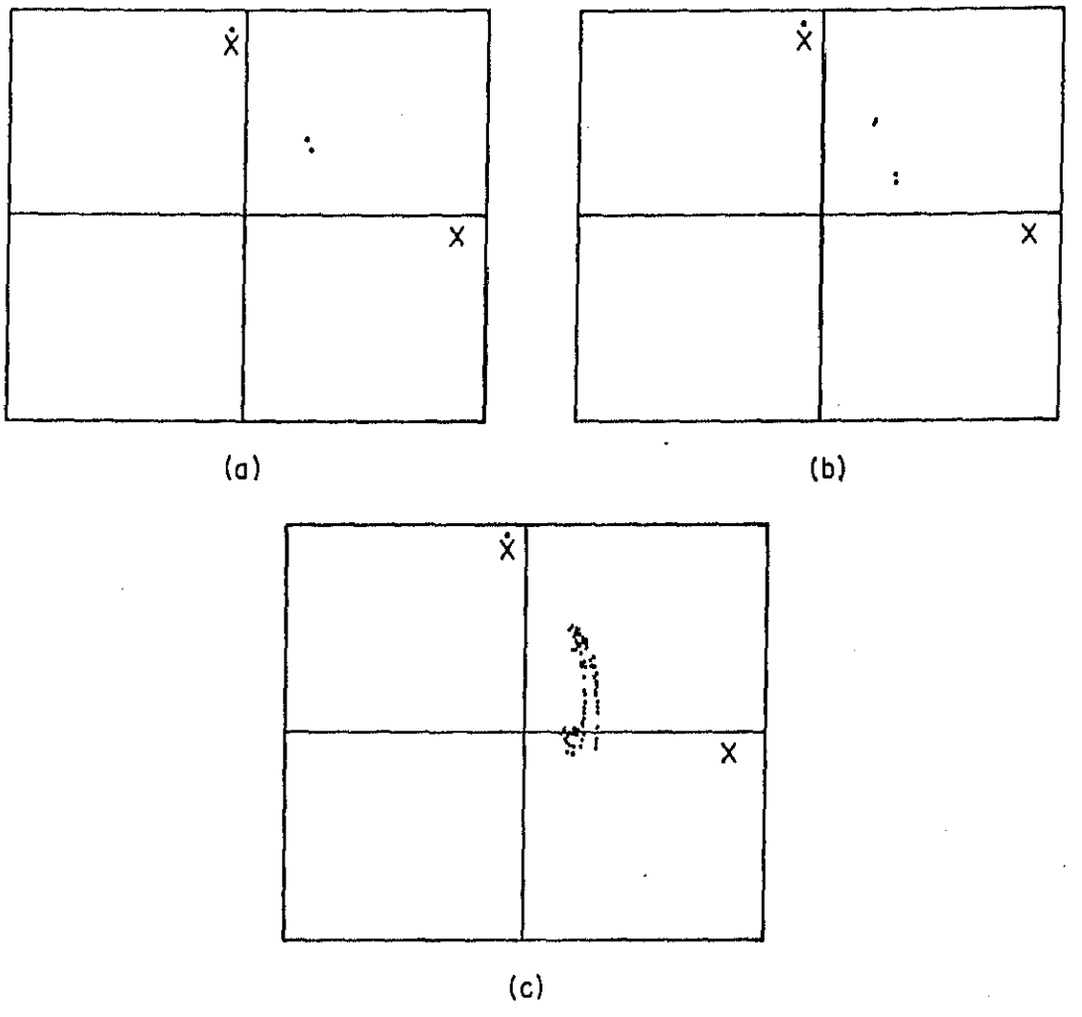

Figure 5.3 Stroboscopic maps of the period-doubling route to chaos with ζ=0.05 and ζ_f=0.005. (a) F=4.9 (b) F=5.5 (c) F=5.7

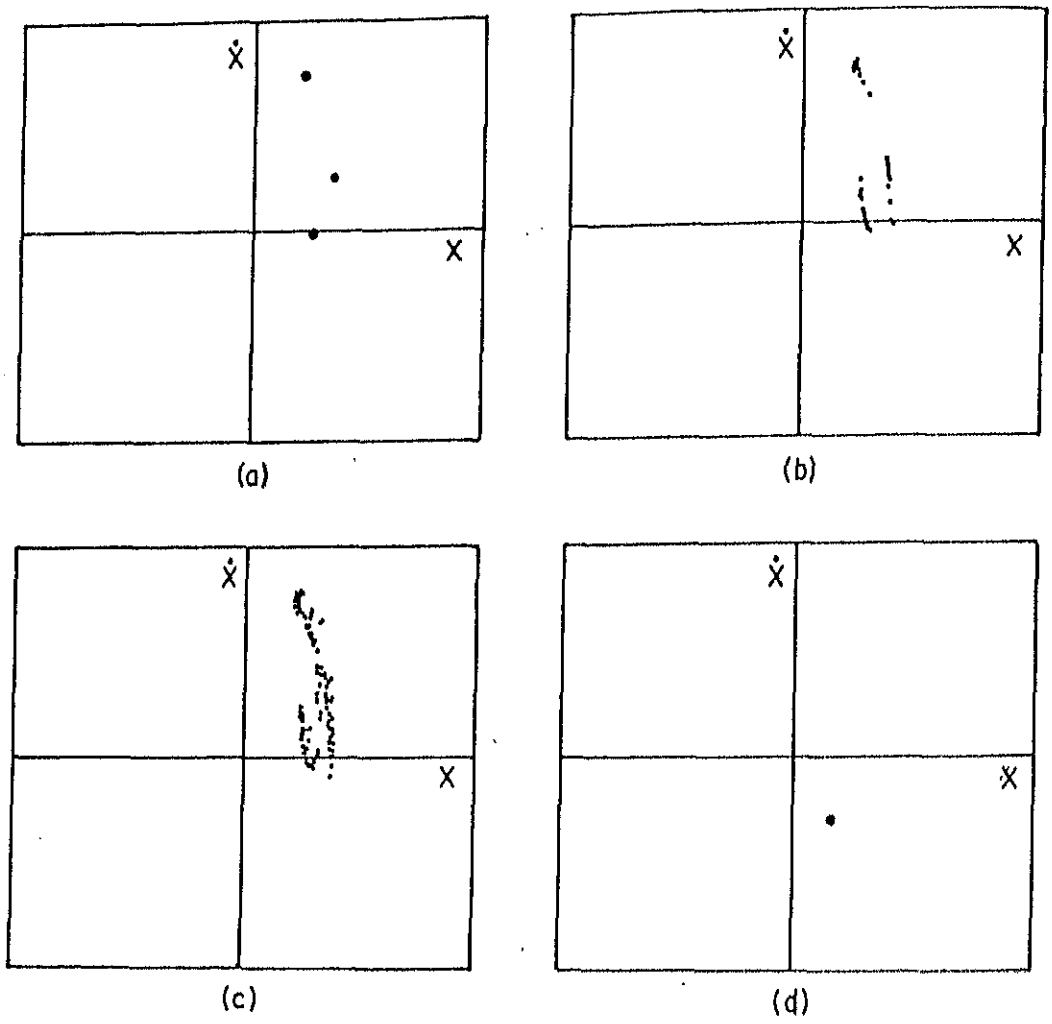

Figure 5.4 Stroboscopic maps of the (Type I) intermittency route to chaos with ζ=0.05 and ζ_f=0.005. (a) F=9.8 (b) F=9.9 (c) F=10.0 (d) F=13.4

of a period-three orbit to a period-one orbit via a chaotic zone has also been observed in references [53, 70].

It may be mentioned that Ueda [53] presented a detailed set of results for the same parameter values as above and ζ_f=0.0. A comparison of Ueda's results with those presented in this section indicates that the bifurcation structure seems to be unaffected by friction damping. Numerical simulation carried out for ζ_f up to a value of 0.02 confirms this. It is also observed that the critical values of F needed to cause the symmetry-breaking and period-doubling are relatively insensitive to the value of ζ_f. Just as in the case of a base-excited system, the analysis presented in this section does not encompass the stick-slip motions.

5.4 Conclusions

It has been demonstrated by numerical simulation that the instabilities associated with the secondary resonances and chaotic motion, encountered in the low frequency regime of a base-excited system, can be eliminated by using a suitably designed friction damper. The bifurcation structure of a force-excited, hard system seems to be unaltered by the addition of friction damping.

CHAPTER 6

ROLE OF NONLINEAR DISSIPATION IN SOFT DUFFING'S OSCILLATORS

6.1 Introduction

Soft Duffing's oscillators (with a saddle point in the unforced situation) are employed as models of various physical and engineering situations such as Josephson junctions, optical bistability, plasma oscillations, buckled beam, ship dynamics, vibration isolators and elctrical circuits, etc.,[43-60]. The effect of a strictly dissipative force (velocity to the pth-power model) on the response and bifurcations of driven, soft Duffing's oscillators is considered. The method of harmonic balance is used to obtain the steady state harmonic response. An anomalous jump in the harmonic response (signifying a break in the resonance curve), obtained in the case of linearly damped, soft Duffing's oscillators, is shown to persist even in the presence of nonlinear damping. It is shown that the bifurcation structure and the structure of the chaotic attractor are quite insensitive to the damping exponent p. However, the threshold values of the parameters, at which bifurcations occur, depend both on the damping index and the damping coefficient. The Melinkov criterion and an analytical criterion for the period-doubling bifurcation have been obtained in the presence of combined linear and cubic damping.

6.2. Single-Well Potential Oscillator

Consider the governing equation of motion in the non-dimensional form as

$$\ddot{x} + 2\zeta\,\dot{x} + 2\zeta_p\,\dot{x}|\dot{x}|^{p-1} + x + \varepsilon\,x^3 = F\cos\Omega\tau, \quad \varepsilon<0, p>0 \qquad (6.1)$$

where p is the damping exponent, ζ is the coefficient of viscous damping, ζ_p is the coefficient of pth-power damping, ε is the nonlinearity parameter, F is the amplitude of excitation and Ω is the frequency of excitation. The dot denotes differentiation with respect to time τ. In this section we illustrate the effects of nonlinear damping on the harmonic response and bifurcation set.

Assuming the harmonic solution of equation (6.1) in the form

$$x = A\cos(\Omega\tau-\phi) \qquad (6.2)$$

and using the method of harmonic balance one gets the following equation for A:

$$A^2(1-\Omega^2)^2 + (9/16)\,\varepsilon^2 A^6 + (3/2)(1-\Omega^2)\,\varepsilon A^4 + (2\zeta A\Omega + 2\zeta_p A^p \Omega^p \gamma_p)^2 - F^2 = 0 \qquad (6.3)$$

where γ_p is given by

$$\gamma_p = (2/\sqrt{\pi})\Gamma[(p+2)/2]/\Gamma[(p+3)/2], \qquad (6.4)$$

Γ is the standard gamma function.

It should be noted that equation (6.3) can also be obtained using the notion of equivalent viscous damping coefficient [3].

Typical curves of A vs. Ω with p=2 are shown in Figures 6.1a-6.1d for different values of F. One can see from Figures 6.1a-6.1c that apart from the usual jump phenomenon, there exists

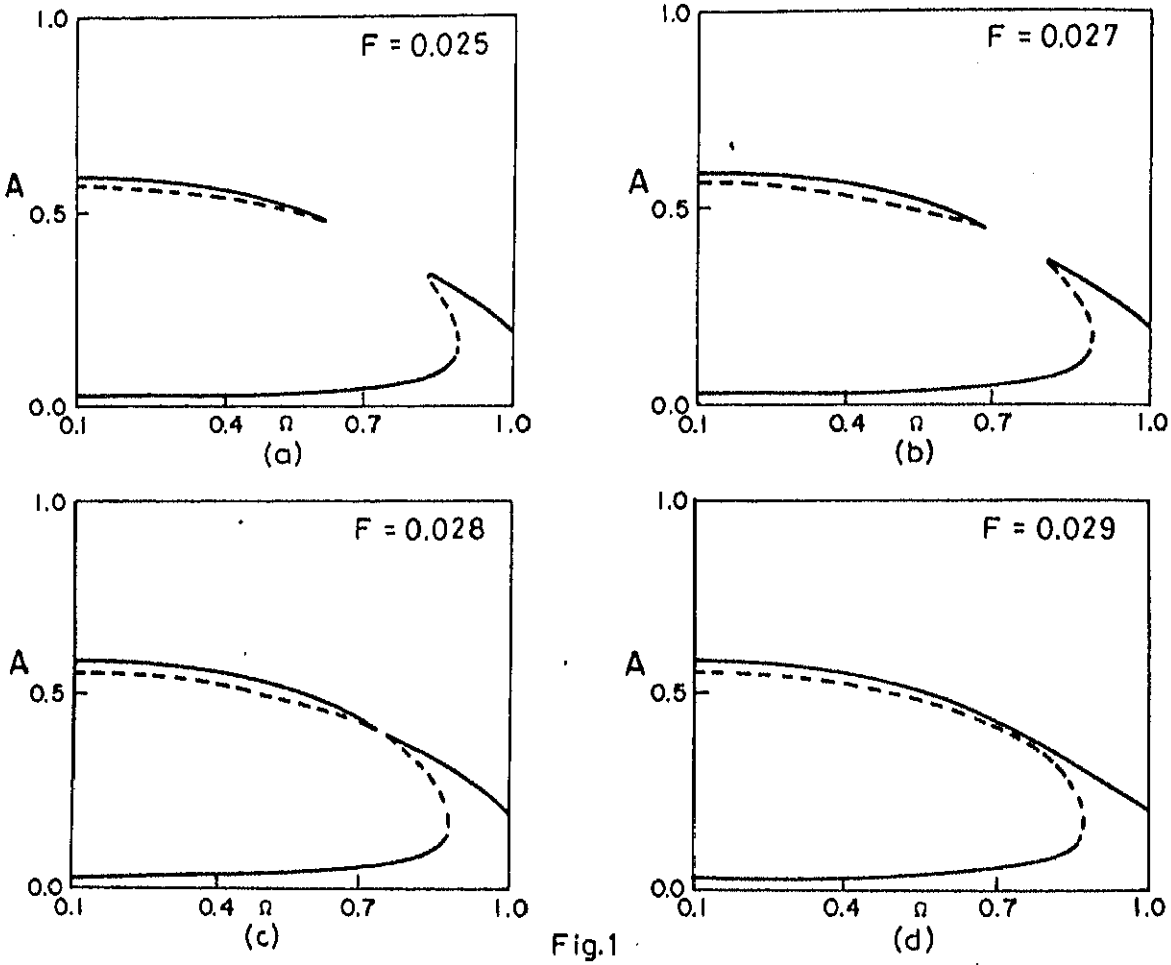

Figure 6.1 Response curve A vs. Ω with ζ=0, ζ_2=0.2 and ε= -4.0

another branch at low frequencies referred to as the 'anomalous jump'. When the forcing amplitude F is increased beyond a critical value, the anomalous jump merges with the main jump and the response curve opens up (similar to the case of an undamped system) as shown in Figure 6.1(d). This phenomenon was observed with p=1 and was related to the symmetry-breaking bifurcation [75-80].

To obtain the bifurcation set depicting the unstable zone in the F-Ω plane, one can define

$$\rho = (1-\Omega^2),\ \sigma = 2\ \zeta\ \Omega \text{ and } \sigma_p = 2\ \zeta_p\ \Omega^p\ \gamma_p \qquad (6.5)$$

and rewrite equation (6.3) as,

$$9\ \varepsilon^2\ A^6 + 24\ \rho\ \varepsilon\ A^4 + 16\ \rho^2\ A^2 + 16\ (\sigma\ A + \sigma_p\ A^p)^2 - 16\ F^2 = 0 \qquad (6.6)$$

So long as $\zeta=0$ the above equation is bi-cubic in A, for p=1,2 and 3. In these cases one can employ the condition for repeated roots of a cubic equation to get the loci of the turning points (the points of vertical tangencies in the response curve) in the F-Ω plane [74]. The bifurcation sets so obtained for p=1 and 2 are shown in Figures 6.2 and 6.3, respectively. It may be seen that the nature of the bifurcation set is similar in both the cases. It may be noted that in the soft system considered here (with $\varepsilon<0$), there is a limiting amplitude beyond which the spring loses its stiffness and the above results are not valid beyond that amplitude.

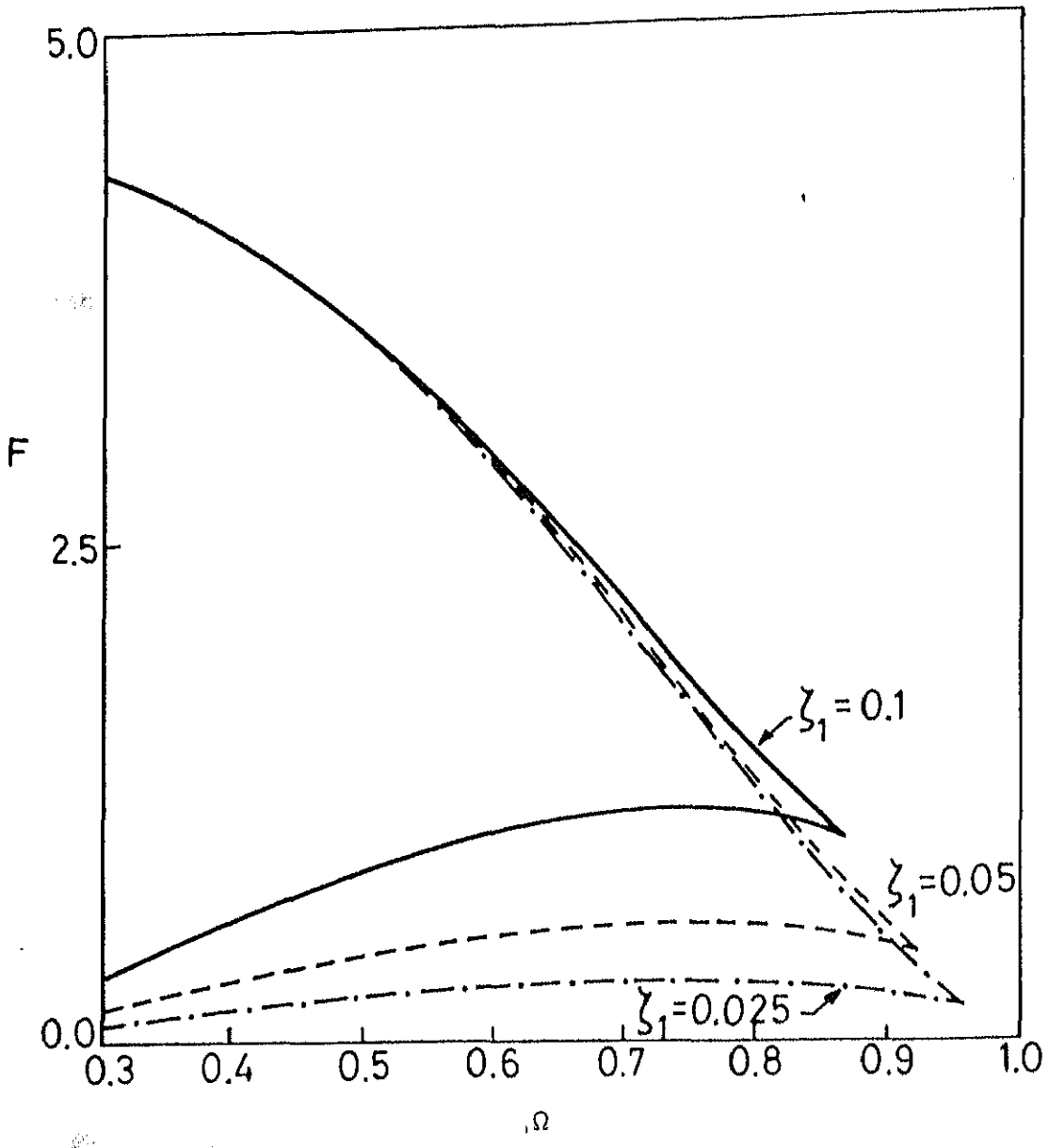

Figure 6.2 Bifurcation set of the harmonic solution with $\zeta=0$, $p=1$ and $\varepsilon= -0.01$

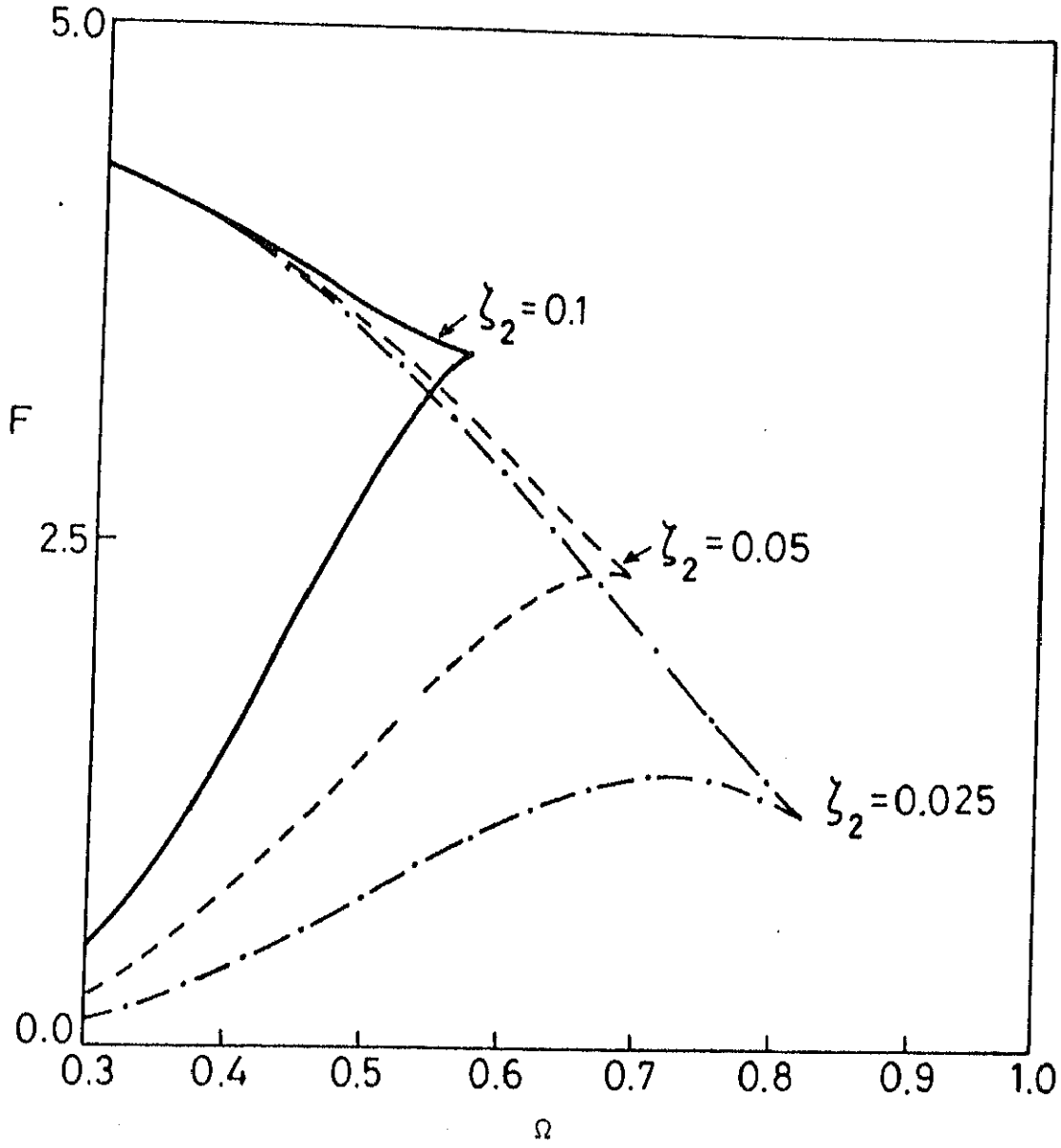

Figure 6.3 Bifurcation set of the harmonic solution with ζ=0, p=2 and ε= -0.01

6.3 Double-Well Potential Oscillator

Consider the following non-dimensional equation

$$\ddot{x} + 2\,\zeta\,\dot{x} + 2\,\zeta_p\,\dot{x}|\dot{x}|^{p-1} + \varepsilon(-x+x^3) = F\cos\Omega\tau,\ \varepsilon>0,\ p>0. \quad (6.7)$$

In this section we study the effects of ζ_p on the period-doubling bifurcation, for p=1, 2 and 3, using numerical simulation. Also an analytical criterion for the period-doubling bifurcation, based on the instability of the harmonic solution, is derived for combined linear and cubic damping ($\zeta\neq0$, p=3). Further, the Melinkov criterion has also been obtained for such combined damping.

6.3.1 Numerical simulation

Equation (6.7) is numerically integrated using Runge-Kutta-Merson method to investigate the role of damping exponent on the structure of the chaotic attractor. The Poincare maps of the chaotic attractors are shown in Figure 6.4 for various values of p. It can be seen from Figure 6.4 that the structure of the chaotic attractor is insensitive to the value of p. Numerical results (not presented here) suggest that both the period-doubling and intermittency routes to chaos observed with linear damping [38, 89] persist even in the presence of nonlinear damping. Though, the bifurcation structure is qualitatively similar for various values of p, the threshold values of the parameters at which the period-doubling bifurcation occurs depend on the values of both p and ζ_p. Table 6.1 shows the critical values of F required to generate a period 2 orbit with ζ=0, ε=1.0 and Ω=1.5.

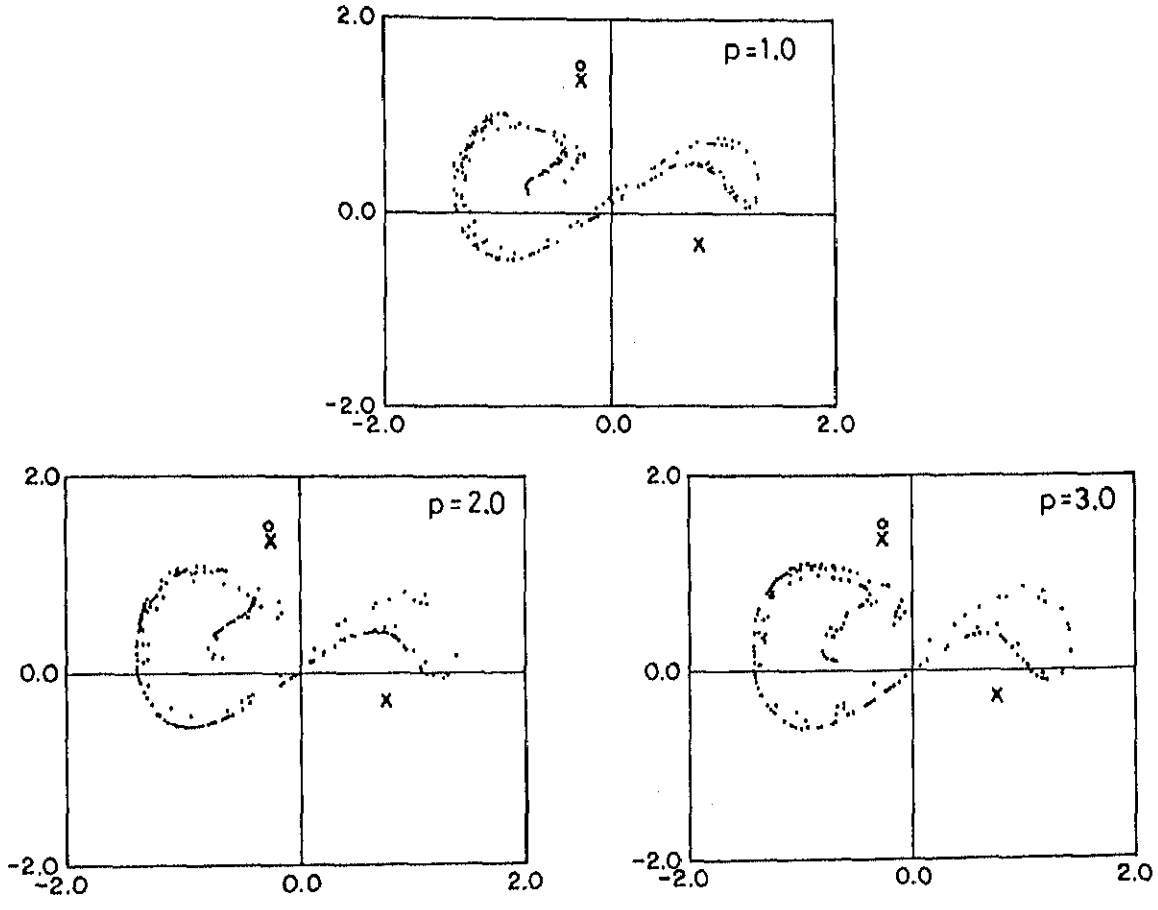

Figure 6.4 Stroboscopic maps of chaotic attractors with ζ=0, ζ_p=0.125, ε=1.0, F=0.4 and Ω=1.0

Table 6.1

ζ_p \ p	1	2	3
0.05	0.38	0.38	0.38
0.1	0.41	0.39	0.38
0.15	0.44	0.40	0.39
0.2	0.49	0.42	0.40
0.25	0.54	0.45	0.41

It can be observed from the above table that, for the same values of $\zeta_p (>0.05)$, the critical values of F decrease with increasing p. This feature is just opposite to what has been observed in the case of a hard, Duffing's oscillator (see chapter 3) where the critical values were seen to increase with increasing p.

6.3.2 Period-doubling criterion

A criterion is derived for the period-doubling bifurcation based on the instability of harmonic solution predicted by the classical stability analysis. Towards this end, we take $\varepsilon=1/2$ and p=3.0 in equation (6.7). Assuming the harmonic solution of equation (6.7) in the form

$$x = A_0 + A \cos(\Omega\tau - \phi) \tag{6.8}$$

and using the method of harmonic balance , we get the following expressions for A_0 and A:

$$A_0 = (2-3A^2)/2 \tag{6.9}$$

and $$(15/8)^2 A^6 - (15/4)(1-\Omega^2) A^4 + (1-\Omega^2)^2 A^2 + (2\zeta A\Omega + 3\zeta_3 A^3\Omega^3/2)^2 - F^2 = 0. \tag{6.10}$$

To analyse the stability of the solution given by equation (6.8), consider $x_0=x+\delta$, where δ is a small perturbation. Employing the usual variational procedure [36] one gets the following linear differential equation with coefficients varying periodically in time:

$$\ddot{\delta} + [\gamma_0+\gamma_1 \cos 2\Omega\tau]\,\dot{\delta} + [\lambda_0+\lambda_1\cos \Omega\tau +\lambda_2 \cos 2\Omega\tau]\,\delta = 0 \qquad (6.11)$$

where
$$\gamma_0 = 2\zeta + 2\zeta_3 A^2\Omega^2,$$
$$\gamma_1 = -3\zeta_3 A^2\Omega^2,$$
$$\lambda_0 = 3A_0^2/2 + 3A^2/4 - 1/2, \qquad (6.12)$$
$$\lambda_1 = 3A_0A,$$
and $$\lambda_2 = 3A^2/4.$$

Let us assume

$$\delta = \delta_{1/2} \cos [(\Omega\tau/2)+\vartheta] \qquad (6.13)$$

to get the first approximate solution for 1/2 subharmonic instability [78]. Substituting equation (6.13) in equation (6.11) and using the method of harmonic balance, one finds that for nontrivial solution, the following condition must be satisfied:

$$(\lambda_0-\Omega^2/4)^2 + (\zeta+3\zeta_3 A^2\Omega^2/2)^2\Omega^2 - \lambda_1^2/4 = 0 \qquad (6.14)$$

Equation (6.14) in conjunction with equation (6.10) determines the boundary of the period-doubling bifurcation in the F-Ω plane for combined linear and cubic damping. Figure 5 shows the results for linear (p=1) and cubic damping (p=3). These results have been obtained as special cases from the analysis presented above by assuming, in turn $\zeta_3=0$ and $\zeta=0$, respectively. It may be pointed out that the results for p=1 are in perfect agreement with those

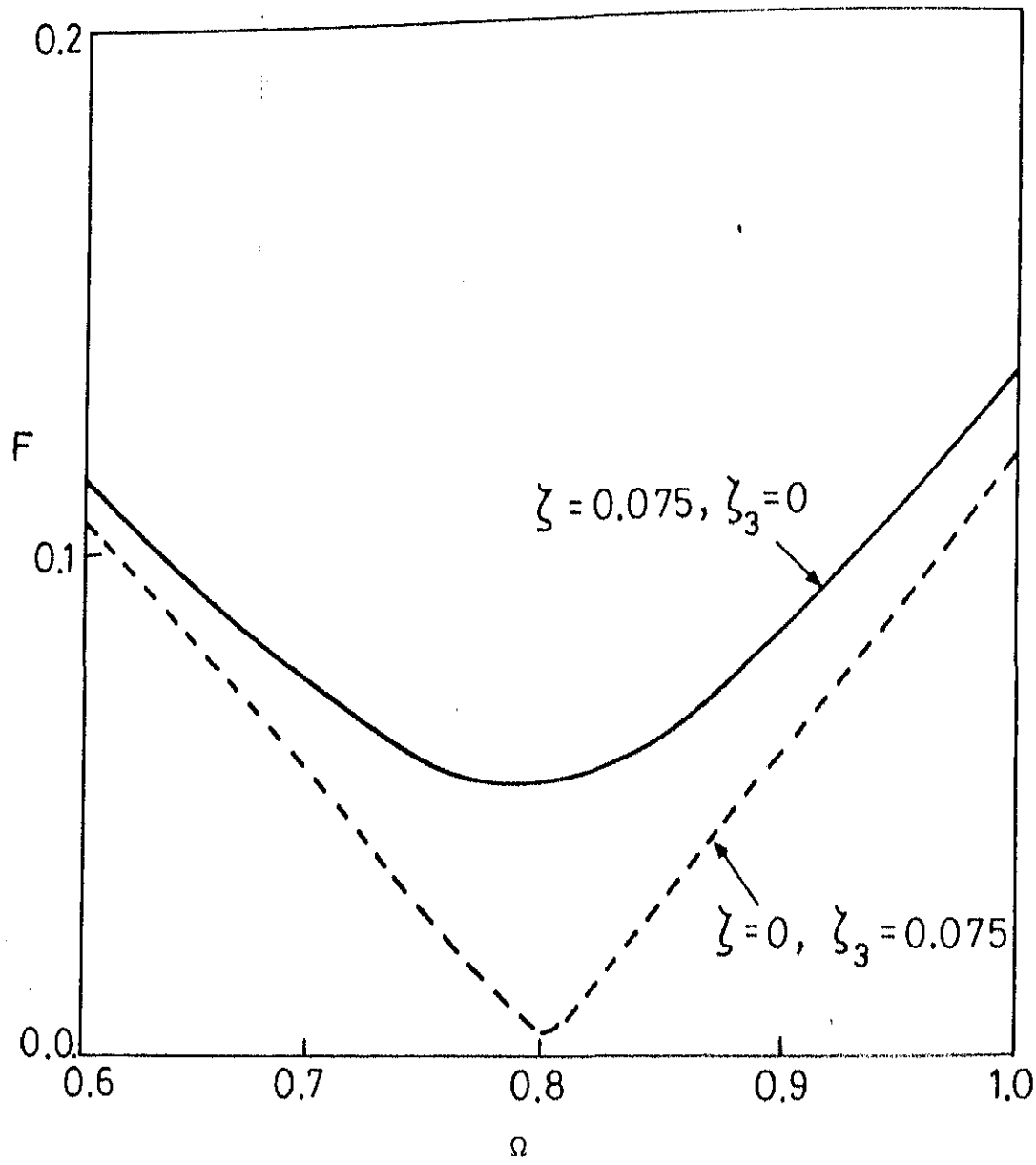

Figure 6.5 Period-doubling criterion with c=1/2

reported in reference [78]. It can be seen from Figure 6.5 that the excitation amplitude needed to generate the period-doubling bifurcation for p=3 is lower than that for p=1. So this trend is in conformity with the numerical results presented in Table 6.1.

6.3.3 Melinkov Criterion

The Melinkov criterion for the double-well potential oscillator has been obtained in the case of linear damping [43]. It has been pointed out that the Melinkov criterion depicts the occurence of fractal basin boundaries rather than the onset of chaos [44]. Following reference [43], the Melinkov criterion for combined linear and cubic damping has been obtained for ε=0.5 as

$$F = \left(\frac{8}{3}\,\zeta + 8\,\zeta_3 \int_{-\infty}^{\infty} \sec^4 ht\, \tan^4 ht\, dt\right) \frac{\cosh(\pi\Omega/2)}{\sqrt{2}\,\pi\Omega} \qquad (6.15)$$

Evaluating the integral in equation (6.15) one gets,

$$F = \left(\frac{8}{3}\,\zeta + \frac{32}{35}\,\zeta_3\right) \frac{\cosh(\pi\Omega/2)}{\sqrt{2}\,\pi\Omega} \qquad (6.16)$$

The coefficient of ζ_3 in the above equation is smaller than that of ζ. One can, thus, conclude that the fractal basin boundaries, just like the period-doubling bifurcation, occur for a lower value of F in the case of cubic damping as compared to linear damping (of course with $\zeta=\zeta_3$).

It should be noted that the present analysis can be easily extended to the case of a harmonically driven pendulum (with periodic potential) [76]. Following reference [50] it can be shown that for a driven pendulum the Melinkov criterion is obtained as

$$F = (8\,\zeta + \frac{128}{3}\,\zeta_3)\,\frac{\cos h(\pi\Omega/2)}{\pi} \qquad (6.17)$$

It is worthwhile to note the difference in the coefficients of ζ and ζ_3 in equations (6.16) and (6.17). For the driven pendulum (which is also a soft Duffing's oscillator), the critical value of F, predicted by the Melinkov criterion, is more for p=3 than that for p=1 with $\zeta=\zeta_3$. This is in contradiction to what has been just observed for the double-well potential oscillator.

6.4 Conclusions

A detailed investigation of the effects of strictly dissipative nonlinear damping on the harmonic response, bifurcation set and chaotic motion of harmonically driven soft Duffing's oscillators is carried out. Numerical results indicate that the structure of the chaotic attractor and the routes to chaos are quite insensitive to the value of the damping exponent p. A parametric study is reported to show the influence of the nonlinear damping on the onset of period-doubling route to chaos. An analytical criterion has been derived, in the presence of combined linear and cubic damping, to estimate the critical values of the excitation at which the period-doubling bifurcation takes place. The Melinkov criterion for such systems has also been obtained. These results indicate that the correct model of damping nonlinearity is important in accurate prediction of the onset of chaos.

CHAPTER 7

EXPERIMENTAL INVESTIGATIONS

7.1 Introduction

In this chapter, some preliminary experimental results are presented for a nonlinear vibration isolator made in the form of a hollow rubber tube. This isolator has softening type restoring force characteristics. The jump phenomenon has been observed in the experiments. The transmissibility characteristics of this system obtained experimentally indicate that the soft characteristics of the hollow rubber tube are beneficial for effective vibration isolation.

7.2 Experiment

The isolation system under consideration is shown in Figure 7.1. A hollow rubber tube (length=102mm, inner diameter=24mm, outer diameter=32mm and Hardness=40 IRHD) clamped to the projections in the top and bottom plates acts as the isolator. In addition to the internal damping of the rubber, provision is made to include two rubber pads with adjustable pressure which can provide additional damping as the top plate rubs against them. The static stiffness of the isolator is obtained from a compressive test carried out on a universal testing machine. The resulting force-displacement curve, shown in Figure 7.2, indicates a soft characteristic of the isolator at small deformation. However, as the load is increased further, the

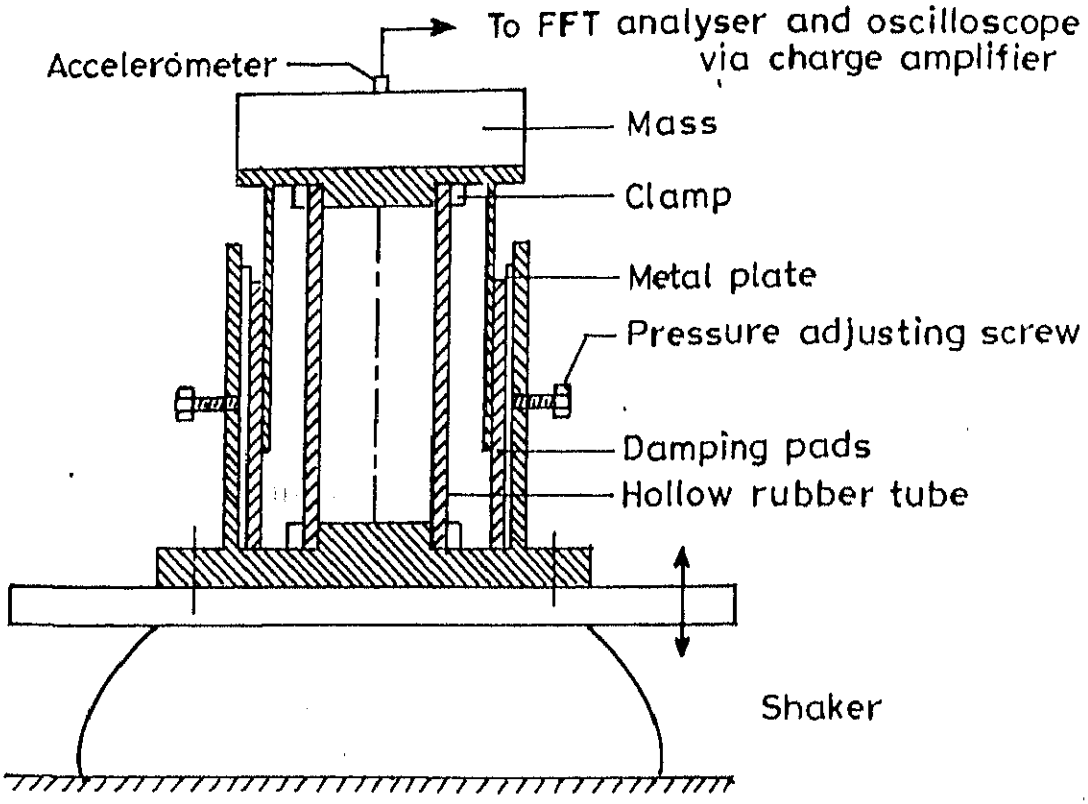

Figure 7.1 Experimental set-up

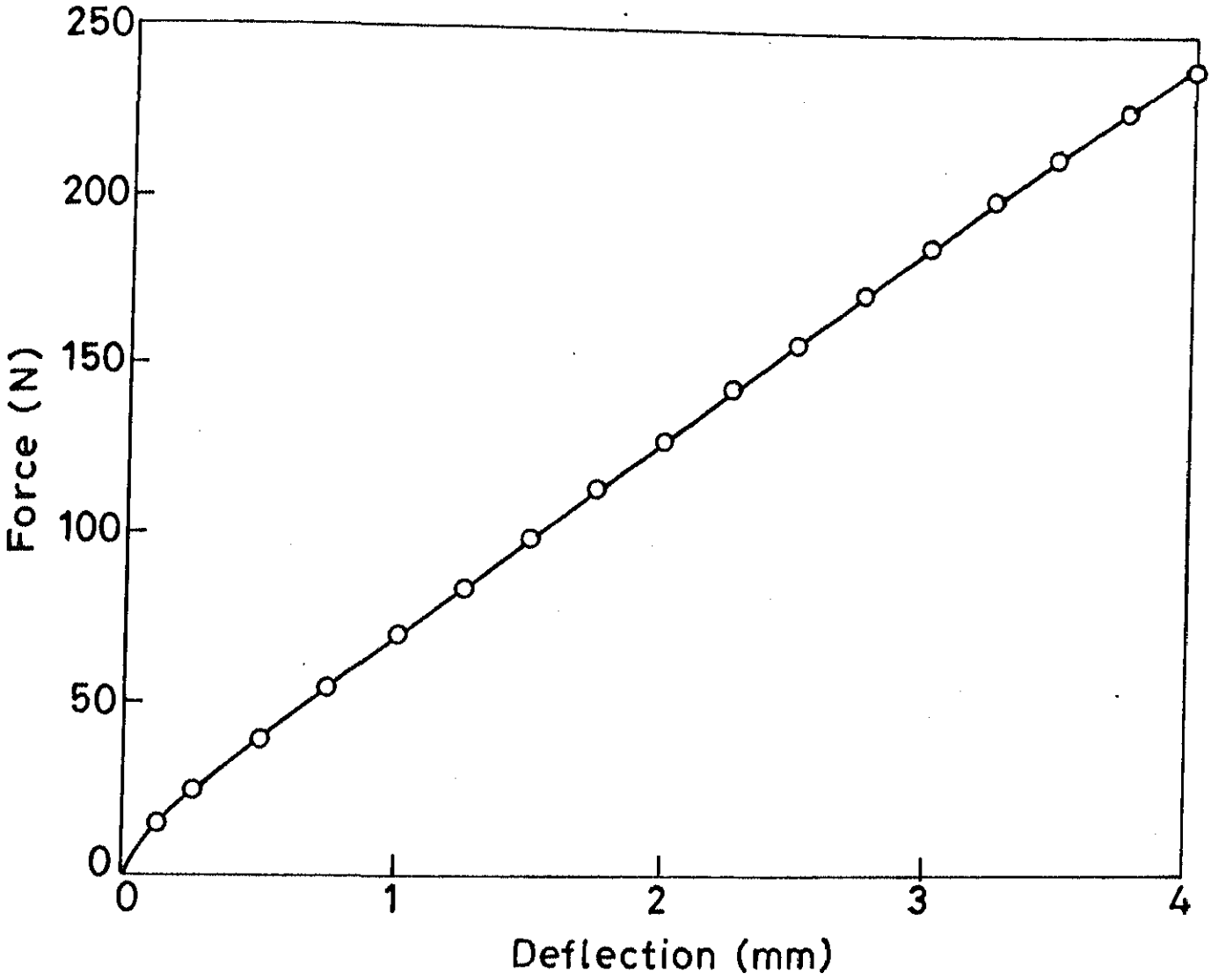

Figure 7.2 Stiffness characteristics

isolator has an almost linear stiffness characteristic.

In order to measure the transmissibility characteristics, the bottom plate of the isolator is clamped on to a mechanical shaker which provides a sinusoidal base excitation whose frequency and amplitude can be set to desired values. A mass (1.95 Kg) is fixed to the top plate of the isolator. The vibration of the mass is sensed by an accelerometer (B&K 4370), and the output signal is fed to a Digital storage oscilloscope and a H.P. real time spectrum analyser via a charge amplifier (B&K 2635) (see Figure 7.1).

The displacement transmissibility (T_d) is obtained as the ratio of the maximum displacement of the mass to the amplitude of the base excitation. The transmissibility values are obtained for both increasing and decreasing values of frequency. The results obtained are shown in Figures 7.3 and 7.4 for two different values of the base amplitude. The transmissibility curves are bent to the left clearly indicating the softening nature of the isolator. To depict the jump phenomenon clearly, the zone around the resonance is expanded as shown in Figures 7.5 and 7.6. It may be observed that as the base excitation is increased the jump region also increases as expected. Also the value of the frequency at which the maximum transmissibility occurs is shifted to a lower value (from 33.2 Hz to 28 Hz) and the value of the maximum transmissibility increases as the base excitation is increased.

A curious observation worth mentioning is that the transients are very long at the frequency when the jump occurs. This phenomenon is analogous to the case of a first order phase

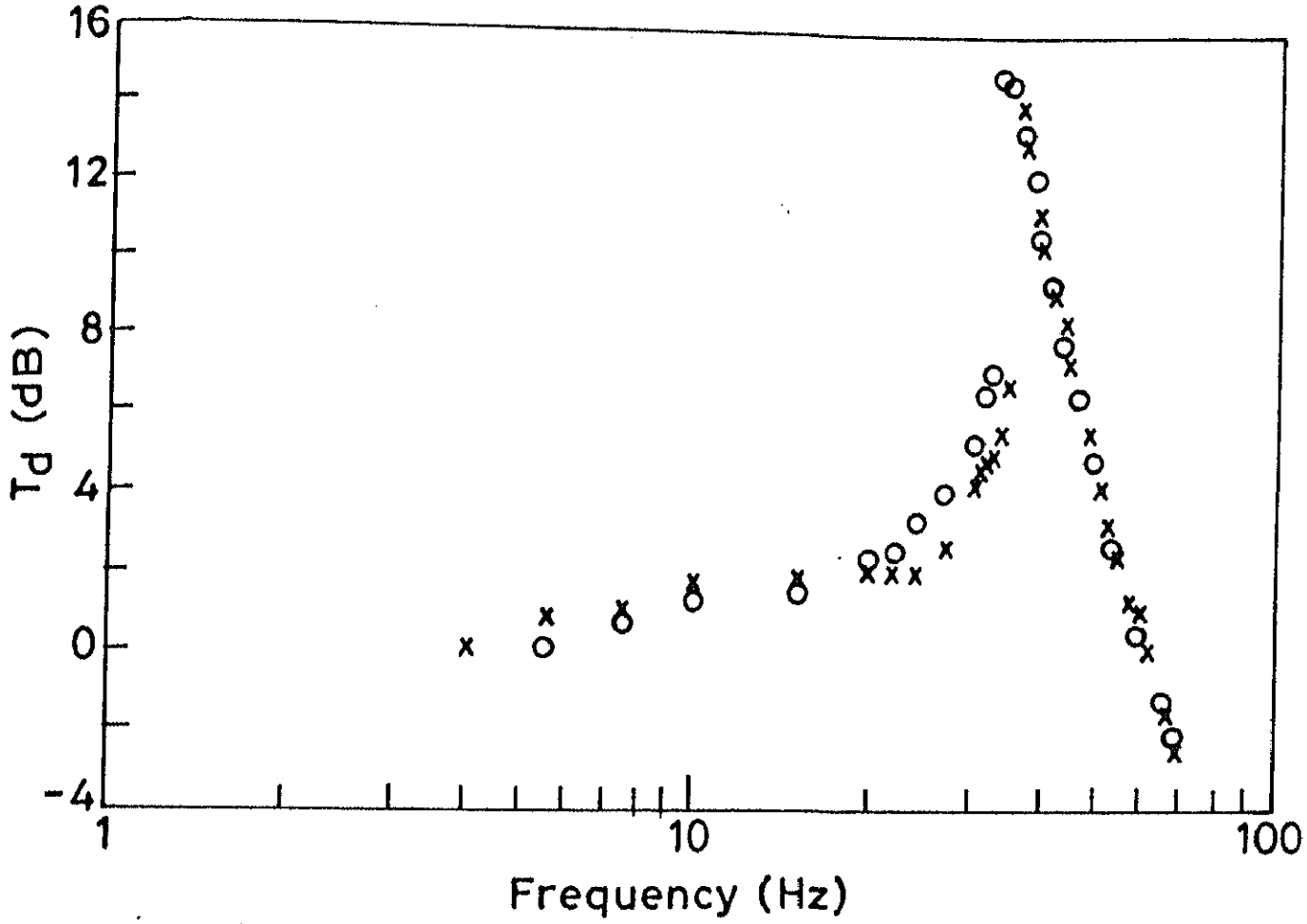

Figure 7.3 Variation of transmissibility with frequency with base amplitude = 0.28 mm. × × × Increasing frequency; o o o Decreasing frequency;

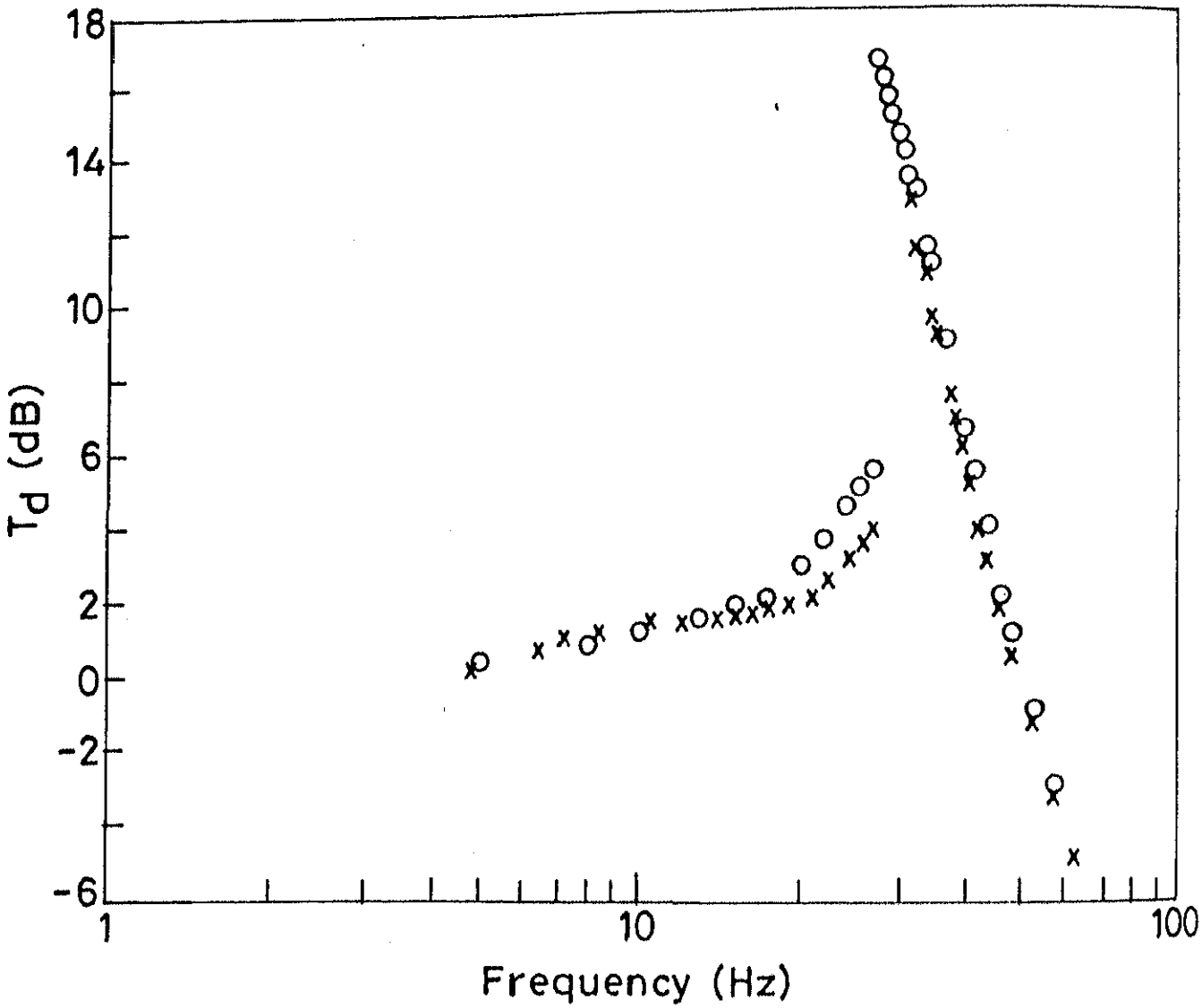

Figure 7.4 Variation of transmissibility with frequency with base amplitude = 0.625 mm. × × × Increasing frequency; o o o Decreasing frequency;

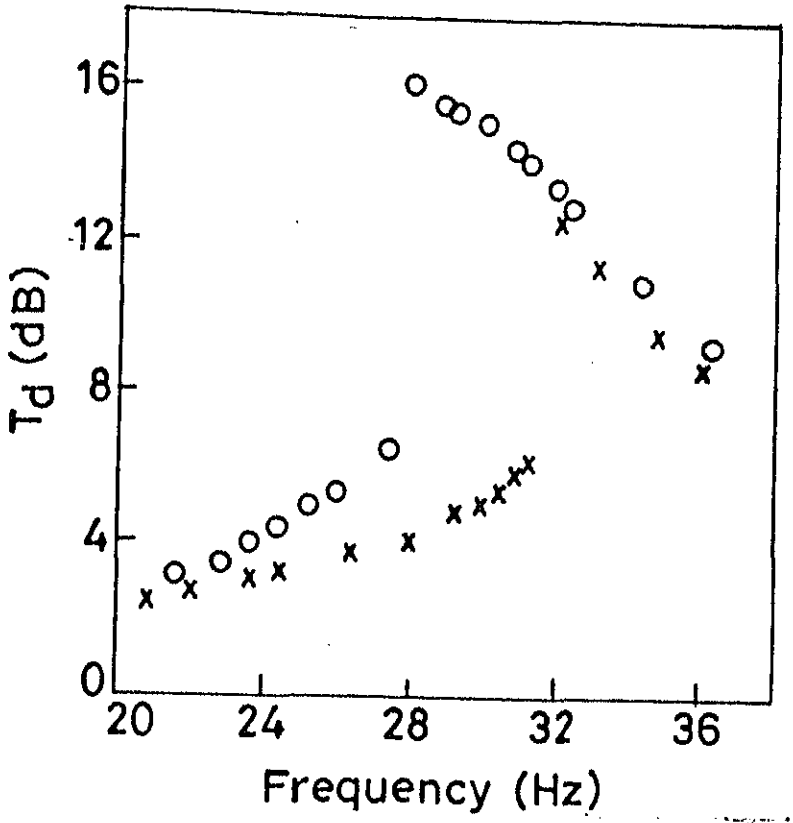

Figure 7.5 Jump phenomena with base amplitude = 0.28 mm. × × × Increasing frequency; o o o Decreasing frequency;

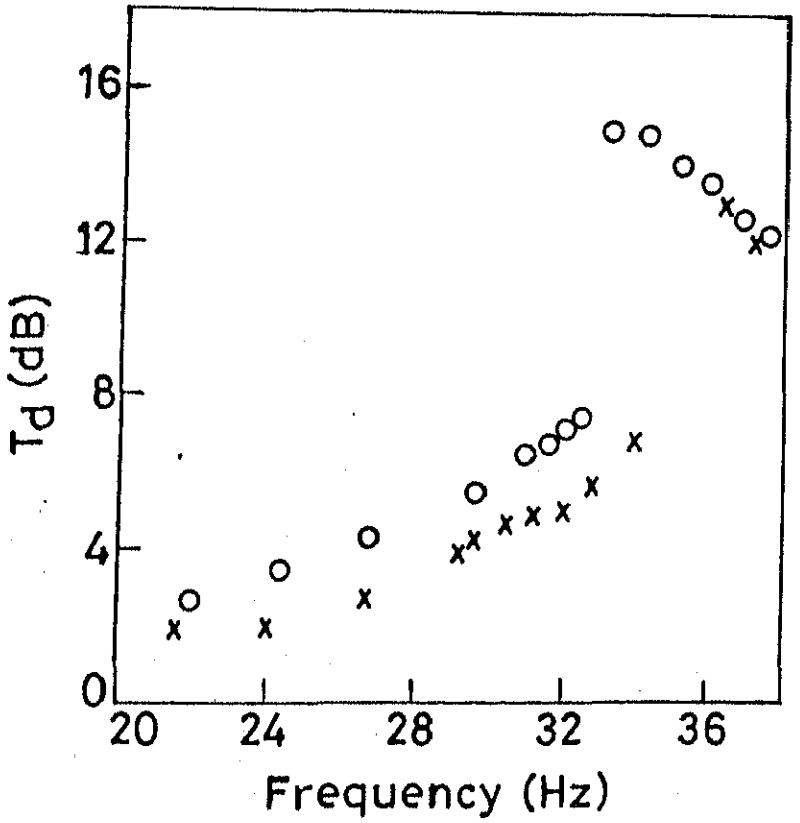

Figure 7.6 Jump phenomena with base amplitude = 0.625 mm. × × × Increasing frequency; o o o Decreasing frequency;

transition. It appears that the role of noise on the onset of bifurcation is the cause for these long transients. Another point to note is that the values of T_d obtained while decreasing the frequency are found to be more than those obtained while increasing frequency around the jump region. This could be attributed to the fact that due to the long transients mentioned above, there is a considerable increase in the temperature of the rubber isolator (with associated change in the property values) while decreasing frequency.

One important observation from the view point of vibration isolation is, that as the base amplitude is increased (Figures 7.3 and 7.4), the frequency at which T_d (in dB) becomes negative decreases substantially from 60 Hz to 49 Hz. This indicates that there is a substantial increase in both the operational frequency range and the high frequency attennuation rate due to the softening nature of the isolator. However, as mentioned above the maximum value of T_d is increased from 14.8 dB to 16.2 dB as the base excitation is increased. This increase in T_d can be offset by suitably increasing the damping. To see the effect of increasing the damping, two settings of the adjustable damping pads are used and the resulting transmissibility values are plotted in Figures 7.7 and 7.8. For both these settings of damping, the base amplitude is fixed at 0.625 mm. Comparing Figures 7.4, 7.7 and 7.8 it can be said that the increased damping eliminates the jump, reduces the maximum value of T_d and increases the frequency at which T_d (in dB) becomes negative. As expected, the high frequency attennuation rate is poorer with higher damping. But a suitable

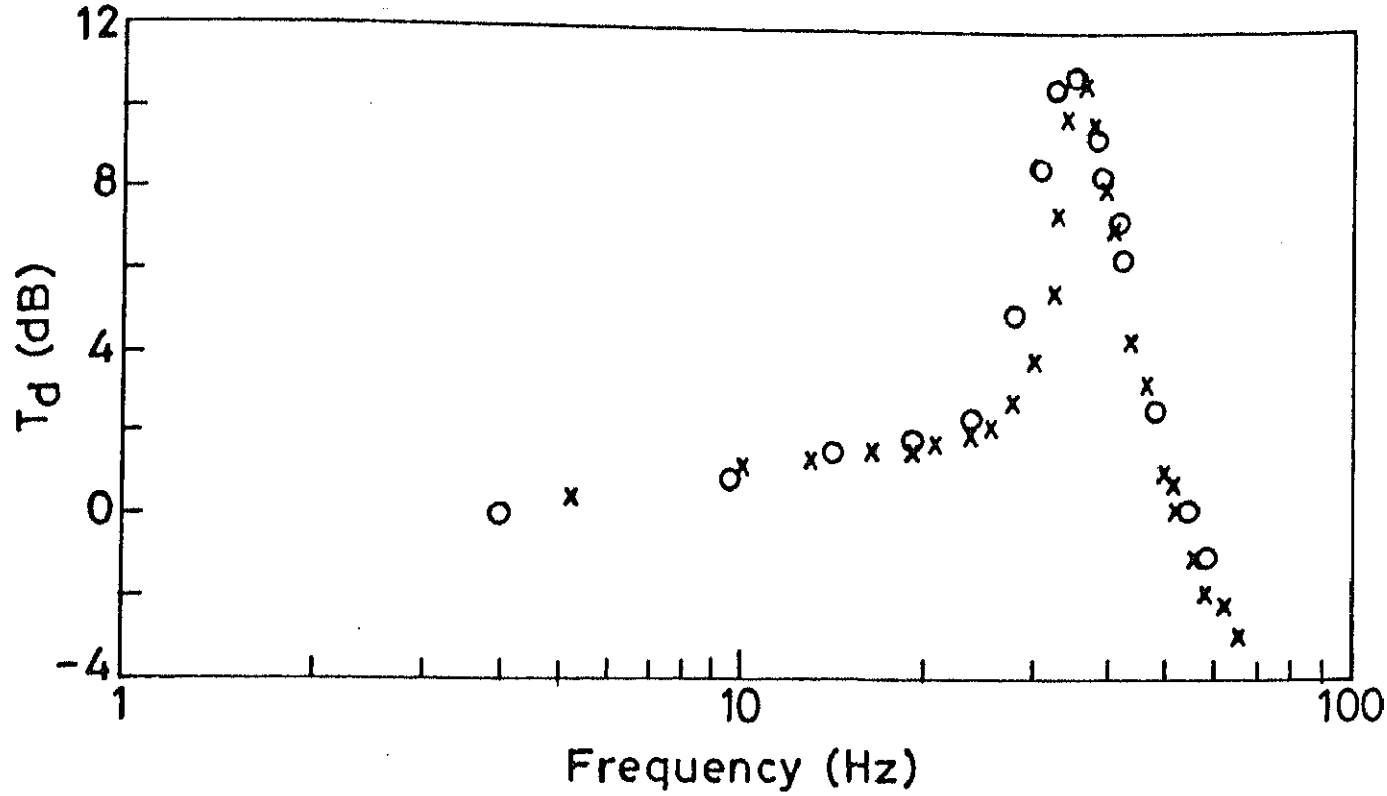

Figure 7.7 Variation of transmissibility with frequency with base amplitude = 0.625mm and increase in damping. × × × Increasing frequency; o o o Decreasing frequency;

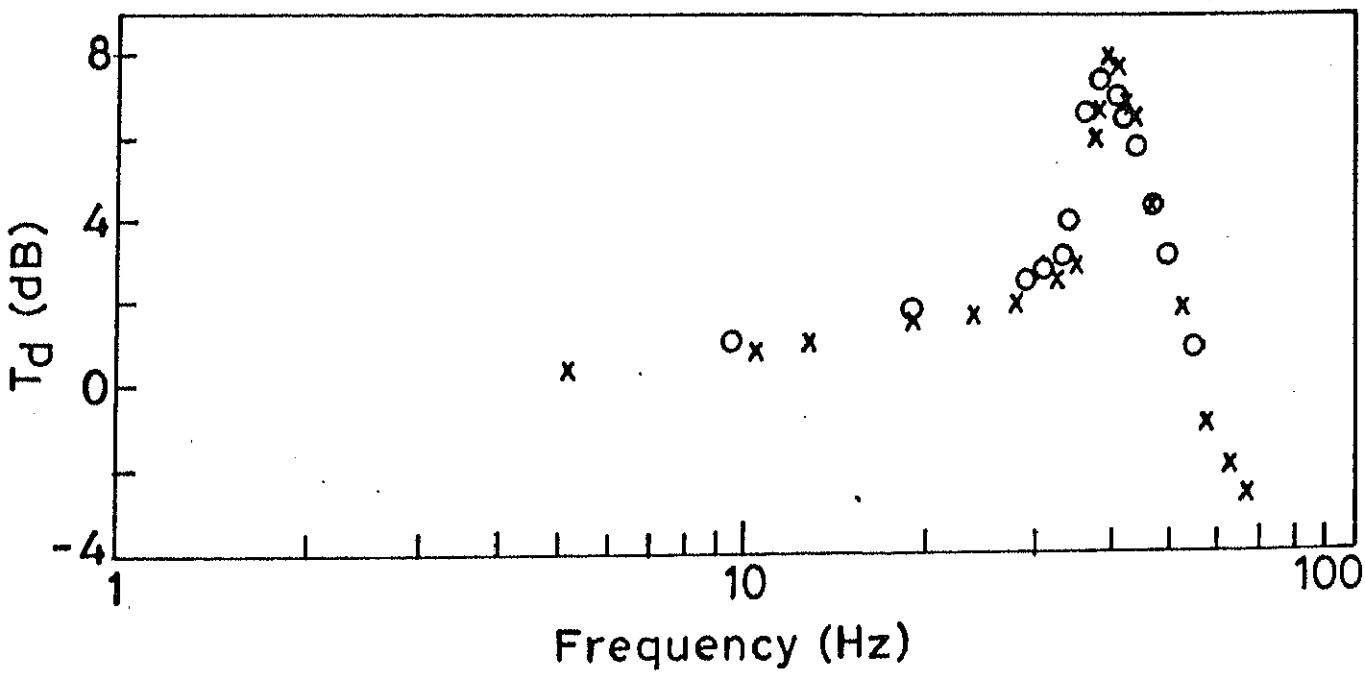

Figure 7.8 Variation of transmissibility with frequency with base amplitude = 0.625 mm and further increase in damping. × × × Increasing frequency; o o o Decreasing frequency;

combination of a soft nonlinear spring and the optimum value of damping can yield a better design than the linear isolator.

The Fourier spectrum of the response of the isolator is obtained by feeding the signal to a real time spectrum analyser. As the base amplitude is increased, a 3/4 subharmonic appears in the response as shown in Figure 7.9. At some other excitation frequency with the same base amplitude, a 1/2 subharmonic is also revealed as shown in Figure 7.10. However, no further bifurcations could be observed with this level of excitation.

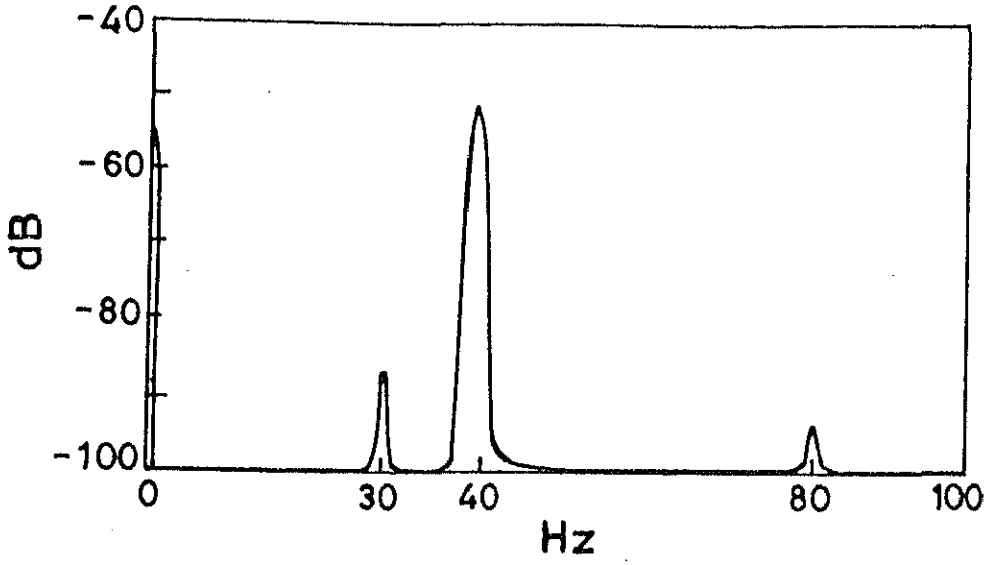

Figure 7.9 Fourier spectrum of 3/4 subharmonic with base amplitude = 1.25 mm.

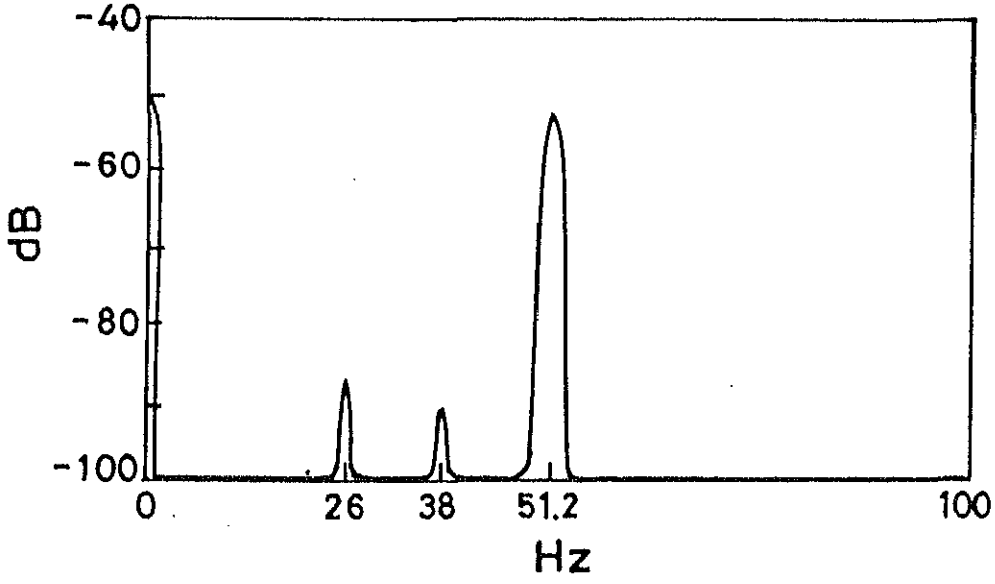

Figure 7.10 Fourier spectrum of 1/2 subharmonic with base amplitude = 1.25 mm.

CHAPTER 8

CONCLUSIONS

In the present thesis, harmonic and chaotic responses of a single degree-of-freedom vibration isolation system with nonlinearity in both stiffness and damping have been studied. While the method of harmonic balance has been used to obtain the harmonic response, the chaotic responses are investigated through numerical simulation. Both force- and base-excited systems have been considered. Also special attention is paid to understand the role of strictly dissipative nonlinear damping in the chaotic dynamics of such systems. The main conclusions that can be drawn from this work are summarised below:

1. Detailed performance characteristics of nonlinear vibration isolators presented as transmissibility vs frequency plots suggest that, an isolator with a soft characteristic is superior to that with a hard characteristic. With increasing damping index p, the jump width reduces and consequently the unstable zone becomes narrower. It is seen that, for the parameter values considered, an isolator with an asymmetric restoring force may not perform satisfactorily for base excitation.

2. It is shown that both the period-doubling and intermittency routes to chaos occur for all values of p, thus preserving the bifurcation structure of a linearly damped, Duffing's oscillator. It is pointed out that nonlinear damping can be effectively used

for controlling chaos.

3. An anomalous jump in the response of a base-excited, hard Duffing-type vibartion isolator with combined Coulomb and viscous damping is shown to exist when the method of harmonic balance is used. This is also confirmed by direct numerical integration.

4. It is shown that with a suitable choice of Coulomb damping one can maintain the transmissibility at or less than unity over the entire frequency range even for a nonlinear system under base-excitation.

5. It has been demonstrated by numerical simulation, that the instabilities, associated with the secondary resonances and chaotic motion, encountered in the low frequency regime can be eliminated by using a suitably designed friction damper. The bifurcation structure of a force-excited, hard system seems to be unaltered by the addition of friction damping.

6. With the same value of the damping coefficient, the threshold values of forcing required to cause period-doubling bifurcation are seen to decrease with increasing p in the case of a double-well potential oscillator. This feature is just opposite to what has been observed in the case of a hard, Duffing's oscillator where the critical excitation values are seen to increase with increasing p.

7. Experimental results indicate that a suitable combination of a soft nonlinear spring and the optimum value of the damping can yield a better design than a linear isolator.

8.1 Suggestions for future work

The following directions may be taken up to extend the work carried out in the present thesis:

1. The stability analysis of isolators with Coulomb damping should be expanded to include the stick-slip phenomena. Also more realistic models of Coulomb damping with variable friction force need to be considered.

2. The emphasis of the experiment carried out in the present work is to obtain a qualitative understanding of a soft isolator subjected to a base excitation. No attempt is made to model the isolator and obtain the quantitative predictions. A detailed modelling of the damping phenomena needs to be carried out. Also the design of friction damper to exploit the break-loose phenomena in the case of base excitation needs to be examined.

3. Characterisation of the chaotic attractor via Liapunov exponents, fractal dimensions and entropies also deserves attention.

REFERENCES

1. C.E. CREDE 1951 Vibration and Shock Isolation, NewYork: Wiley.
2. C.M. HARRIS and C.E. CREDE 1976 Shock and Vibration Handbook (2nd edition), NewYork: McGraw-Hill Book Company, Inc.
3. A. K. MALLIK 1990 Principles of Vibration Control, New Delhi: Affliated East-West Press Pvt Ltd.
4. J.C. SNOWDON 1968 Vibration and Shock in Damped Mechanical Systems, New York: John Wiley and Sons, Inc.
5. J.C. SNOWDON 1979 Journal of Acoustical Society of America 66, p1245. Vibration isolation: use and characterisation.
6. J. A. MACINANTE 1984 Seismic Mountings for Vibration Isolation, New York: John Wiley and Sons, Inc.
7. E. I. RIVIN 1979 Transactions of ASME, Journal of Mechanical Design 101, p682. Principles and criteria for vibration isolation of machinery.
8. H. G. D. GOYDER and R. G. WHITE 1980 Journal of Sound and Vibration 68, p97. Vibrational power flow from machines into builtup structures, Part III.
9. R. J. PINNINGTON and R. G. WHITE 1981 Journal of Sound and Vibration 75, p179. Power flow through machine isolators to resonant and nonresonant beams.
10. J. A. GOLINSKI 1977 Transactions of ASME, Journal of Engineering for Industry 199, p24. On some problems associated with vibration isolation of ship machinery.
11. E. E. UNGAR and C. W. DIETRICH 1966 Journal of Sound and Vibration 4, p224. High frequency vibration isolation.
12. M. L. MUNJAL 1975 Journal of Sound and Vibration 39, p247. A rational synthesis of vibration isolators.

13. S. A. PAIPETIS and A. F. VAKAKIS 1985 Journal of Sound and Vibration 98, p13. A method of analysis for unidirectional vibration isolators with many degrees of freedom.

14. J. C. SNOWDON 1971 Journal of Sound and Vibration 15, p307. Mechanical four-pole parameters and their applications.

15. A. F. VAKAKIS 1985 Journal of Sound and Vibration 103, p25. Dynamic analysis of a unidirectional periodic isolator, consisting of identical masses and intermediate distributed resilient blocks.

16. B. RAVINDRA and A. K. MALLIK 1992 Journal of Sound and Vibration 154, p249. Harmonic vibration isolation characteristics of periodic systems.

17. R. J. PINNINGTON 1987 Journal of Sound and Vibration 118, p515. Vibration power transmission to a seating of a vibration isolated motor.

18. M. G. SAINSBURY and D. J. EWINS 1974 Transactions of ASME, Journal of Engineering for Industry 96, p1000. Vibration analysis of a damped machinery foundation structure using the dynamic stiffness coupling technique.

19. H. WAGNER 1965 ZAMP 16, p327. On the concept of transmissibility for randomly excited elastic structures.

20. B. RAVINDRA 1989 M. Tech. Thesis. IIT Kanpur. Vibration isolation of finite-impedance foundations by parallel rubber mountings.

21. M.L. TINKER and M.A. CUTCHINS 1992 Journal of Sound and Vibration 157, p7. Damping phenomena in a wire rope vibration isolation system.

22. J.E. RUZICKA and T.F. DERBY 1971 Influence of Damping in Vibration Isolation, Washington: The Shock and Vibration Information Center.

23. C.L. KIRK 1988 Journal of Sound and Vibration 124, p157. Nonlinear random vibration isolators.

24. A. MURATA et al. 1987 Journal of Sound and Vibration 112, p31. Application of catastrophe theory to forced vibration of a diaphragm air spring.

25. S.M. METWALLI 1986 Transactions of ASME, Journal of Mechanism, Transmission and Automation in Design 108, p197. Optimum nonlinear suspension systems.

26. N. C. HILYARD 1985 Journal of Sound and Vibration 101, p593. Response of a vibration isolator with distributed nonlinear stiffness at large excitations.

27. M. F. BEATTY 1984 Transactions of ASME, Journal of Applied Mechanics 51, p361. Finite amplitude vibrations of a body supported on simple shear bushings.

28. M. F. BEATTY 1988 Journal of Elasticity 20, p203. Finite amplitude, periodic motion of a body supported by arbitrary isotropic, elastic shear mountings.

29. M. F. BEATTY 1989 International Journal of Non-linear Mechanics 24, p65. Stability of a body supported by a simple vehicular shear suspension system.

30. J. A. HARRIS 1989 Rubber Chemistry and Technology 62, p515. Design principles for vibration isolation and damping with elastomers including nonlinearity.

31. A. D. ROBERTS (Ed) 1988 Natural Rubber Science and Technology, Oxford: Oxford University Press.

32. I. J. BUSCH-VISHNIAC 1987 Journal of Acoustical Society of America 81, p1801. Fundamental problem with mobility analysis of vibration isolation systems.

33. C. KNOSPE and P. ALLAIRE 1990 Journal of Spacecraft 27, p642. Limitations on vibration isolation for microgravity space experiments.

34. A. SINHA and Y. P. WANG 1993 Transactions of ASME, Journal of Vibration and Acoustics 115, p256. Digital control algorithms for microgravity isolation systems.

35. B.RAVINDRA and A.K. MALLIK 1994 Journal of Sound and Vibration (To be published in 1994). Performance of nonlinear vibration isolators under harmonic excitation.

36. J.J. STOKER 1950 Nonlinear Vibrations, New York: Interscience Publishers, 1961 Fourth printing.

37. C. HAYASHI 1985 Nonlinear Oscillations in Physical Systems. Princeton: Princeton University Press.

38. A. H. NAYFEH AND D.T. MOOK 1979 Nonlinear Oscillations, New York: Wiley.

39. P. HAGEDORN 1981 Nonlinear Oscillations. Oxford University Press.

40. W. SZEMPLINSKA-STUPNICKA 1990 The behaviour of Nonlinear Vibratory systems vol I and II, Netherlands, Kluwer Academic Publishers.

41. J.B.ROBERTS and P.D. SPANOS 1990 Random Vibration and Statistical Linearisation, Chichester, John Wiley.

42. D.W. JORDAN and P. SMITH 1987 Nonlinear Ordinary Differential Equations, Oxford: Clarendon Press.

43. J. GUCKENHEIMER and P. J. HOLMES 1983 Nonlinear Oscillations, Dynamical Systems and Bifurcation of Vector Fields, New York: Springer.

44. F. C. MOON 1992 Chaotic and Fractal Dynamics, New York: John Wiley and Sons.

45. P.BERGE', Y. POMEAU and C. VIDAL 1984 Order within Chaos, Paris: Hermann and John Wiley & Sons, Inc.

46. H.G. SCHUSTER 1984 Deterministic Chaos, D-6940 Weinheim, (Federal Republic of Germany), Physik-Verlag GmbH.

47. J. M. T. THOMPSON and H. B. STEWART 1986 Nonlinear Dynamics and Chaos, Geometric Methods for Engineers and Scientists, New York: John Wiley and Sons.

48. P. J. HOLMES and F. C. MOON 1983 Transactions of ASME, Journal of Applied Mechanics 50, p1021. Strange attractors and chaos in nonlinear mechanics.

49. P. J. HOLMES 1990 Applied Mechanics Reviews 43, ps23. Nonlinear dynamics, chaos and mechanics.

50. P. HOLMES 1989 in Proceedings of Symposia in Applied Mathematics, American Mathematical Society, 39, p25.

51. A. H. NAYFEH AND A.A. KHDEIR 1986 International Ship Building Progress 33, p40. Nonlinear rolling of ships in regular beam seas.

52. J.M.T. THOMPSON et al. 1990 Philosophical Transactions of Royal Society London Ser A 332, p149. Stability criteria based on chaotic transients from incursive fractals.

53. Y.UEDA 1979 Journal of Statistical Physics 20, p181. Randomly transitional phenomena in the systems governed by Duffing's equation.

54. Y.UEDA 1980 Annals of the New York Academy of Sciences 357, p422. Explosions of strange attractors exhibited by Duffing's equation.

55. Y.UEDA 1981 New Approaches to Nonlinear Problems in Dynamics. SIAM, Philadelphia 1980. Steady motions exhibited by *Duffing's equation*: a picture book of regular and chaotic motions.

56. S. NOVAK and R.G. FREHLICH 1982 Physical Review A 26, p3660. Transition to chaos in the Duffing oscillator.

57. B. A. HUBERMAN, J. P. CRUTCHFIELD 1979 Physical Review Letters 43, p1743. Chaotic states of anharmonic systems in periodic fields.

58. J. P. CRUTCHFIELD and B. A. HUBERMAN 1980 Physics Letters 77A, p407. Fluctuations and the onset of chaos.

59. K. WIESENFELD et al. 1984 Physical Review A 29, p2102. Calculation of period doubling in a Josephson circuit.

60. K. WIESENFELD 1985 Physical Review A 32, p1744. Virtual Hopf phenomenon: A new precursor of period-doubling bifurcations.

61. J.SWIFT and K. WIESENFELD 1984 Physical Review Letters 52, p705. Suppression of period doubling in symmetric systems.

62. U. PARLITZ and W. LAUTERBORN 1985 Physics Letters 107A, p351. Superstucture in the bifurcation set of the Duffing equation.

63. U. PARLITZ and W. LAUTERBORN 1986 Z. Naturforsch. 41a, p605. Resonances and torsion numbers of driven dissipative nonlinear oscillators.

64. C. SCHEFFCZYK et al. 1991 Physical Review A 43(12). Comparision of bifurcation structures of driven dissipative nonlinear oscillators.

65. U. PARLITZ et al. 1991 International Series of Numerical Mathematics 97, p283. Two-dimensional maps modelling periodically driven strictly dissipative oscillators.

66. U. PARLITZ et al. 1991 International Journal of Bifurcation and Chaos 1, p261. On modelling driven oscillators by maps.

67. T. FANG and E.H. DOWELL 1987 International Journal of Non-linear Mechanics 22, p401. Numerical simulations of periodic and chaotic responses in a stable Duffing system.

68. C.S. WANG et al. 1992 Physical Review A 45, p3471. Potential dependence of the bifurcation structure in generalised Duffing oscillators.

69. W. SZEMPLINSKA-STUPNICKA and J. BAJKOWSKI 1986 International Jounal of Non-linear Mechanics 21, p401. The 1/2 subharmonic resonance and its transition to chaotic motion in a nonlinear oscillator.

70. W. SZEMPLINSKA-STUPNICKA 1987 Journal of Sound and Vibration 113, p155. Secondary resonances and approximate models of routes to chaotic motion in nonlinear oscillators.

71. W. SZEMPLINSKA-STUPNICKA and P. NIEZGODZKI 1990 Journal of Sound and Vibration 141, p181. The approximate approach to chaos phenomena in oscillators having single equilibrium position.

72. K. MAGNUS 1965 Vibrations. London: Blakie & Son Limited.

73. F. DINCA and C. TEODOSIU 1973 Nonlinear and Random Vibrations, New York and London: Academic Press Inc.

74. P. J. HOLMES and D. A. RAND 1976 Journal of Sound and Vibration 44, p237. The bifurcation of Duffing's equation: An application of catastrophe theory.

75. J. MILES 1988 Physics Letters 130A, p276. Resonance and Symmetry breaking for a nonlinear oscillator.

76. J. MILES 1988 Physica D 31, p252. Resonance and symmetry breaking for the pendulum.

77. W. SZEMPLINSKA-STUPNICKA 1988 International Journal of Non-linear Mechanics 23, p257. Bifurcations of harmonic solution leading to chaotic motion in the softening type Duffing's oscillator.

78. K. R. ASFAR and K.K. MASOUD 1992 Transactions of ASME, Journal of Vibration and Acoustics 114, p489. On the period-doubling bifurcations in the Duffing's oscillator with negative linear stiffness.

79. A. Y. T. LEUNG 1991 Journal of Sound and Vibration 149, p147. Rigorous studies of a Duffing oscillator.

80. R. VAN DOOREN 1992 Journal of Sound and Vibration 153, p368. Reply to A. Y. T. Leung: Rigorous studies of a Duffing oscillator.

81. A. B. PIPPARD 1989 The Physics of Vibration. Cambridge: Cambridge university press.

82. P. C. WRAIGHT 1971 Philosophical Magazine 23, p1261. Mechanical effects in flux motion.

83. P. H. KES et al. 1990 Physical Review Letters 64, p1063. Dissipation in highly anisotropic superconductors.

84. A. O. CALDEIRA and A. J. LEGGETT 1983 Annals of Physics (N.Y.) 149, p374. Quantum tunnelling in a dissipative system.

85. R. LANDAUER 1989 in Selected Topics in Signal Processing, S.Haykin, ed. Prentice Hall, Englewood Cliffs, NJ.

86. S. SMALE 1980 The Mathematics of Time: essays on dynamical systems, Economic processes and related topics. New York: Springer-Verlag.

87. J. MILNOR 1985 Communications of Mathematical Physics 99, p177. On the concept of an attractor.

88. S. H. CRANDALL 1970 Journal of Sound and Vibration 11, p3. The role of damping in vibration theory.

89. B. RAVINDRA and A. K. MALLIK 1994 Journal of Sound and Vibration (submitted). Chaotic response of a harmonically excited mass on an isolator with nonlinear stiffness and damping characteristics.

90. B. RAVINDRA and A. K. MALLIK 1994 Physical Review E (Accepted). Role of nonlinear dissipation in soft Duffing oscillators.

91. J. P. DEN HARTOG 1931 Transactions of the ASME 53, p107. (APM-53-9). Forced vibrations with combined Coulomb and viscous friction.

92. M. S. HUNDAL 1979 Journal of Sound and Vibration 64, p371. Response of a base excited system with Coulomb and viscous friction.

93. R. PARNES 1984 Journal of Sound and Vibration 94, p469. Response of an oscillator to a ground motion with Coulomb friction slippage.

94. T. K. PRATT and R. WILLIAMS 1981 Journal of Sound and Vibration 74, p531. Nonlinear analysis of stick-slip motion.

95. S. W. SHAW 1986 Journal of Sound and Vibration 108, p305. On the dynamic response of a system with dry friction.

96. N. MAKRIS and M. C. CONSTANTINOU 1991 Mechanics of Structures and Machines 19, p477. Analysis of motion resisted by friction.I. constant Coulomb and linear/Coulomb friction.

97. E. H. DOWELL 1983 Journal of Sound and Vibration 89, p65. The behaviour of a linear damped modal system with a nonlinear spring-mass-dry friction damper system attached.

98 . A. A. FERRI and E. H. DOWELL 1985 Journal of Sound and Vibration 101, p55. The behaviour of a linear damped modal system with a nonlinear spring-mass-dry friction damper system attached, part II.

99. C. PIERRE, A. A. FERRI and E. H. DOWELL 1985 Transactions of ASME, Journal Of Applied Mechanics 52, p958. Multi-Harmonic analysis of dry friction damped systems using an incremental harmonic balance method.

100. J. AWREJCEWICZ 1986 Journal of Sound and Vibration 109, p178. Chaos in simple mechanical systems with friction.

101. S. NARAYANAN and K. JAYARAMAN 1991 Journal of Sound and Vibration 146, p17. Chaotic vibration in a non-linear oscillator with Coulomb damping.

102. J. AWREJCEWICZ and J. DELFS 1990 European Journal of Mechanics A/solids 9, p269. Dynamics of a self-excited stick-slip oscillator with two degrees of freedom Part I: Investigation of equilibria.

103. J. AWREJCEWICZ and J. DELFS 1990 European Journal of Mechanics A/solids 9, p397. Dynamics of a self-excited stick-slip oscillator with two degrees of freedom Part II: slip-stick, slip-slip, stick-slip tranisitions, periodic and chaotic orbits.

104. E. REITHMEIER 1991 Periodic Solutions of Nonlinear Dynamical systems. Lecture Notes in Mathematics 1483. Berlin: Springer-Verlag.

105. B. RAVINDRA and A. K. MALLIK 1993 International Journal of Non-linear Mechanics 28, p427. Hard Duffing-type vibration isolator with combined Coulomb and viscous damping.

106. B. RAVINDRA and A. K. MALLIK 1994 Journal of Sound and Vibration (submitted). Chaotic response of a hard Duffing-Type vibration isolator with combined Coulomb and viscous damping.

107. R. LANGRETH 1991 (May) Science 252, p776. Engineering dogma gives way to chaos.

108. E. OTT, C. GREBOGI and J. A. YORKE 1990 Physical Review Letters 64, p1196. Controlling chaos.

109. W. L. DITTO, S. N. RAUSEO and M. L. SPANO 1990 Physical Review Letters 65, p3211. Experimental control of chaos.

110. T. K. CAUGHEY 1963 Journal of Acoustical Society of America 35, p1706. Equivalent linearization techniques.

111. D. CAPECCHI and F. VESTRONI 1990 International Journal of Non-linear Mechanics 25, p309. Periodic response of a class of hysteretic oscillators.

112. B.RAVINDRA and A.K. MALLIK 1994 Journal of Sound and Vibration (To be published in 1994). Stability analysis of a nonlinearly damped Duffing oscillator.

113. S.N. CHOW AND J.K. HALE 1982 Methods of Bifurcation Theory, New York: Springer-Verlag.

114. Y.H. KAO, C.S. WANG AND T.H. YANG 1992 Journal of Sound and Vibration 159, p13. Influences of harmonic coupling on bifurcations in Duffing Oscillator with bounded potential well.

115. S.F. MASRI AND T.K. CAUGHEY 1966 Transactions of A.S.M.E. Journal of Applied Mechanics 33, p586.. On the stability of impact damper.

116. S. PRADEEP AND S.K. SHRIVASTAVA 1988 Mechanics Research Communications 15, p353. On the stability of the damped Mathieu equation.

117. T.Y. LI and J.A. YORKE 1975 American Mathematical Monthly 82, p985. Period three implies chaos.

118. Y. POMEAU and P. MANNEVILLE 1980 Communications of Mathematical Physics 74, p189. Intermittent transition to turbulence in dissipative dynamical systems.

119. H. KAPLAN 1992 Physical Review Letters 68, p553. Return to type I intermittency.

120. A. G. KUROSH 1977 Algebraic Equations of Arbitrary Degrees. Moscow: Mir Publishers.

APPENDIX A

STABILITY ANALYSIS OF A NONLINEARLY DAMPED DUFFING'S OSCILLATOR

A.1 Introduction

The equation of motion of a harmonically excited, hard, Duffing's oscillator with generalized pth-power damping model [112], is given by

$$\ddot{X} + C' \dot{X}|\dot{X}|^{p-1} + \alpha X + \beta X^3 = F' \cos \omega' t \qquad (A.1)$$

where $\alpha > 0$, $\beta > 0$, $p > 0$ and the dot denotes differentiation with respect to time t. The parameters C' and p are called the damping coefficient and exponent, respectively. The harmonic solution of equation (A.1) is sought in the form

$$X_o = A' \cos (\omega' t - \phi). \qquad (A.2)$$

which can be easily obtained by any standard method like the equivalent linearisation technique or the harmonic balance method.

In the standard variational technique [36] of stability analysis of the solution given by equation (A.2), a small variation η is considered in the form

$$X = X_o + \eta. \qquad (A.3)$$

Substituting equation (A.3) in equation (A.1) and using the fact that X_o satisfies equation (A.1), one gets a linear differential equation in η with time varying coefficients (after neglecting terms higher than linear in η). This approach has been termed dynamic analysis [113] as opposed to the static analysis where the bifurcation of the steady state harmonic solution is investigated

through the turning points having vertical tangents to the response curves in the A'-ω' plane. Only the dynamic analysis can capture unstable regions of secondary and higher orders. The dynamic analysis is increasingly becoming popular towards obtaining approximate analytical criteria for the onset of symmetry-breaking and chaotic motion of a Duffing's oscillator [114].

It must be emphasized that the dynamic analysis cannot be carried out in the usual manner unless the damping exponent p is an odd integer. Moreover, in the range $0 < p < 1$, the derivative of the damping force is discontinuous. Consequently, approximate methods have been attempted in the past. For example, in reference [51], quadratic damping (p=2) has been replaced by a linear plus cubic model. Some other methods have been proposed while carrying out the stability analysis of the responses of impact dampers [115] and hysteretic oscillators [111].

In this appendix, another approximate method is proposed using the notion of equivalent viscous damping coefficient. The method is based on the correspondence between the static analysis and the primary unstable region obtained from the dynamic analysis for $p = 1$ and 3. Following the usual method of variational technique, one obtains a Mathieu equation for $p = 1$ and a Hill equation for $p = 3$. It is shown that one can get away with only Mathieu equation for all values of p by suitably modifying the equivalent viscous damping coefficient in this variational equation. This simplification has been justified from the fact that strictly dissipative, velocity-dependent nonlinear damping alone does not give rise to any instability. Numerical results

for p = 2 obtained by the present method show good agreement with those obtained by another approximate method [111] which uses, after some approximation, the van der Pol plane. Unlike this van der Pol plane method, the present analysis, however, can also be used to obtain approximately the higher order unstable regions.

A.2. Static Analysis

The static analysis or the classical jump phenomena in the response curve for the harmonic solution of equation (A.1) is carried out as follows. It is known that for the pth-power damping model, the equivalent viscous damping coefficient can be obtained as [112]

$$C'_{e_p} = C' A'^{(p-1)} \omega'^{(p-1)} \gamma_p \tag{A.4}$$

where $$\gamma_p = \frac{2}{\sqrt{\pi}} \frac{\Gamma[(p+2)/2]}{\Gamma[(p+3)/2]} \tag{A.5}$$

with Γ representing the standard gamma function.

Now equation (A.1) can be rewritten as

$$\ddot{X} + C'_{e_p} \dot{X} + \alpha X + \beta X^3 = F' \cos \omega' t \tag{A.6}$$

and the amplitude A' of equation (A.2) is known to satisfy the relation [3]

$$A'^2 = \frac{F'^2}{C'^2_{e_p} \omega'^2 + \left(\omega'^2 - \alpha - \frac{3}{4}\beta A'^2\right)^2} \tag{A.7}$$

Introducing the following non-dimensional parameters:

$$\omega = \omega'/\sqrt{\alpha},\quad C_p = C'\,\frac{\alpha^{(2p-3)/2}}{\beta^{(p-1)/2}},\quad A = (\beta/\alpha)^{\frac{1}{2}}A',\quad F=(\beta/\alpha^3)^{1/2}F'$$

$$\text{and } C_{e_p} = \gamma_p\, C_p A^{(p-1)}\omega^{(p-1)}, \tag{A.8}$$

one can write equation (A.7) as

$$A^2 = \frac{F^2}{C_{e_p}^2\,\omega^2 + \{\omega^2 - 1 - \frac{3}{4}A^2\}^2} \tag{A.9}$$

It has been shown [35] that irrespective of the value of p, the response curve given by equation (A.9) yields the usual jump phenomenon observed in the case of p=1. The use of equivalent viscous damping coefficient is nothing but the method of equivalent linearisation [3]. The same result, as given by equation (A.9), is also obtained by the method of harmonic balance [35].

For a given value of F', differentiating both sides of equations (A.7) with respect to ω', one obtains an expression for $\frac{dA'}{d\omega'}$. Setting the denominator of this expression to zero, i.e. $\frac{dA'}{d\omega'} \to \infty$, one gets the locus of the points in the A'-ω' plane having vertical tangents to the response curves. The expression thus resulted can be put in the following non-dimensional form:

$$p\,C_{e_p}^2\,\omega^2 + \left(\omega^2 - 1 - \frac{3}{4}A^2\right)^2 - \frac{3}{2}A^2\left(\omega^2 - 1 - \frac{3}{4}A^2\right) = 0 \tag{A.10}$$

One can rewrite equation (A.10) as

$$\left[\frac{1+\frac{3}{2}A^2}{\omega^2} - 1\right]^2 = \left[\frac{3}{4}\frac{A^2}{\omega^2}\right]^2 - \left[\sqrt{p}\frac{C_{e_p}}{\omega}\right]^2 . \qquad (A.11)$$

Introducing a new set of non-dimensional parameters μ_p, δ and ε given by

$$2\mu_p = \sqrt{p}\,\frac{C_{e_p}}{\omega},\quad \delta = \frac{1+\frac{3}{2}A^2}{\omega^2} \quad \text{and} \quad \varepsilon = \frac{3}{4}\frac{A^2}{\omega^2} \qquad (A.12)$$

equation (A.10) can be recast in the form

$$(\delta - 1)^2 = \varepsilon^2 - 4\mu_p^2$$

or, $$\delta = 1 \pm\sqrt{\varepsilon^2 - 4\mu_p^2} . \qquad (A.13)$$

Attention may be drawn to the appearance of the term $\sqrt{p}$ in the parameter μ_p and dependence of C_{e_p} on A, ω and p.

A.3 Dynamic Analysis

A.3.1 Linear damping (p=1)

With p = 1.0, i.e., in the case of a viscously damped Duffing's oscillator, the variational technique yields the standard damped Mathieu equation in η [36],

$$\frac{d^2\eta}{dz^2} + 2\mu_1\frac{d\eta}{dz} + [\delta + 2\varepsilon\cos 2z]\,\eta = 0 \qquad (A.14)$$

where μ_1, δ and ε are given equation (A.12) after substituting p = 1 (i.e., $C_{e_p} = C_1 = C'/\sqrt{\alpha}$) and $z = \omega' t - \phi$.

The transition curves (in the δ-ε plane) bounding the primary unstable zone of equation (A.14) are given approximately by [36-40]

$$\delta = 1 \pm \left(\varepsilon^2 - 4\mu_1^2\right)^{1/2} + 0(\varepsilon^2) \qquad (A.15)$$

which is nothing but equation (A.13), thus confirming the fact that the loci of the points vertical tangencies of the response curve in the amplitude-frequency plane correspond to the boundaries of the primary unstable region of equation (A.14). It is easy to show that the curves bounding the primary unstable zone are given on the A-ω plane by [112]

$$A^2 = \frac{8}{9}(\omega^2-1) + \frac{4}{9}\left[(\omega^2-1)^2 - 3C_1^2\omega^2\right]^{1/2} \qquad (A.16)$$

and

$$A^2 = \frac{8}{9}(\omega^2-1) - \frac{4}{9}\left[(\omega^2-1)^2 - 3C_1^2\omega^2\right]^{1/2} . \qquad (A.17)$$

The transition curves bounding the secondary unstable zone of equation (A.14) are given by [36-40],

$$\delta = 4 + \frac{1}{6}\varepsilon^2 \mp \left(\varepsilon^4/16 - 16\mu_1^2\right)^{1/2} + 0(\varepsilon^3) . \qquad (A.18)$$

In the absence of damping (i.e., with $\mu = 0$ in equation (A.18)), employing equation (A.12) the transition curves bounding the secondary unstable zones can be obtained in the A-ω plane as

$$A^2 = \frac{16}{5}\omega^2 - \frac{32}{5}\omega^2\left[\frac{15}{16\omega^2} - \frac{3}{2}\right]^{1/2} \qquad (A.19)$$

and

$$A^2 = -\frac{16}{5}\omega^2 + \frac{32}{5}\omega^2\left[3 - \frac{15}{16\omega^2}\right]^{1/2} \qquad (A.20)$$

Following the results given in reference [37], it may be observed that equation (A.19) is quite accurate for $\omega > 0.5$ whereas equation (A.20) is accurate only in the range $0.5 < \omega < 0.8$. Figure A.1 shows the primary and secondary unstable zones in the A-ω plane for the undamped Duffing's oscillator. In this figure, curves I (the backbone curve) and II (the locus of the single turning points) are given by equations (A.16) and (A.17) respectively with $C_1 = 0$. It can easily be shown from equations (A.16), (A.17) and (A.12) that for this undamped situation, the primary unstable region bounded by curves I & II is quite accurate for the entire range of frequency. The secondary unstable region starts from $\omega = 0.5$ and equation (A.19) produces the curve CPQ which, beyond the point Q, deviates drastically from the exact curve CPQ'. The exact curve can be obtained through numerical computation of the transition curve of the Mathieu equation. In the same figure, the response curve for $F = 1.0$ is also shown whose unstable portions are indicated by the dashed lines.

The secondary unstable region in the presence of viscous damping can be obtained through the use of equation (A.18). The two transition curves can be put together as

$$\left(\delta - 4 - \frac{\varepsilon^2}{6}\right)^2 = \frac{\varepsilon^4}{16} - 16\,\mu_1^2 \,. \qquad (A.21)$$

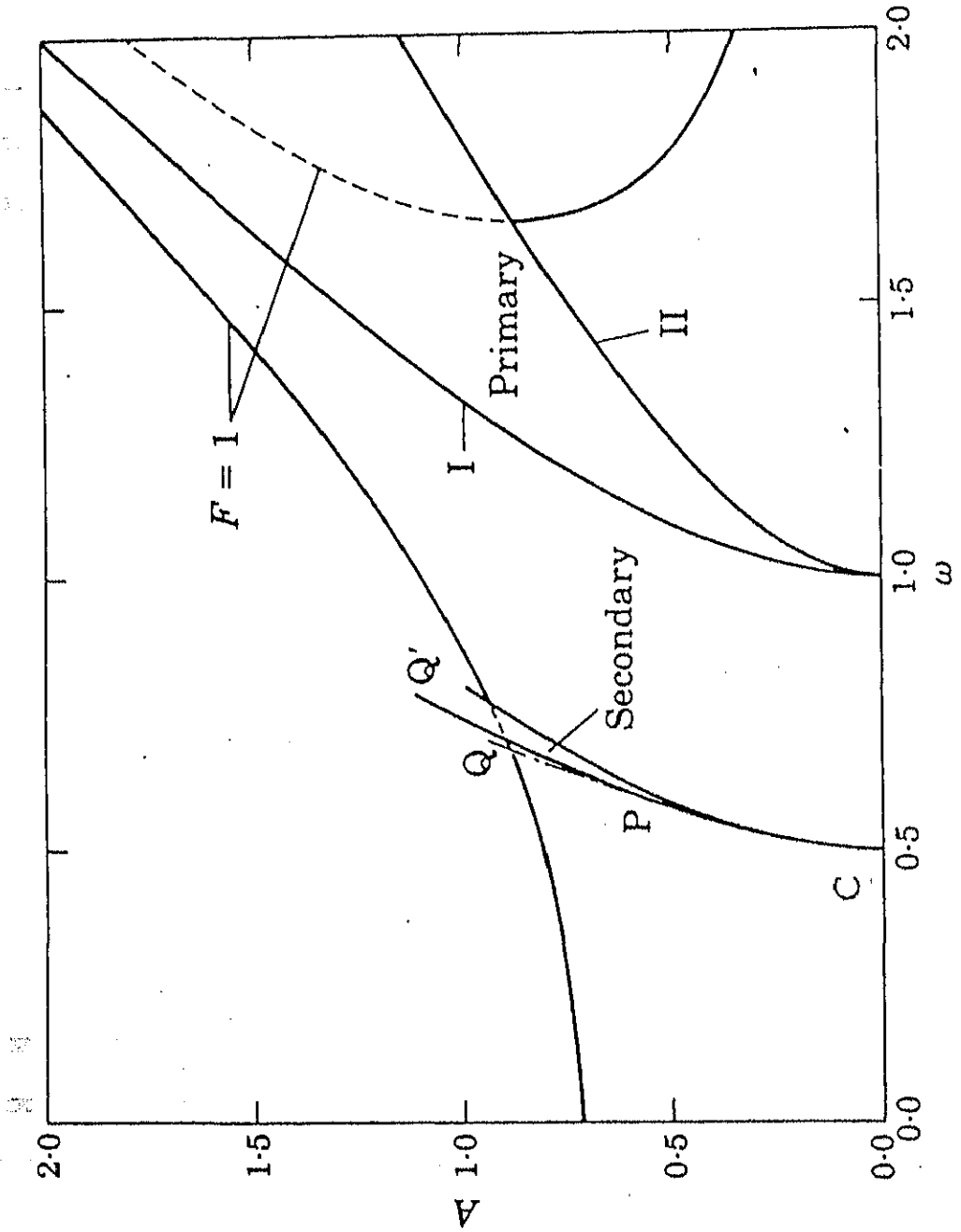

Figure A.1 Primary and Secondary instability regions with a typical response curve for an undamped Duffing's oscillator

Now, substituting for δ, ε and μ_1 from equation (A.12) (with p = 1) in the above equation and simplifying one gets the following quartic equation in A^2:

$$a_1(A^2)^4 + a_2(A^2)^3 + a_3(A^2)^2 + a_4(A^2) + a_5 = 0 \qquad (A.22)$$

where $a_1 = 45/256$, $a_2 = \frac{9}{2}\omega^2$, $a_3 = 3\omega^2 - 48\omega^4$, $a_4 = 192\omega^6 - 48\omega^4$,

and $a_5 = 128\omega^6 - 16\omega^4 - 256\,\omega^8 - 64C_{e_1}^2\,\omega^6$.

Solving equation (A.22) numerically and retaining only the real, positive roots one can obtain the secondary unstable region in the A-ω plane. Figures A.2 and A.3 show respectively, the primary and secondary unstable regions for some low values of damping. The representation of the primary and secondary unstable zones on the A-ω plane may help in locating the chaotic response of equation (A.1) with reference to the classical jump curves [114].

A.3.2 Cubic damping (p=3)

With p=3 in equation (A.1), considering the variation of the solution given by equation (A.2) and carrying out the usual procedure, one gets the following non-dimensional equation:

$$\frac{d^2\eta}{dz^2} + \left[\frac{4\mu_3}{\sqrt{3}} - \frac{4\mu_3}{\sqrt{3}}\cos 2z\right]\frac{d\eta}{dz} + [\delta + 2\varepsilon\cos 2z]\,\eta = 0 \qquad (A.23)$$

where μ_3, δ and ε are still given by equation (A.12) with p=3 and $z = \omega' t - \phi$.

The Lindstedt - Poincare technique [38] can be used to

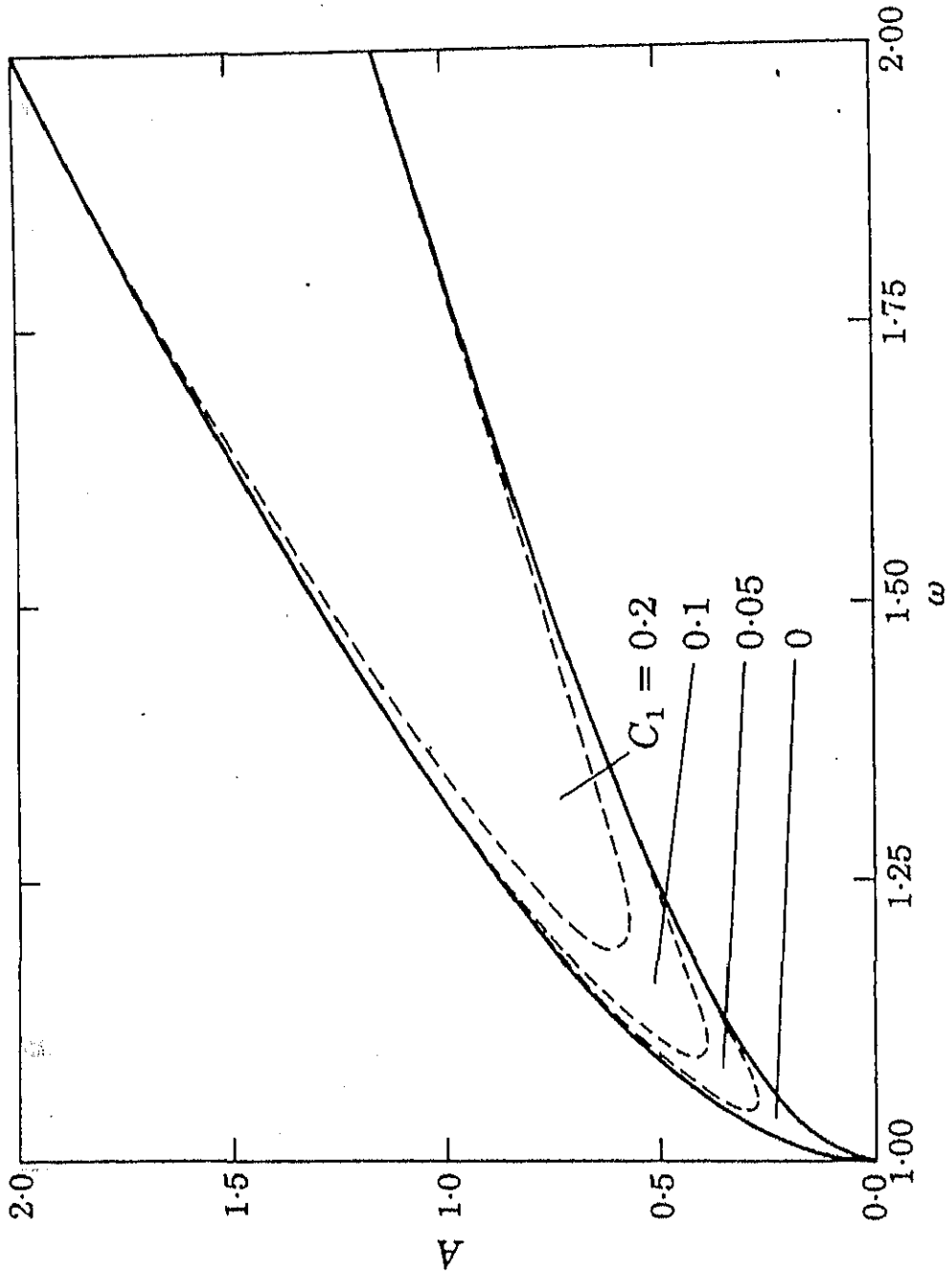

Figure A.2 Primary unstable regions for various coefficients of linear damping

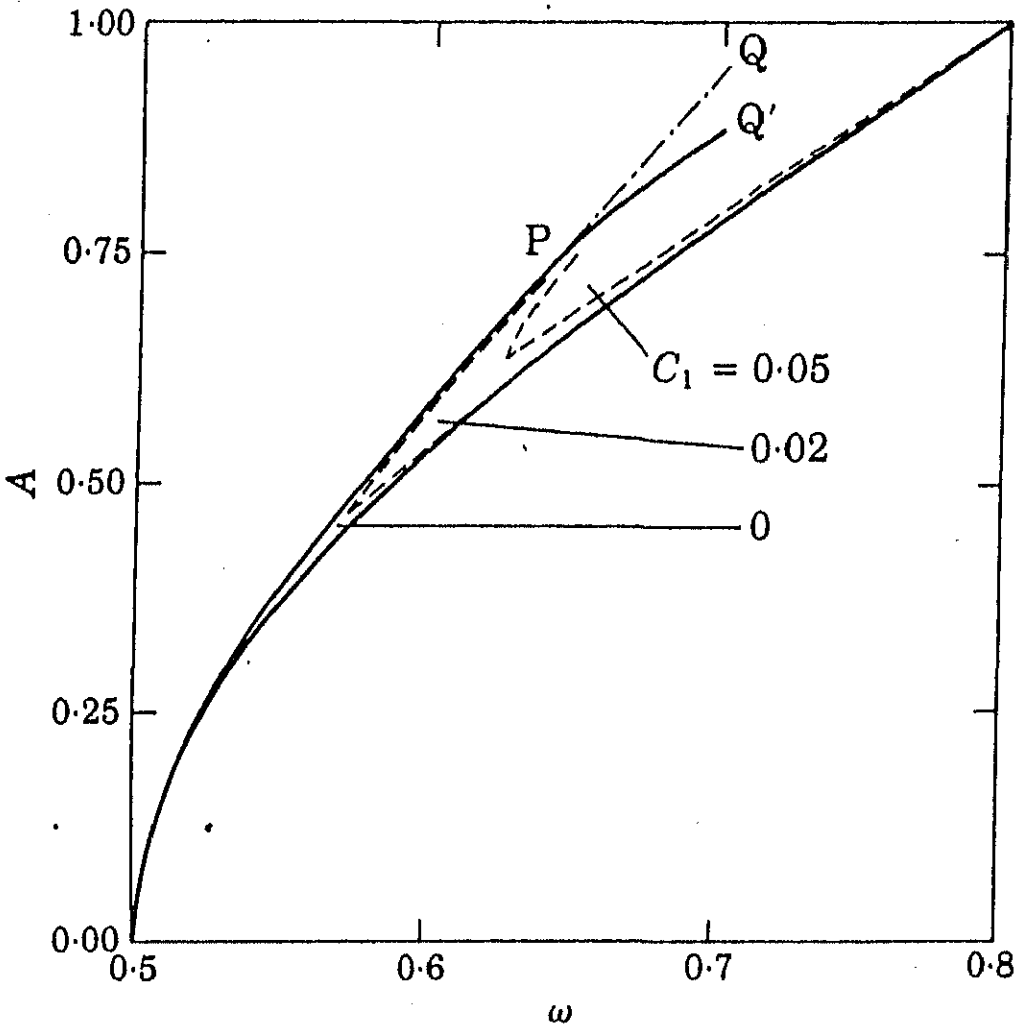

Figure A.3 Secondary unstable regions for various coefficients of linear damping.

obtain the transition curves for the primary unstable zone. Towards this end, one sets $\mu_3 = \varepsilon \hat{\mu}_3$ and writes

$$\eta(z, \varepsilon) = \eta_o(z) + \varepsilon \eta_1(z) + \varepsilon^2 \eta_2(z) + \cdots\cdots \quad (A.24)$$

and $$\delta(\varepsilon) = \delta_o + \varepsilon\delta_1 + \varepsilon^2\delta_2 + \cdots\cdots \quad (A.25)$$

Substituting equations (A.24) and (A.25) in equation (A.23) and equating coefficients of like powers of ε, one obtains

$$\frac{d^2\eta_o}{dz^2} + \delta_o \eta_o = 0 \quad (A.26)$$

$$\frac{d^2\eta_1}{dz^2} + \delta_o \eta_1 = -\left[\frac{4\hat{\mu}_3}{\sqrt{3}} - \frac{4\hat{\mu}_3}{\sqrt{3}} \cos 2z\right] \frac{d\eta_o}{dz} - [\delta_1 + 2\cos 2z] \eta_o \quad (A.27)$$

and

$$\frac{d^2\eta_2}{dz^2} + \delta_o \eta_2 = -\left[\frac{4\hat{\mu}_3}{\sqrt{3}} - \frac{4\hat{\mu}_3}{\sqrt{3}} \cos 2z\right] \frac{d\eta_1}{dz} - [\delta_1 + 2\cos 2z] \eta_1 - \delta_2 \eta_0 . \quad (A.28)$$

According to the Floquet theory [36], η has the period either π or 2π along the transition curves.

Therefore, one can write

$$\eta_o = a_o \cos nz + b_o \sin nz \quad (A.29)$$

where n is a non-zero integer related to δo by

$$n^2 = \delta_o \quad (A.30)$$

and a_o and b_o are arbitrary constants at this point.

For the transition curves bounding the primary unstable zone, n is unity and hence

$$\delta_0 = 1 \text{ and } \eta_0 = a_0 \cos z + b_0 \sin z.$$

Substituting for η_o into equation (A.27) and simplifying one obtains

$$\frac{d^2\eta_1}{dz^2} + \delta_o \eta_1 = \left[\frac{4\hat{\mu}_3}{\sqrt{3}} a_o - b_o\delta_1 + \frac{1}{2}\left(\frac{4\hat{\mu}_3}{\sqrt{3}} a_o + 2b_o\right)\right] \sin z$$

$$-\left[\frac{4\hat{\mu}_3}{\sqrt{3}} b_o + a_o\delta_1 - \frac{1}{2}\left(\frac{4\hat{\mu}_3}{\sqrt{3}} b_o - 2a_o\right)\right] \cos z$$

$$- \frac{1}{2}\left(\frac{4\hat{\mu}_3}{\sqrt{3}} a_o + 2b_o\right) \sin 3z + \frac{1}{2}\left(\frac{4\hat{\mu}_3}{\sqrt{3}} b_o - 2a_o\right) \cos 3z. \tag{A.31}$$

Thus the conditions for eliminating secular terms from η_1 are given by

$$\left(\frac{4\hat{\mu}_3}{\sqrt{3}} + \frac{2\hat{\mu}_3}{\sqrt{3}}\right) a_o + (1-\delta_1)\, b_o = 0 \tag{A.32}$$

and

$$(1 + \delta_1)\, a_o + \left(\frac{4\hat{\mu}_3}{\sqrt{3}} - \frac{2\hat{\mu}_3}{\sqrt{3}}\right) b_o = 0 \,. \tag{A.33}$$

For a nontrivial solution to exist for a_o and b_o, one equates the coefficient determinant for equations (A.32) and (A.33) to zero and obtains the following equation :

$$\delta_1 = \mp (1-4\,\hat{\mu}_3^2)^{1/2} \tag{A.34}$$

Substituting for δ_o and δ_1 in equation (A.25), the transition curves for the primary unstable zone are obtained as

$$\delta = 1 \mp (\varepsilon^2 - 4\,\mu_3^2)^{1/2} + 0\,(\varepsilon^2) \tag{A.35}$$

Once again it can be seen that equation (A.35) is nothing but equation (A.13).

For deriving the transition curves bounding the secondary unstable zone it is assumed that $\mu_3 = 0(\varepsilon^2) = \varepsilon^2\,\hat{\mu}_3$ and carrying out a similar procedure outlined above, one gets

$$\delta = 4 + \frac{1}{6}\,\varepsilon^2 \mp \left(\frac{\varepsilon^4}{16} - \frac{64}{3}\,\mu_3^2\right)^{1/2} \tag{A.36}$$

A.3.3 Proposed method

Comparing equations (A.15) and (A.35) one can conclude that the form of the expression defining the bounds of the primary unstable zone is identical for p = 1 and p =3. The only difference is in the corresponding subscript used for μ. It should be noted that equation (A.23) differs from equation (A.14) since the coefficient of $\frac{d\eta}{dz}$ in the former varies periodically with time. However, as shown in the appendix B, the time variations of the coefficient of $\frac{d\eta}{dz}$ alone, in equation (A.23), does not result in any instability. Therefore, with time varying coefficient of η, it is proposed to approximate the time varying coefficient of $\frac{d\eta}{dz}$ in equation (A.23) by some average value. Comparing equations (A.15) and (A.35) it is clearly seen that for p = 3, this average value turns out to be $\sqrt{3}/2$ times the constant part of the coefficient. This approximation may be tested by obtaining

results for the secondary unstable zones. The transition curves bounding the secondary unstable zone are given by equation (A.36). Equation (A.18) with μ_1 replaced by μ_3 yields the approximation of this secondary unstable zone. A comparison of equation (A.36) with equation (A.18) indicates that the approximation, though a little more conservative (resulting in a wider secondary unstable zone), is quite good, specially for low values of the damping coefficient.

As mentioned in section 1, for a general value of the damping exponent p, the variational method is not amenable for analytical treatment. Keeping in mind that equations (A.15) and (A.18) give satisfactory results even for p=3 when μ_1 is replaced by μ_3 as discussed in the preceeding paragraph, it is proposed to use the same equations for any value of p ($o<p<3$) with μ_1 replaced by μ_p. The proposed method is illustrated for the following set of parameter values : p=2.0, $F'=1.0$, $\omega'=2.0$ and $C'=0.05$. The three roots of the amplitude of the response can be obtained by using equation (A.8) as

$$A_1 = 0.34339,\ A_2 = 1.847,\ A_3 = 2.1022.$$

The first root corresponds to the non-resonant branch (stable), the second to the unstable branch and the third one to the (stable) resonant branch. The stability/instability of these three roots are confirmed by the van der Pol plane method outlined in reference [111]. In this reference also, an approximation was made by neglecting the higher harmonics in the Fourier expansion of the damping force. Using equation (A.12) the value of δ, ε and μ_2 corresponding to the above three roots of A are obtained as given below:

	μ_2	δ	ε
A_1	0.0103	0.2942	0.0221
A_2	0.0554	1.5293	0.6397
A_3	0.0631	1.9073	0.8286

The transition curves bounding the primary unstable zones for p=2 given by equation (A.15) with μ_1 replaced by μ_2 are shown in Figures A.4a-A.4c. The shaded portions correspond to the unstable regions. The points corresponding to the roots of A are also indicated in the some figure by a cross mark. One can see that points A_1 and A_3 lie outside the shaded portions as shown in Figures A.4a and A.4c, respectively, and hence stable; where as the point A_2 is inside the shaded portion as shown in Figure A.4b and hence unstable. Thus, the results are consistent with those obtained by using the method of reference [111]. Similar numerical checks have confirmed the validity of the present approximate method of obtaining the primary unstable zone by using equation (A.15) for a number of values of p in the range $0 < p \leq 3$. The method, however, cannot be used for p=0 i.e., a Duffing's oscillator with Coulomb damping.

A.4 Conclusions

An approximate procedure using a modified equivalent viscous damping coefficient and the variational formulation, has been proposed to obtain the primary (and higher order) unstable zones of the steady state harmonic solutions of the Duffing's oscillator with pth-power damping model. Simple Mathieu equation is used irrespective of the damping exponent p. Numerical results obtained for the primary unstable zone are found to be in

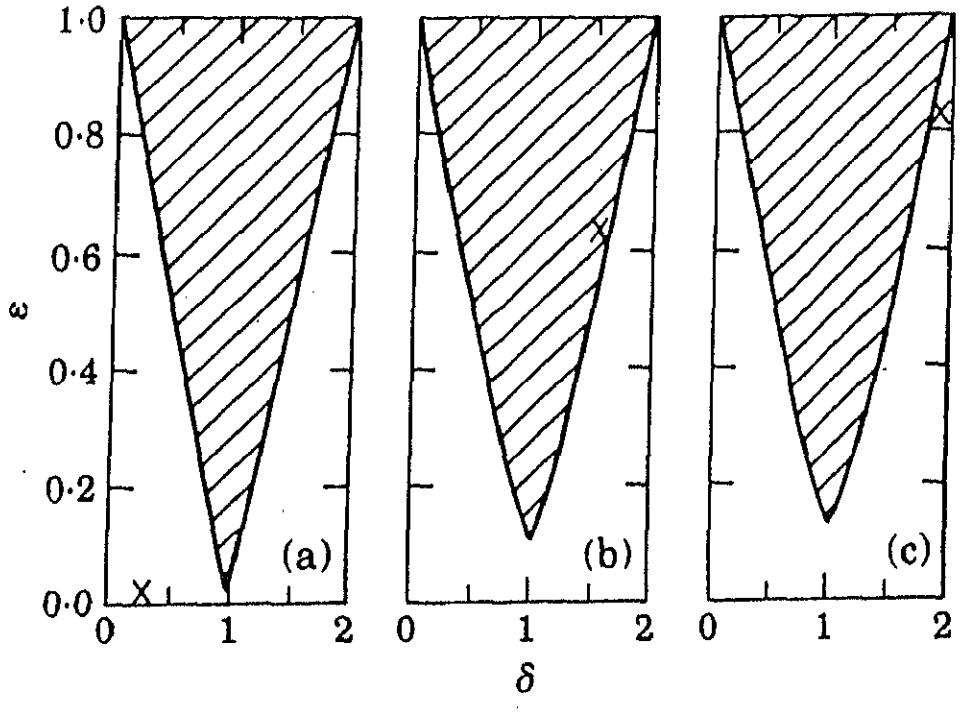

Figure A.4 Primary unstable zones for quadratic damping (p=2) (a) μ_2 = 0.0103; (b) μ_2 = 0.0554; (c) μ_2=0.0631

agreement with that predicted by another approximate method. An analytical procedure to depict the primary and secondary unstable zones on the amplitude-frequency plane is outlined which may enable one to obtain approximate analytical criteria for chaotic responses based on the stability of the harmonic solution.

APPENDIX B

STABILITY ANALYSIS OF AN OSCILLATOR WITH LINEAR STIFFNESS AND CUBIC DAMPING

Consider an equation of the following form [116]

$$\ddot{\eta} + d(t)\,\dot{\eta} + e(t)\,\eta = 0 \qquad \text{(B.1)}$$

where d(t) and e(t) are continuous and differentiable functions of time. Following reference [116], one obtains the conditions for stability of equation (B.1) as

$$e(t) > 0 \qquad \text{(B.2)}$$

and

$$2\,d(t)\,e(t) + \dot{e}(t) \geq 0\ . \qquad \text{(B.3)}$$

Now consider a system with a linear spring and a cubic damper (by putting p=3 and β=0 in equation (A.1)) governed by

$$\ddot{X} + C'\dot{X}^3 + \alpha X = F' \cos \omega' t \text{ with } C' > 0 \text{ and } \alpha > 0 \qquad \text{(B.4)}$$

Applying the variational technique to the harmonic solution of equation (B.4), one obtains,

$$\ddot{\eta} + \left[\frac{4\mu_3}{\sqrt{3}} - \frac{4\mu_3}{\sqrt{3}} \cos 2z\right] \dot{\eta} + \eta = 0 \quad \text{with } z=\omega' t-\phi \qquad \text{(B.5)}$$

Comparing equation (B.5) and (B.1) one can write that

$$d(t) = \frac{4\mu_3}{\sqrt{3}} [\ 1-\cos\ 2z]$$

and $e(t) = 1.0$. (B.6)

Noting that in equations (B.6), $d(t) \geq 0$, $e(t) > 0$ and $\dot{e}(t) = 0$, one can easily see that the conditions for stability of equation (B.5), as dictated by equations (B.2) and (B.3), are satisfied. This implies that there are no unstable zones for equation (B.5) and consequently there is no jump phenomenon in the response of equation (B.4) [3]. This analysis shows that the time variation in the coefficient of $\dot{\eta}$ alone in equation (B.5) does not give rise to any unstable zone.

APPENDIX C

SOME ANALYTICAL CRITERIA

In this appendix, some simple analytical expressions for quantities related to the anomalous jump response have been derived. The response equation, for the base excited system given by equation (4.6), can be put in the form of a cubic equation with the transformation $\Delta_2 = \Delta_1^2$, to yield:

$$\Delta_2^3 + a_1 \Delta_2^2 + a_2 \Delta_2 + a_3 = 0 \qquad (C.1)$$

where $a_1 = -2\Omega^2/\alpha$, $a_2 = \Omega^4/\alpha^2$ and $a_3 = (4\beta^2 \zeta_f^2 - \Omega^4)/\alpha^2$. (C.2)

Equation (C.1) can be put in the standard form with the transformation $\Delta_2 = \Delta_3 - a_1/3$, resulting in the following equation

$$\Delta_3^3 + q_1 \Delta_3 + q_2 = 0 \qquad (C.3)$$

where $q_1 = -a_1^2/3 + a_2$

(C.4)

and $q_2 = 2a_1^3/27 - a_1 a_2/3 + a_3$.

Applying the condition for repeated roots of equation (C.3) [120], we get

$$q_2^2/4 + q_1^3/27 = 0 \Rightarrow 4\beta^2 \zeta_f^2 - \Omega^4 = 0 \qquad (C.5a)$$

or $$4\beta^2 \zeta_f^2 - \Omega^4 + 4/(27\alpha)\,\Omega^6 = 0 \,. \qquad (C.5b)$$

The first of the above equations corresponds to the break-loose frequency. For $\Omega > \Omega_b$ (i.e., $\Omega > (8\zeta_f/\pi)^{1/2}$), the values of Ω obtained by solving equation (C.5b) for a particular ζ_f correspond to the critical frequency of the anomalous jump (Ω_a) and the non-resonance critical frequency of the usual jump (Ω_n). The values of Ω_a and Ω_n, so obtained, are shown in Figure 4.4 for various values of ζ_f.

Now it is interesting to find out the value of $\zeta_f = (\zeta_f)_m$ at which Ω_a and Ω_n coincide i.e., when the anomalous jump just meets the usual jump. This corresponds to the condition for repeated roots of equation (C.5b). Noticing that equation (C.5b) is also a cubic equation in Ω^2 (say W) and substituting for α and β in (C.5b), one obtains

$$W^3 - 3^4/2^4\, W^2 + 3^4\, 2^2/(\pi)^2\, \zeta_f^{\,2} = 0. \qquad (C.6)$$

The condition for repeated roots of equation (C.6), is obtained, in case $\zeta_f > 0$, as

$$(2\zeta_f/\pi)^2 = 3^5/2^{10} \Rightarrow (\zeta_f)_m = 3^{5/2}/2^6\, \pi \approx \pi/4. \qquad (C.7)$$

Beyond this value of ζ_f (i.e., $\zeta_f > (\zeta_f)_m$), the usual jump opens up as in the soft Duffing's case [77], and merges with the anomalous jump. The break-loose frequency corresponding to $(\zeta_f)_m$ is given by (see equation (4.8))

$$(\Omega_b)_m = [\ 8\ (\zeta_f)_m/\pi\ ]^{1/2} \approx [\ 8\ (3^{5/2}/2^6)\ ]^{1/2} \approx \sqrt{2}. \qquad (C.8)$$

ME-1994-D-RAV-HAR